ULTRA-WIDEBAND PHASED ARRAYS

Chao Chun Chen, et al

Hughes Aircraft Company

Prepared for:

Air Force Cambridge Research Laboratories

July 1973

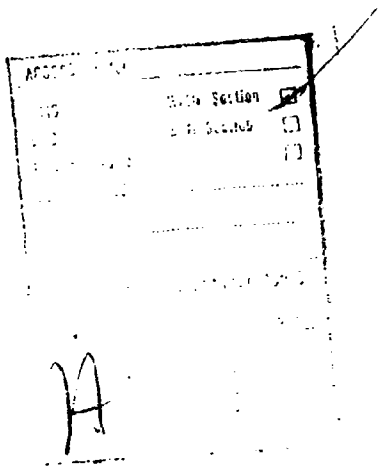

Qualified requestors may obtain additional copies from the Defense Documentation Center. All others should apply to the National Technical Information Service.

UNCLASSIFIED
Security Classification

AD-769965

DOCUMENT CONTROL DATA - R & D

(Security classification of title, body of abstract and indexing annotation must be entered when the overall report is classified)

1. ORIGINATING ACTIVITY *(Corporate author)*
Hughes Aircraft Company/Microwave Techniques Department
Electromagnetic Laboratory/Communications and Radar Div.
Fullerton, California 92634

2a. REPORT SECURITY CLASSIFICATION
Unclassified

2b. GROUP

3. REPORT TITLE

Ultra-Wideband Phased Arrays

4. DESCRIPTIVE NOTES *(Type of report and inclusive dates)*
Scientific. Final. 15 March 1972 – 15 June 1973 approved 18 Sept 1973

5. AUTHOR(S) *(First name, middle initial, last name)*
Chao Chun Chen
N. S. Wong
R. Tang

6. REPORT DATE
July 1973

7a. TOTAL NO. OF PAGES
~~74~~ 72

7b. NO. OF REFS
15

8a. CONTRACT OR GRANT NO
F19628-72-C-0224

b. PROJECT NO Task, Work Unit Nos.
4600-10-01

c. DoD Element 62702F

d. DoD Subelement 674600

9a. ORIGINATOR'S REPORT NUMBER(S)
FR 73-14-922

9b. OTHER REPORT NO(S) *(Any other numbers that may be assigned this report)*
AFCRL-TR-73-0569

10. DISTRIBUTION STATEMENT
A – Approved for public release, distribution unlimited.

Letter qualifications in this document may be better studied on microfiche.

11. SUPPLEMENTARY NOTES
TECH, OTHER

12. SPONSORING MILITARY ACTIVITY
Air Force Cambridge Research Laboratories
L.G. Hanscom Field (LZ)
Bedford, Massachusetts 01730

13. ABSTRACT

This report describes the analysis, design and development of Ultra Wideband Phased Arrays. Four different waveguide radiators were studied for wideband and for ±60° half-angle conical scan coverage. Rectangular waveguides with thin iris and double ridge-loaded rectangular waveguides were considered for linearly polarized, two dimensional array antennas. Dielectric-loaded circular waveguides and quadruple ridge-loaded circular waveguides were considered for arbitrarily polarized antennas.

A maximum VSWR of 2.3:1 is achieved over a 50 percent bandwidth by using a thin iris in the open end of rectangular waveguides. The same array can be operated over a 58 percent band with a maximum VSWR of 2.75:1. Applying the iris matching technique to an array of double ridge-loaded waveguides, an octave bandwidth with a maximum VSWR of 3.3:1 over ±60° scan angle is achieved.

The requirements of dual polarization and ±60° scan limits the bandwidth of an arbitrarily polarized phased array. A 20 percent band design for a dielectrically loaded circular waveguide arrays and a 15 percent band design for a quadruple ridge-loaded waveguide arrays are described. The maximum transmission loss is less than 1.83 dB within the 60-degree conical scan angle and throughout the entire bandwidth. The variation of axial ratio and polarization isolation between the two orthogonal modes of operation as a function of scan angle is also presented in detail.

All data presented in this report are based on an element spacing six percent less than the condition required for grating lobe suppression unless specified. Reduction in element spacing, scan volume, or bandwidth will result in an even better impedance match and polarization characteristics. Simplicity and low fabrication cost are the features of these radiating elements.

DD FORM 1 NOV 65 1473

UNCLASSIFIED
Security Classification

14 KEY WORDS	LINK A		LINK B		LINK C	
	ROLE	WT	ROLE	WT	ROLE	WT
Phased Arrays						
Waveguide Radiators						
Ultra-Wideband						
Wide-Angle Scan						
Aperture Matching						
Octave Bandwidth						
Arbitrary Polarization						
Dual Polarization						
Arial Ratio						
Polarization Isolation						

ABSTRACT

This report describes the analysis, design and development of Ultra Wideband Phased Arrays. Four different waveguide radiators were studied for wideband and for $+60^{\circ}$ half-angle conical scan coverage. Rectangular waveguides with thin iris and double ridge-loaded rectangular waveguides were considered for linearly polarized, two dimensional array antennas. Dielectric-loaded circular waveguides and quadruple ridge-loaded circular waveguides were considered for arbitrarily polarized antennas.

A maximum VSWR of 2.3:1 is achieved over a 50 percent bandwidth by using a thin iris in the open end of rectangular waveguides. The same array can be operated over a 58 percent band with a maximum VSWR of 2.75:1. Applying the iris matching technique to an array of double ridge-loaded waveguides, an octave bandwidth with a maximum VSWR of 3.3:1 over a $\pm 60^{\circ}$ scan angle is achieved.

The requirements of dual polarization and $\pm 60^{\circ}$ scan limits the bandwidth of an arbitrarily polarized phased array. A 20 percent band design for a dielectrically loaded circular waveguide arrays and a 15 percent band design for a quadruple ridge-loaded waveguide arrays are described. The maximum transmission loss is less than 1.83 dB within the 60-degree conical scan angle and throughout the entire bandwidth. The variation of axial ratio and polarization isolation between the two orthogonal modes of operation as a function of scan angle is also presented in detail.

All data presented in this report are based on an element spacing six percent less than the conditions required for grating lobe suppression unless specified. Reduction in element spacing, scan volume, or bandwidth will result in an even better impedance match and polarization characteristics. Simplicity and low fabrication cost are the features of these radiating elements.

FOREWORD

This report was prepared by the Microwave Technique Department, Communication and Radar Division, Hughes Ground Systems Group, at Fullerton, California. Research was conducted under Contract F19628-72-C-0224. Dr. Richard Mack, LZR of the Air Force Research Laboratories at Bedford, Massachusetts was the program monitor for this research.

The material reported herein represents the results of the investigation into techniques applicable to the design and development of Ultra Wideband Phased Arrays.

The author wishes to acknowledge the contributions of Mr. E.E. Barber, J.W. McFarland and J.K. Jasperson in the experimental measurements performed and reported.

TABLE OF CONTENTS

BLANK PAGE FOLLOWS v/vi

SECTION I
INTRODUCTION AND SUMMARY

This final report describes the activities and accomplishments associated with the two major technical tasks of this project. The first task is the development of a linearly polarized two-dimensional phased array which is well matched simultaneously over a large scan angle range and over an octave bandwidth. The second task is to extend the impedance matching of the linearly polarized element to an arbitrarily polarized element for wide-angle scaning and wide tunable bandwidth.

1.1 BACKGROUND

Due to the demands of sophisticated radar capabilities, modern military aircraft and ships are equipped with a large number of antennas for various radar and communication systems. Installation of many antennas not only increases the cost and weight, but also becomes impractical in a space limited environment. Consequently, there are increasing demands for a broadband radiating aperture, which can be shared by many microwave antennas to satisfy the needs of multifunction shipboard or airborne radar systems. In addition, a phased array with broadband capability is advantageous for ECM and ECCM applications. The current state of the art in the design of broadband phase shifters, feed networks, and other components appears to be more advanced than broadband apertures for waveguide phased arrays; therefore, the concern here is primarily with the aperture design.

The problems of wide-angle impedance matching of phased arrays have been investigated extensively in the past decade. A survey of various matching schemes was made by Knittel[1] in 1970. Most designs have a bandwidth of about 10 percent, and none of the designs shown were capable of operating over a 20 percent bandwidth without serious degradation of impedance performance. Recently, Tsandoulas[2] and Laughlin, et al[3] developed some wide-band elements which operate over nearly an octave frequency band. However, the number of elements per unit area in the array and the average impedance mismatch loss over the scan volume were not efficiently minimized in the cases requiring 50% or more bandwidth.

1.2 PROGRAM OBJECTIVES

The purpose of this study is to analyze and develop the design of two-dimensional phased arrays which satisfy the following requirements:

1) Radiation impedance of arrays with linearly polarized elements should be well matched simultaneously over a 60-degree half-angle core and over an octave bandwidth.

2) Radiation impedance of arrays with arbitrarily polarized elements should be well matched ovar a 60-degree half-angle cone and over at least a 20 percent tunable frequency band.

3) The arbitrarily polarized radiators should be capable of electronically adjusting their polarization to any elliptical value including either circular or any linear.

4) The total number of elements in an array must be minimized.

5) All radiators should be rigid and mechanically simple so that the array would be most advantageous from the standpoint of weight, performance cost of fabrication, and practicality.

6) Fabricate test array to verify analytical results.

1.3 DESIGN CONSIDERATIONS OF WIDEBAND RADIATORS

Spirals and log periodics have been used as wideband radiators for most applications. In those cases, either a single element or a few is used where the interaction between the elements is unimportant. In the case where an ultra-wide band radiator in terms of an octave bandwidth or more is required for application in phased arrays, the application of log periodics or spirals may present problems in physical interference as well as mutual coupling problems. In any case, the fact that the radiator may be broadband in an isolated environment does not necessarily carry over into the case of a large phased array.

The important conditions which must be satisfied by ultra-wide band radiator in a large phased array are enumerated as follows: (1) the interelement spacing between radiating elements must be less than roughly 0.6 λ at the high end of the frequency band in order to avoid grating lobe formation, (2) the radiation impedance as a function of scan must be well behaved over the frequency band, and (3) the transmission line to the radiator must be capable of satisfactory operation over the frequency band. The first condition rules out the use of most of the popular broadband elements such as log periodic, spirals, and so on because these elements are physically many wavelengths in size and they cannot be packaged into the available space. Dipoles, slots, and other resonant elements probably are also poor candidates because of rapid change in radiation impedance with frequency. Open ended waveguide radiators appear to possess the disadvantage of waveguide cutoff at low frequencies. However, this can be overcome by ridge loading of the waveguide elements.

1.4 PROGRAM OVERVIEW

Section II deals with the case of using straight rectangular waveguide radiators. The design utilizes a simple iris in the aperture to obtain an impedance match having a maximum VSWR of 2.3:1 over a 50 percent band and for a 60-degree half-angle conical coverage using an element spacing which is 6 percent less than the conditions required for grating lobe suppression.* With the relaxation of the aperture matching conditions, the same array can be operated over a 58 percent frequency band with a maximum VSWR of 3.3:1. The design procedure has been well established.

The radiation characteristics of the array has been verified by taking active element patterns as well as reflection measurements in three H-plane waveguide simulators. Section III is an extension of the work presented in Section II to cover an octave band of frequencies (67 percent bandwidth) by ridge loading of the rectangular waveguide radiators.

*The condition required for grating lobe suppression implies that the grating lobe peak is at end fire when the main beam is scanned to the edge of the scan volume at the high end of the frequency band.

Section IV deals with arrays of dielectric-loaded circular waveguide elements. A design which provides 20 percent frequency band over a 60-degree half-angle conical coverage is achieved. Performance of the arrays is based on a tradeoff studies between aperture mismatch loss and axial ratio of the array as a function of scan. Detailed analysis of the polarization characteristics such as cross polarization, axial ratio and polarization coupling between two senses of circular modes were investigated. Section V is concerned with the development of quadruple ridge loaded circular waveguide arrays. Design curves of quadruple ridge-loaded circular waveguides and a procedure for aperture matching has been established. Finally, a short conclusion is given in Section VI.

1.5 ACCOMPLISHMENTS

In Task I, the design objective of an octave band phased array has been achieved successfully. The maximum VSWR is less than 3.6:1 over an octave bandwidth and over a 60 degree half-angle conical scan range. If the bandwidth is reduced slightly to 50%, the maximum VSWR is improved to less than 2.3:1 over the same scan coverage. A tradeoff between VSWR and bandwidth for 60° coverage is shown in Figure 1.1. Simplicity and cost effectiveness is the features of these designs.

In Task II, we have accomplished a 20 percent design for an arbitrarily polarized phased array. Significant improvement in axial ratio and polarization isolation between the two opposite senses of the polarization ellipses in space are obtained for a circular waveguide array comparing to that of the square waveguide arrays.

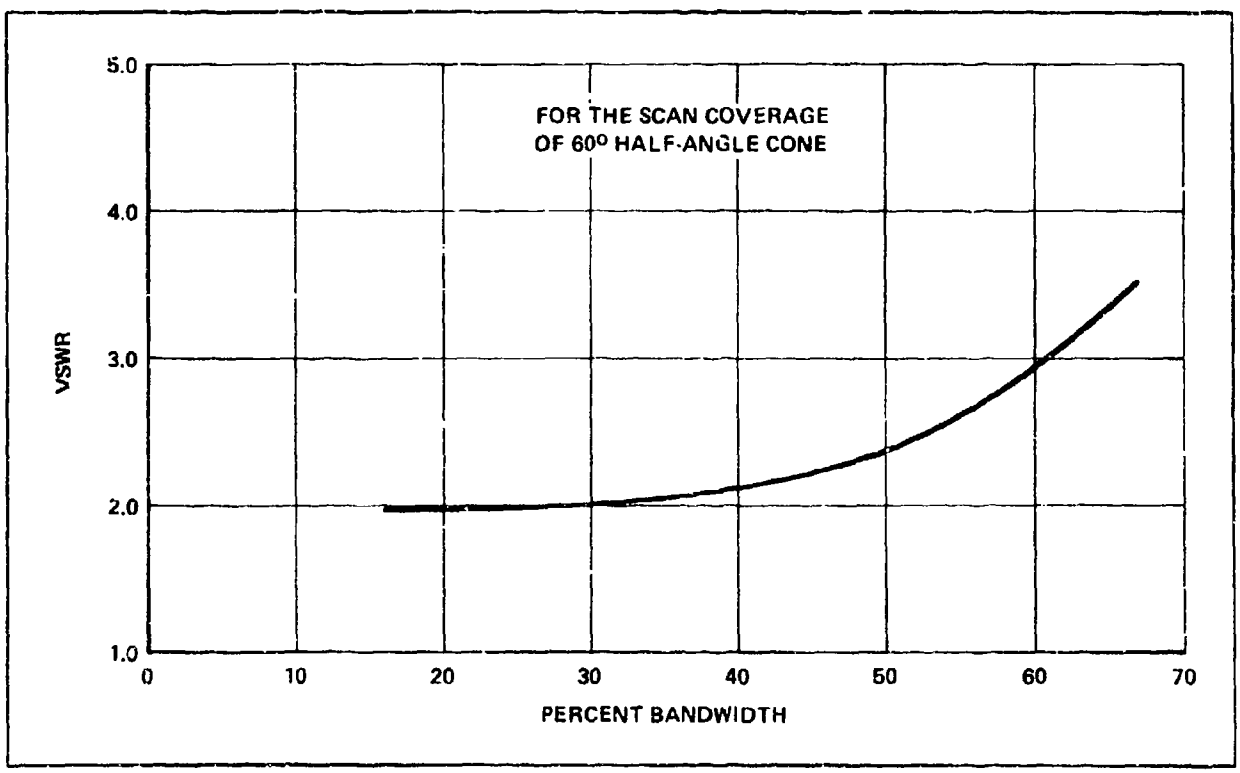

Figure 1.1. Tradeoff Between VSWR with Bandwidth for Rectangular Waveguide Arrays.

SECTION II
RECTANGULAR WAVEGUIDE ARRAYS

2.1 DESIGN CONSIDERATION OF THE ELEMENT CONFIGURATION

The radiation impedance of an infinite phased array of rectangular waveguides can be predicted precisely. Mutual coupling between array elements and the change of the driving impedance as a function of scan is completely understood. However, no significant improvement in aperture matching has been made, since Magill and Wheeler's[4] invention of using a thin dielectric sheet for wide-angle impedance matching (WAIM).

The technique of using a thin iris at the open ends of the waveguide radiators has been investigated by Lee and Jones[5]. Installation of a thin iris in the aperture yields a remarkable effect on the elimination of radiation nulls and improvement of aperture mismatch. However, the advantages of broadbanding inherent in this iris matching technique is not clearly shown in their paper[5]. It is suspected that the multimode dielectric plugs used in their array has limitations on broadband aperture matching. Therefore, it was decided to remove the multimode dielectric plug.
The model used in this study is an array of rectangular waveguides with a thin iris in each waveguide aperture. A thin dielectric sheet placed in front of the array aperture is used for wide-angle impedance matching. Figure 2-1 shows the array structure under consideration.

2.2 INTEGRAL REPRESENTATION OF THE ELECTROMAGNETIC FIELD AND METHOD OF SOLUTIONS

The aperture admittance of a waveguide element in a uniformly excited infinite planar array has been investigated extensively in the past decade. Among these works, the most effective numerical approach is to solve the integral equation for the unknown tangential aperture fields by the method of moments.

A unit cell in an infinite two-dimensional array and its equivalent circuit are shown in Figure 2-2. The basic procedure is to describe the internal fields in terms of waveguide modes $\bar{\psi}_j$, and the external fields in terms of Floquet's modes $\bar{\Phi}_{pqr}$. The subscript p and q are the order of two dimensional spatial harmonics and the third subscript r = 1 or 2, is used to indicate TE or TM waves, respectively. The tangential electric and magnetic fields in each region are related by the modal admittance Y_j in the waveguide and Y_{pqr} in the external unit cell. By matching the tangential field components E_t and H_t at the aperture, we can obtain an integral equation:

$$2\sum_{j=1}^{J} A_j Y_j \bar{\psi}_j = \sum_{j=1}^{\infty} Y_j \bar{\psi}_j \iint \bar{E}_t \cdot \bar{\psi}_j^* \, da$$

$$+ \sum_{p}\sum_{q}\sum_{r=1}^{2} Y_{pqr} \bar{\Phi}_{pqr} \iint \bar{E}_t \cdot \bar{\Phi}_{pqr}^* \, da \qquad (2\text{-}1)$$

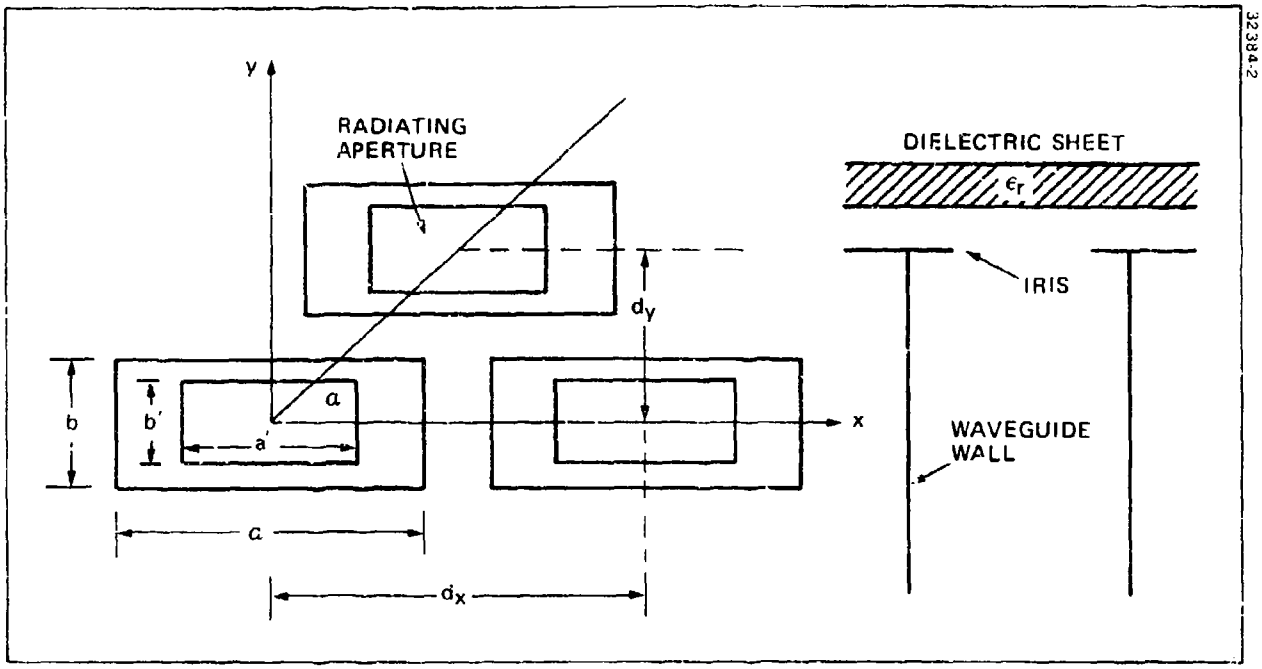

Figure 2-1. Geometry of Radiating Structure

where Φ^*_{pqr} is the complex conjugate of Φ_{pqr}, A_j is the coefficient of the incident waveguide mode. Our approach follows that introduced by Amitay and Galindo[6] except the time convention of e^{jwt} is used.

To solve the integral equation (2-1), the method of moments[7] was used. In applying this technique it is necessary to select a third set of linearly independent modes that satisfy the boundary condition on the radiating aperture in between the irises to represent the electric field $\bar{E}_t$. This last step is necessary in order to obtain a faster convergence to an accurate solution. For the rectangular aperture, one may use the expansion of rectangular waveguide modes $\bar{\psi}'_j$ and let

$$\bar{E}_t = \sum_{j=1}^{\infty} F_j \bar{\psi}'_j, \tag{2-2}$$

When the size of iris reduces to zero, i.e., a' = a and b' = b, the function $\bar{\psi}'_j$ equals to $\bar{\psi}_j$. By taking the inner product of equation (2-1) with each $\bar{\psi}'_j$ the result is a set of simultaneous equations which can be solved to determine the unknown F_j coefficient in equation (2-2). Once the tangential aperture field $\bar{E}_t$ is determined, the transmission coefficient T_{pqr} and the reflection coefficient R_j can be obtained by the following equations:

$$T_{pqr} = \iint \bar{E}_t \cdot \bar{\Phi}^*_{pqr}\, da \tag{2-3}$$

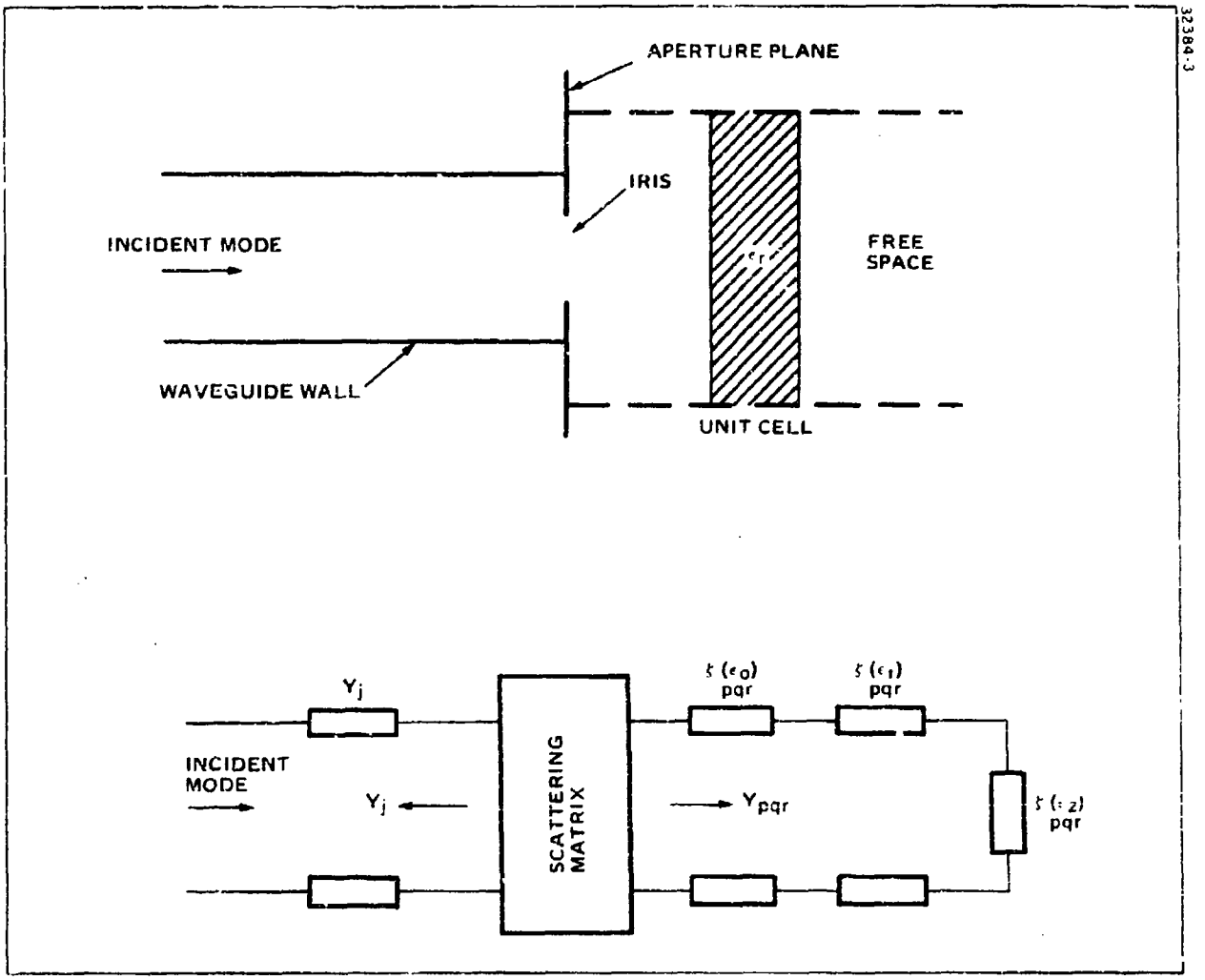

Figure 2-2. Unit Cell in a Planar Array and its' Equivalent Network

and

$$R_j = \iint \bar{E}_t \cdot \bar{\psi}_j \, da - A_j \qquad (2\text{-}4)$$

Equation (2-1) essentially is the result of Ampere's law in the equivalent circuit representation. The left hand side of Equation (2-1) is the current incident at the aperture from the source. The first term on the right hand side is a summation of mode currents reflected back to the internal transmission line and the second term is the currents flowing into the exterior free space. Only the propagating modes whose admittance are real, i.e., conductances contribute to energy flow either back to the source or forward to the exterior free space. All nonpropagating modes whose admittances are pure imaginary, i.e., susceptances result in stored energy around the aperture. . For a wide band element, it is desirable to reduce this stored energy to a minimum. If the size of the waveguide element is close to the cutoff of the higher order mode, or the dielectric plug at the open end of the element propagates more than one mode, the excessive stored energy near the aperture may cause high impedance mismatch or even blind spots in the scan range. These undesirable effects should be avoided in the selection of the type element.

The computer program used in the following computations accounts for the lowest 10 waveguide modes in the rectangular aperture a' by b'. The number of modes in the feeding waveguide and the free space Floquet modes were chosen according to the size of irises as suggested by Lee, et al[8].

2.3 SELECTION OF ARRAY PARAMETERS

The standard procedure for aperture matching of a phased array antenna is as follows: (1) choose proper element lattice and element spacing; (2) select a compact radiator which can be fixed into the element lattice and cover the desired frequent band; (3) design an impedance scheme such as the WAIM sheet or iris; and (4) optimize the array performance.

It is well known that the aperture matching is strongly dependent on scan in the plane where the grating lobes come closest to the real space. For a large phased array, a 6 to 8 percent reduction in element spacing from the grating lobe condition at the high end of the frequency band is commonly used to avoid the excessive mismatch loss at the edge of the scan volume. The array performance of the wideband designs presented in this study is based on a 6 percent reduced element spacing unless otherwise specified. In the selection of the radiating element, a wide width of the rectangular waveguide is desirable, so that the feed waveguide can transmit a wideband of frequencies at a nearly constant impedance level and free from propagating higher order modes. The low end of the frequency band should be kept about 10 percent or more above TE_{10} cutoff since the characteristic impedance of the waveguide near TE_{10} cutoff varies rapidly with frequency. The effect of the iris on the active element impedance of the array can be seen easily in the following example. The array parameters chosen for a 60-degree half-angle conical coverage through a wideband of frequency are:

Lattice:	$d_x = 1.0075\lambda$, $d_y = .2909\lambda$, $\alpha = 30^o$
Waveguide:	$a = .972\lambda$, $b = .1997\lambda$
Raditing Aperture:	$a = .5\lambda, .65\lambda, .8\lambda, .97\lambda$, $b' = b$
Dielectric Sheet:	$\epsilon_r = 7.5$, $.0276\lambda$ thick and $.0884\lambda$ off the array face
Incident Wave:	TE_{10} mode (2-5)

Where λ is the free space wavelength at the high end of the operating frequency band, "f = 1". Performance of this array configuration with a similar choice of array parameters can be found in the papers published by Borgiotti,[9] and by Lee and Jones[5]. Borgiotti did not use an iris, while Lee and Jones used both iris and dielectric plug at the open end of the waveguide. Without the iris, the array has serious aperture mismatch in the H-plane scan, while with both iris and dielectric plug, the broadbanding effect of the iris is offset by the frequency sensitive plug.

2.4 PERFORMANCE OF THE WIDEBAND ARRAY

Without the wide-angle impedance matching sheet (WAIM), the active element impedance does not seem to be well behaved across the frequency band from f = 0.56 to 1.00. Figure 2-3 illustrates the calculated reflection coefficient at f = 0.56 and 1.00, as a function of scan angle θ. from 0 to 60 degrees in E- and H-plane for four different sizes of iris as specified in equation (2-5). With the WAIM, the active element

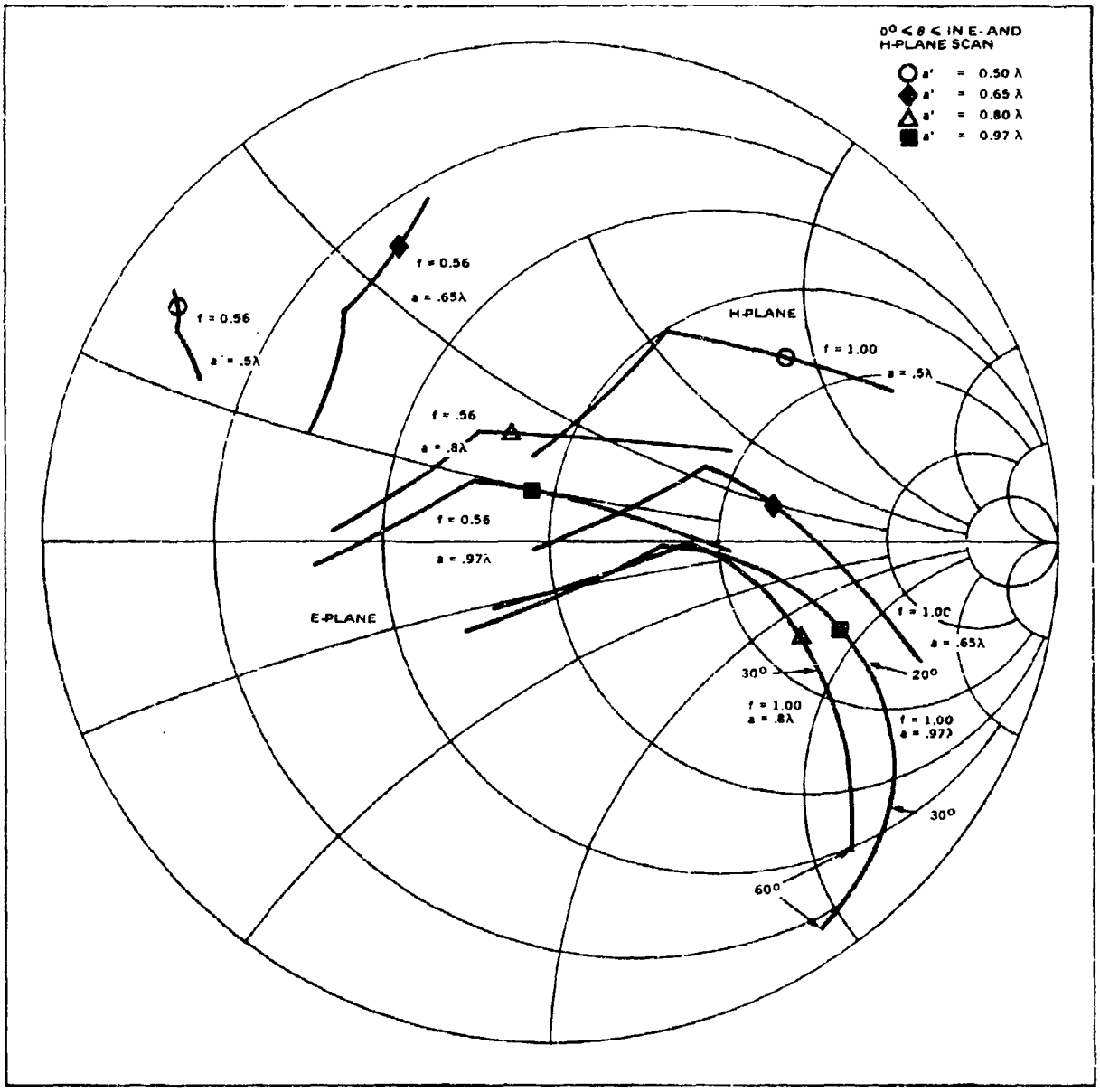

Figure 2-3. Reflection Coefficient of the Array as Specified in Equation (2-5) at f = 0.56 and 1.00, except NO WAIM

impedance is shown in Figure 2-4. At f = 0.56, the feed waveguide is about 9 percent above the TE_{10} cutoff frequency. The amplitude of reflection coefficient increases rapidly towards unity as the frequency approaches cutoff. Figure 2-5 shows the amplitude of the TE_{20} mode induced in each element due to the progressive phase variation across the array aperture as the array is scanned off broadside in the H-plane. It is observed that the amplitude of TE_{20} mode excited depends upon the size of iris, and the large TE_{10} reflection from the array aperture is accompanied by a large TE_{20} evanescent mode excited in the feed waveguide. Since the TE_{20} mode is near cutoff condition at f = 1.00, the radiation blindness which is observed in the H-plane scan for the case of waveguides with small or no iris must be caused by the large amount of energy in the TE_{20} mode trapped in the feed waveguide near the aperture region. A large iris is effective in preventing the TE_{20} mode from being excited. However, an excessively large size iris deteriorates the aperture matching condition in the low frequency region. Figure 2-6 shows the impedance performance of an array with $a' = 0.65\lambda$ at three frequencies, f = 1.0, 0.8, and 0.6. Computations were performed in a five-degree step in four planes of scan: $\varphi = 0^{\circ}$ (H-plane), 30°, 60° and 90° (E-plane). A maximum VSWR of 2.3:1 over a 50 percent bandwidth is obtained. Reduction of element spacing, scan volume, or bandwidth could result in better impedance match. Figure 2-7 shows the impedance loci of the same array except $a' = 0.62\lambda$ and the WAIM sheet raised slightly up to 0.1λ off the array face. The aperture VSWR decreases to less than 2.1:1 over 30 percent bandwidth. Therefore, a true evaluation of the aperture performance should be made on not only the average transmission loss (or VSWR) over the scan volume and bandwidth, but also the element spacing or area per element.

2.5 OPERATION BEYOND TE_{20} CUTOFF FREQUENCY

Observation of the data presented in Figure 2-6 indicates that the bandwidth can be extended further on both ends of the frequency band if the required impedance match condition is relaxed. Basically, the low end of the frequency band is limited by the waveguide cutoff, and the high end of the frequency band is limited by the formation of grating lobes in the visible space. If the scan volume is reduced to stay within the grating lobe constraint, there are two possible ways to operate the TE_{20} cutoff frequency. One is to terminate the TE_{20} mode by an internal matched load and the other is to terminate the TE_{20} mode by an internal short. Since the TE_{20} mode is not excited in the E-plane scan, and the TE_{01} mode remains far below cutoff for the array considered, the impedance matching in the E-plane scan appears to have no problem even operating at frequencies above TE_{20} cutoff. However, the radiation blindness may occur first at the edge of H-plane scan and moves toward broadside when the operating frequency is raised beyond the TE_{20} cutoff frequency.

Assuming that the TE_{20} mode can be terminated into a matched load without affecting the propagation of TE_{10} mode, Figure 2-8 shows the amplitude of the reflected TE_{10} mode in the H-plane scan versus frequency at $\theta = 25$, 35, 45, and 55 degrees of scan for the array with $a' = .65\lambda$. The amplitude of the reflected TE_{10} mode at the scan limits, based on the criteria set by the 6, 8, and 10 percent reduced spacings from that of placing the nearest grating lobe at endfire, are also shown in the same figure. Figure 2-9 shows the total reflected power and the power in TE_{20} mode alone versus frequency. For a 10 percent reduced element spacing in the high frequency region, the array is able to operate up to f = 1.10 with less than 3 dB transmission loss.

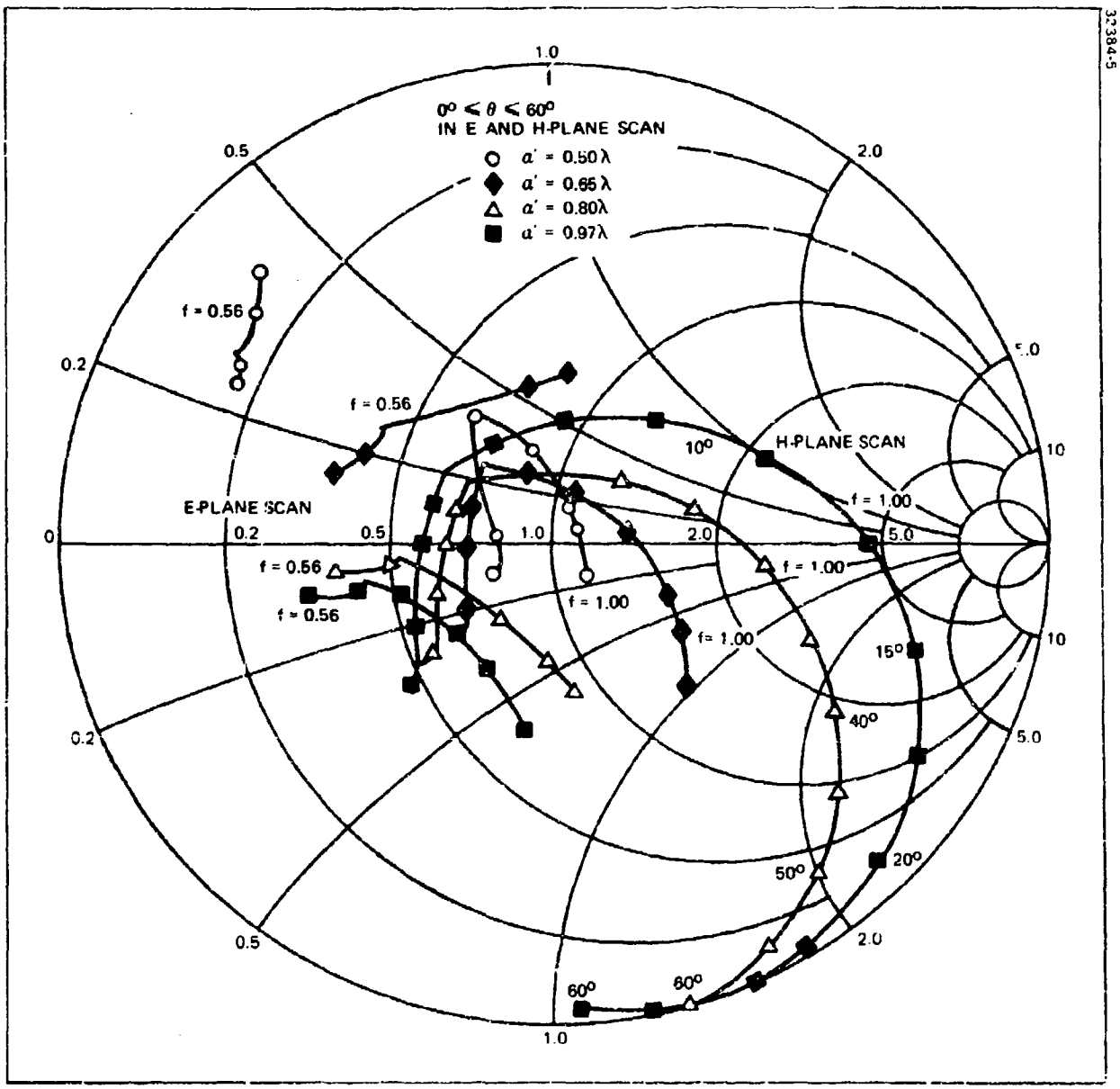

Figure 2-4. Reflection Coefficient of Arrays with Radiating Aperture a' = 0.5λ, 0.65λ, 0.8λ and 0.97λ at f = 1.00 and 0.56

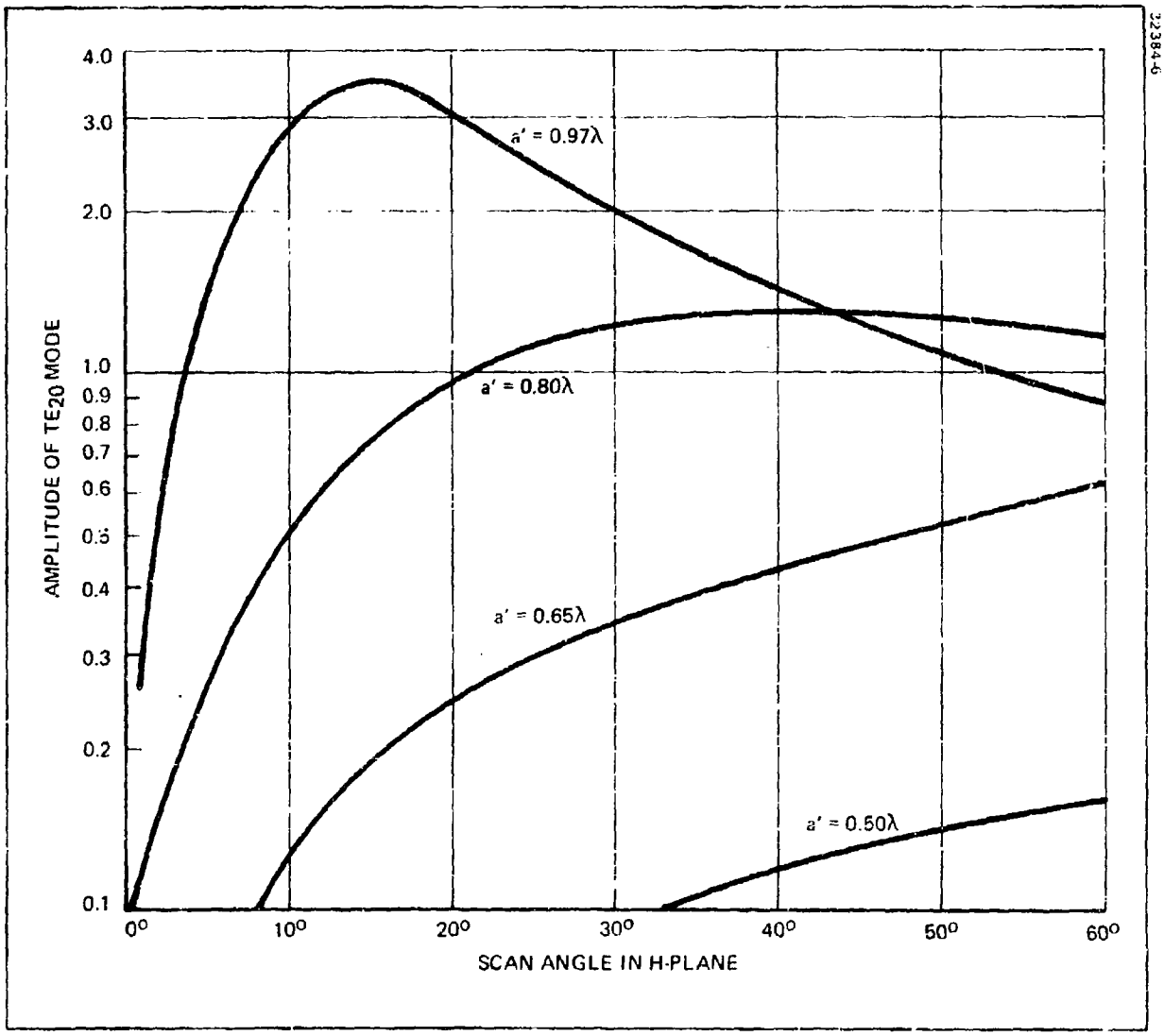

Figure 2-5. Amplitude of TE_{20} Mode Induced in Feed Waveguide with Unit TE_{10} Incidence versus H-Plane Scan Angle *0*

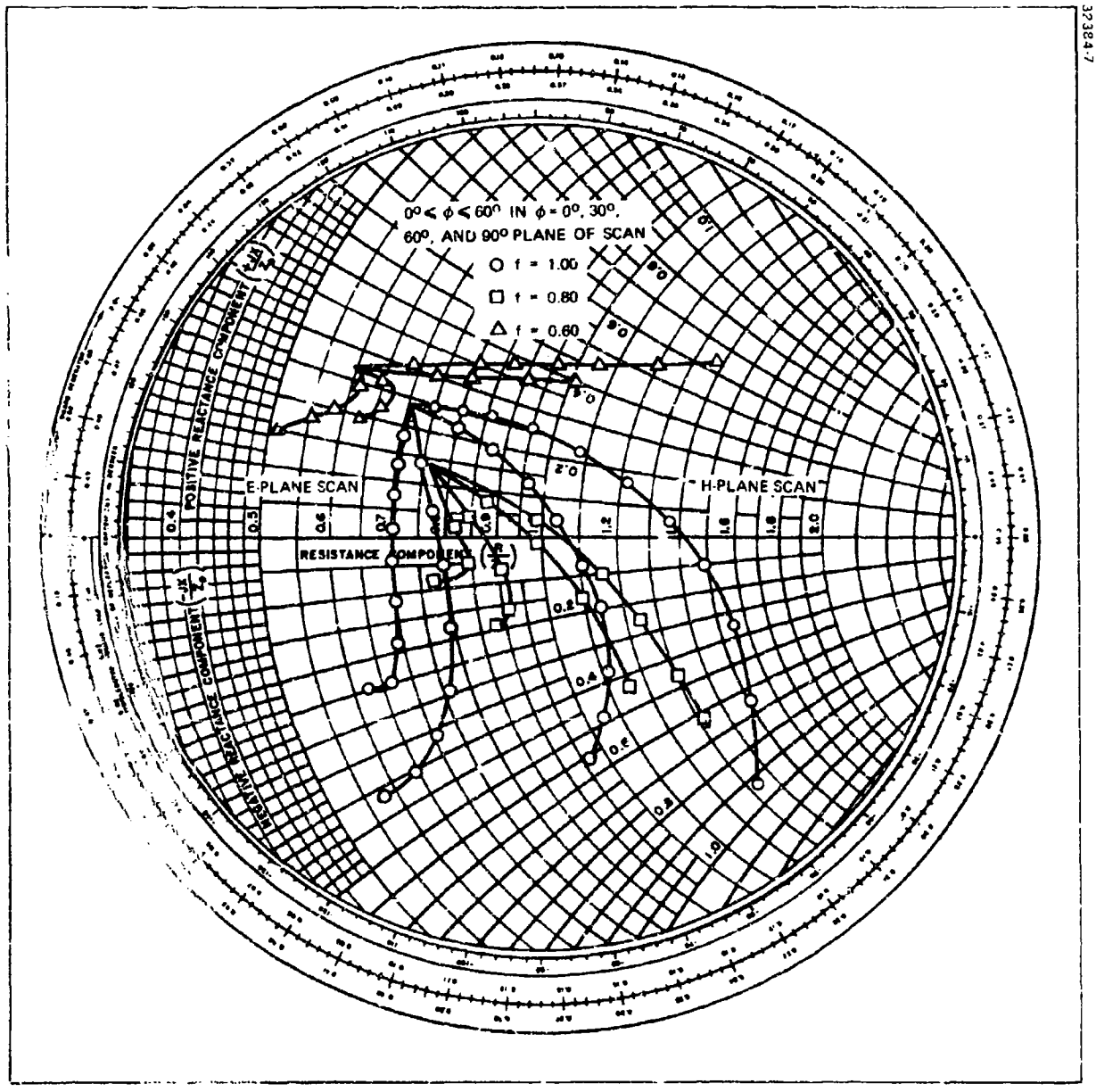

Figure 2-6 Reflection Coefficient of the Array with a' = 0.65λ at f = 1.0, 0.8 and 0.6 in Four Plane of Scan: φ = 0° (E-Plane), 30°, 60° and 90° (H-Plane)

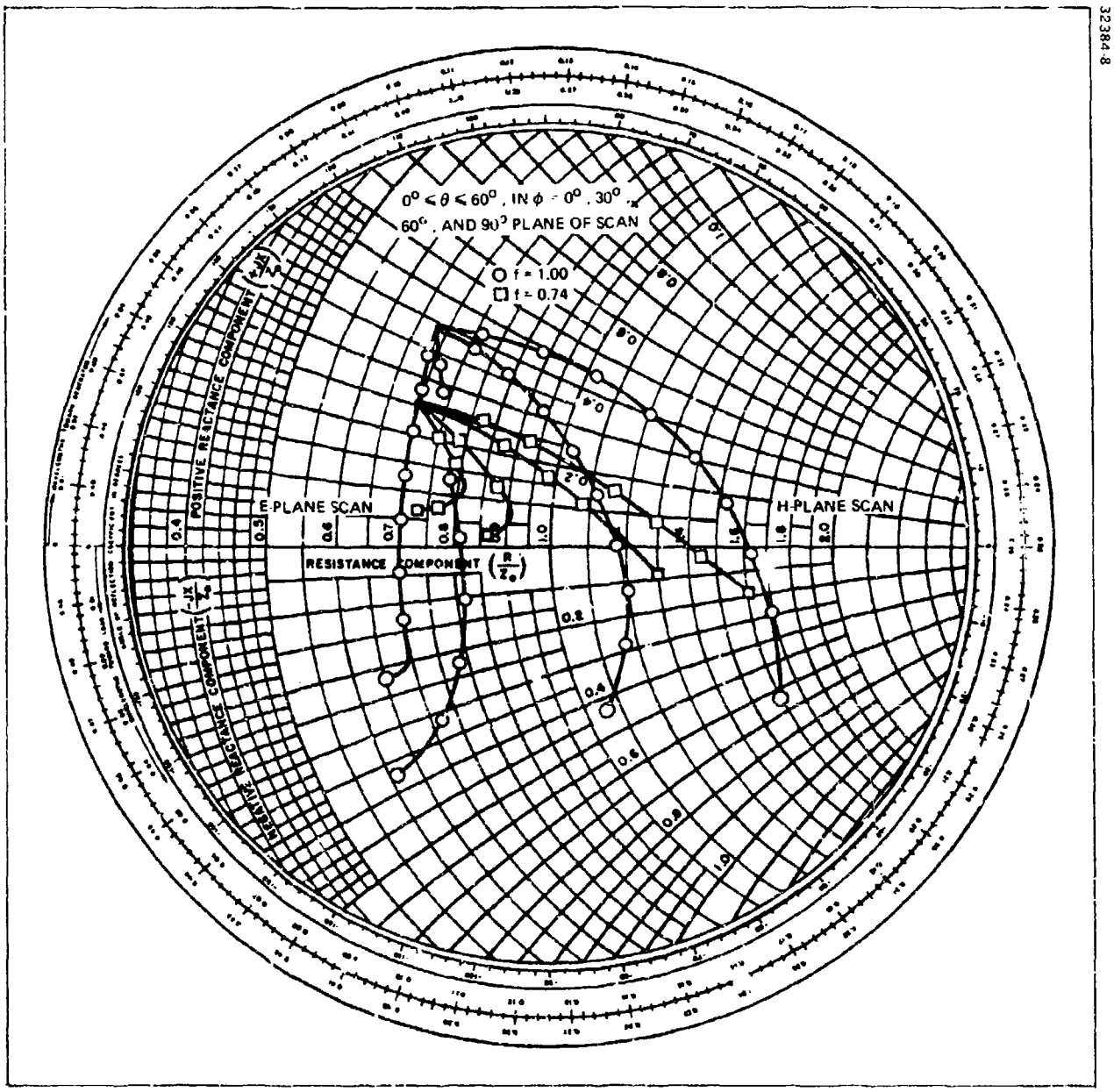

Figure 2-7. Reflection Coefficient of the Array with a' = 0.62λ and WAIM Sheet 0.1λ Off the Array Face at f = 1.00 and 0.74 in Four Planes of Scan: φ = 0° (E-Plane), 30°, 60° and 90° (H-Plane)

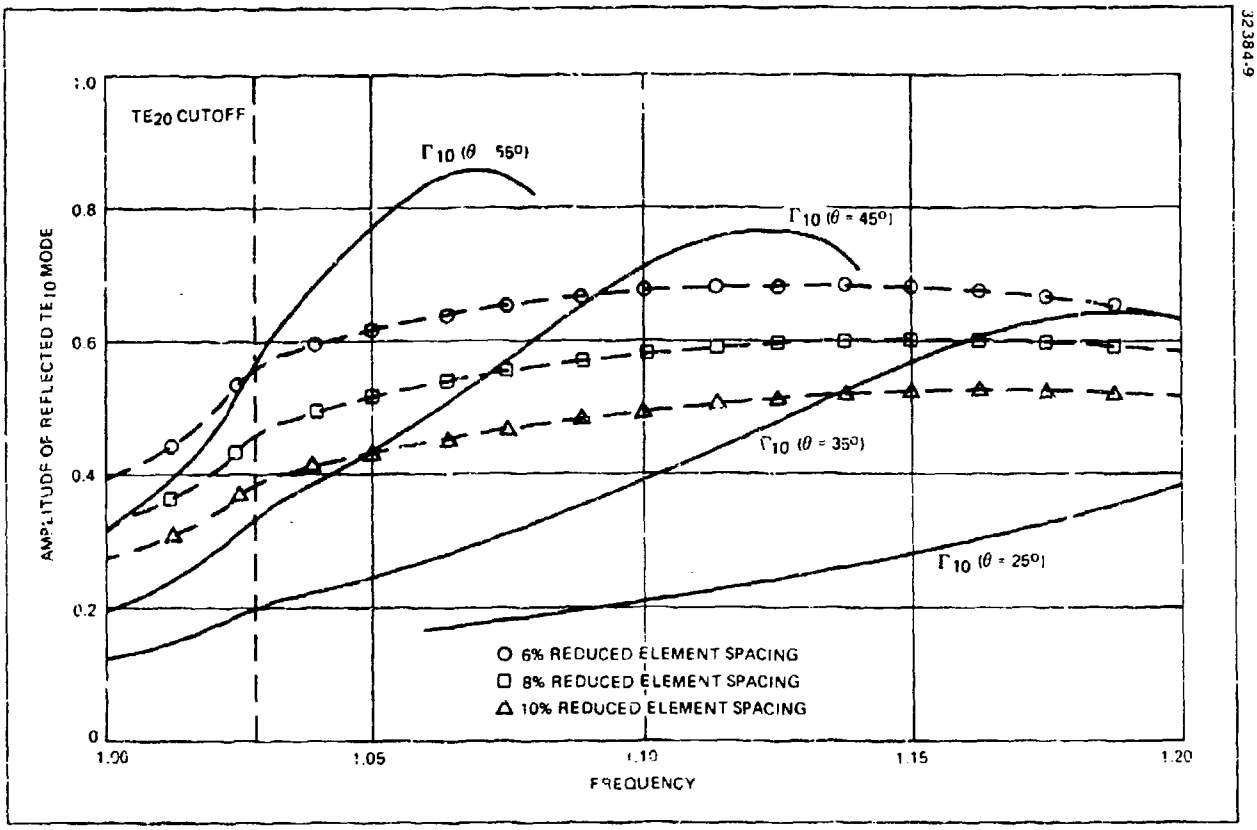

Figure 2-8. Amplitude of Reflected TE_{10} Mode at the Edges of Scan Limit in H-Plane by 6, 8 and 10% Reduced Element Spacings from that of Placing the Nearest Grating Lobe at Endfire. Also reflection at θ = 25°, 35° 45° and 55°.

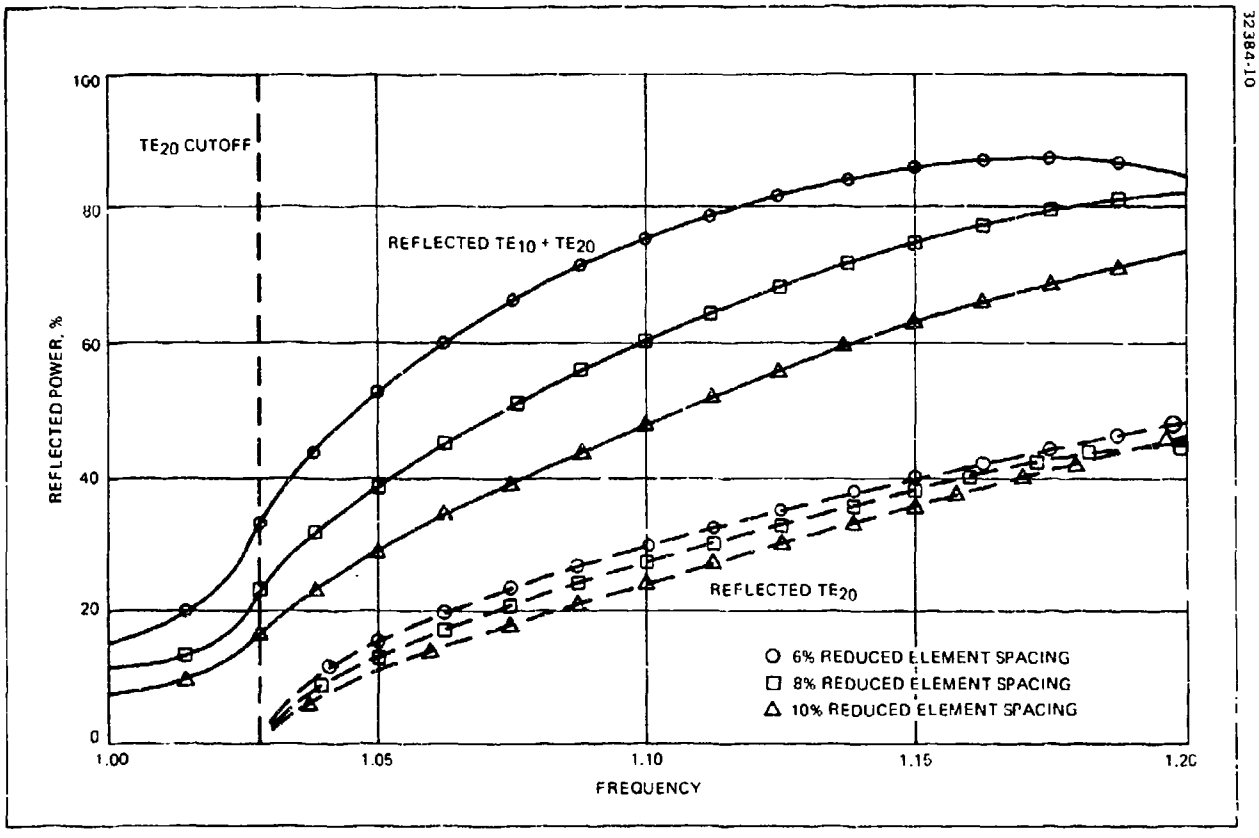

Figure 2-9. Reflected Power Level at Edges of Scan Limit in H-Plane by 6, 8 and 10% Reduced Element Spacings from that of Placing the Nearest Grating Lobe at Endfire.

The alternative way of extending the bandwidth by a TE_{20} short termination can be accomplished by the employment of a coaxial to waveguide transition to launch a TE_{10} mode in the feed waveguide. In this case, the TE_{20} mode looking toward the source is shorted at the end wall of the waveguide and decoupled to the probe or loop which is used to launch the TE_{10} mode in the waveguide. Figure 2-10 shows the amplitudes of the reflected TE_{10} mode and the trapped TE_{20} mode versus location of short termination in terms of the TE_{20} guide wavelength behind the aperture at f = 1.093. It is shown that the TE_{20} short termination behaves like a shunt circuit tuner. The TE_{20} mode can be suppressed effectively at the aperture by placing the end wall of the feed waveguide at half-integer multiples of the TE_{20} guide wavelengths behind the radiating aperture. In so doing, a good impedance match in several narrow bands of frequency above TE_{20} cutoff is obtained. Figure 2-11 shows the difference in TE_{10} coefficient between two arrays; one with a TE_{20} matched termination and the other with a TE_{20} short at the aperture. Since the TE_{20} mode is not excited in the ϕ plane scan, there is no difference expected in this plane between these two arrays. Figure 2-12 shows the amplitude of the reflected TE_{10} mode as a function of frequency if the TE_{20} short is implemented at 2.7λ behind the aperture of the array with $a' = .65\lambda$. It is observed observed that the array can be operated in several discrete narrow bands of frequency above TE_{20} cutoff.

2.6 DESIGN FOR A 1/4 HEMISPHERICAL COVERAGE

Occasionally, phased arrays designed for a one quarter hemispherical coverage is of interest for missile defense radar. Applying the principle and procedure presented in the last section we arrived at a design:

Lattice:	$d_x = 1.126\lambda$, $d_y = .304\lambda$
Waveguide:	$a = .980\lambda$, $b = .205\lambda$
Radiating Aperture:	$a' = .650\lambda$, $b' = b\lambda$
Dielectric Sheet:	$\epsilon_r = 7.5$, $.0284\,\lambda$ thick and $.10\,\lambda$ off the array face
Incident Wave:	TE_{10} mode

The boresight axis of the array is tilted 35.3 degrees from horizon so that a $\theta = 40^\circ$ scan in H-plane and a $\theta = 55^\circ$ in $\phi = 30^\circ$ plane will be able to cover one quarter of the hemispherical volume in the earth coordinate. The calculated active element impedance at f = .55 and 1.00 are shown in Figure 2-13. A maximum VSWR of 2.75:1 over 58 percent band with a unit cell area of $.3426\lambda^2$ at high end of the frequency band. This is a significant improvement over that of the Tsandoulas' design[2] from the standpoint of array performance, area per element, and simplicity in element structure.

2.7 EXPERIMENTAL VERIFICATIONS

Accuracy of the numerical results obtained from this computer program was verified by measurement of the reflection coefficient in a H-plane simulator. The waveguide element used in this experiment has a 2.20 x .452 inches rectangular cross section. The cutoff frequency is 2.68 GHz for the TE_{10} mode. Reflection from the array aperture for a simulated H-plane incidence was measured from 2.75 GHz to 6.5 GHz by

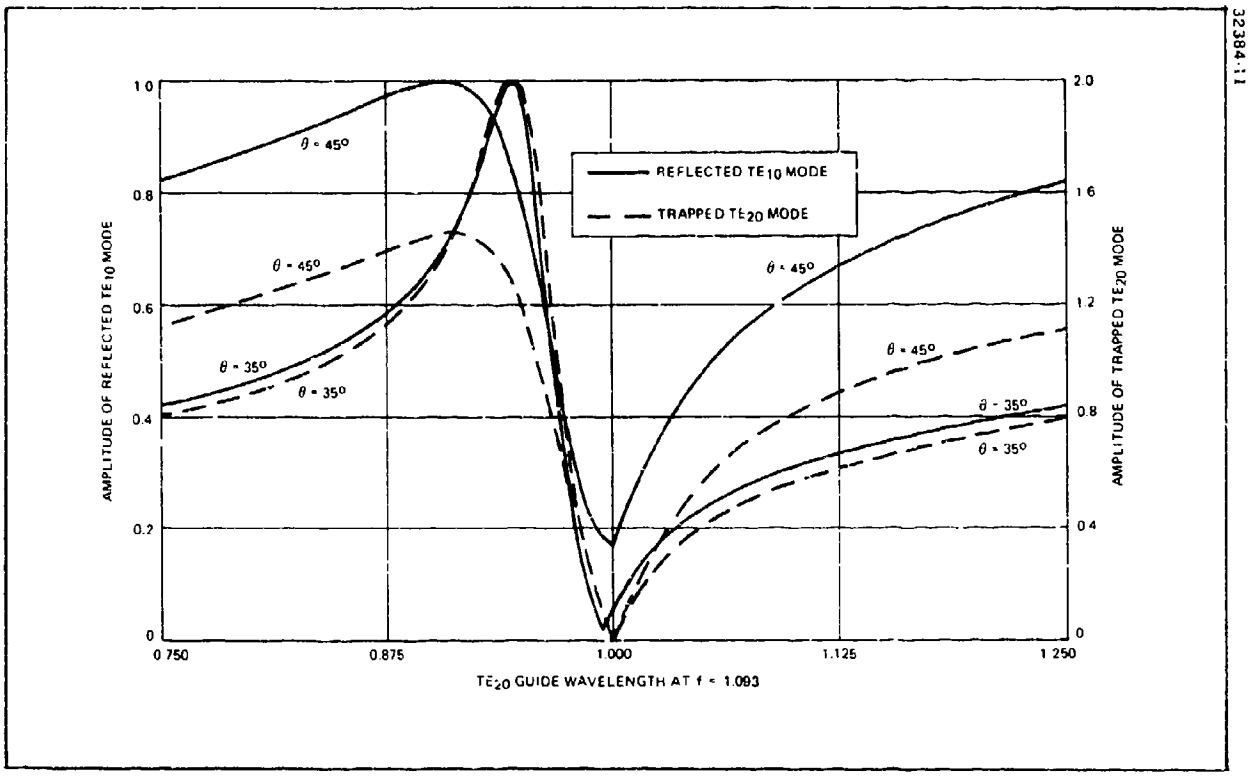

Figure 2-10. Amplitude of Reflected TE_{10} Mode and Trapped TE_{20} Mode for the Array with a' = 0.65λ at f = 1.093 versus Location of TE_{20} Short Termination in the Feed Waveguide.

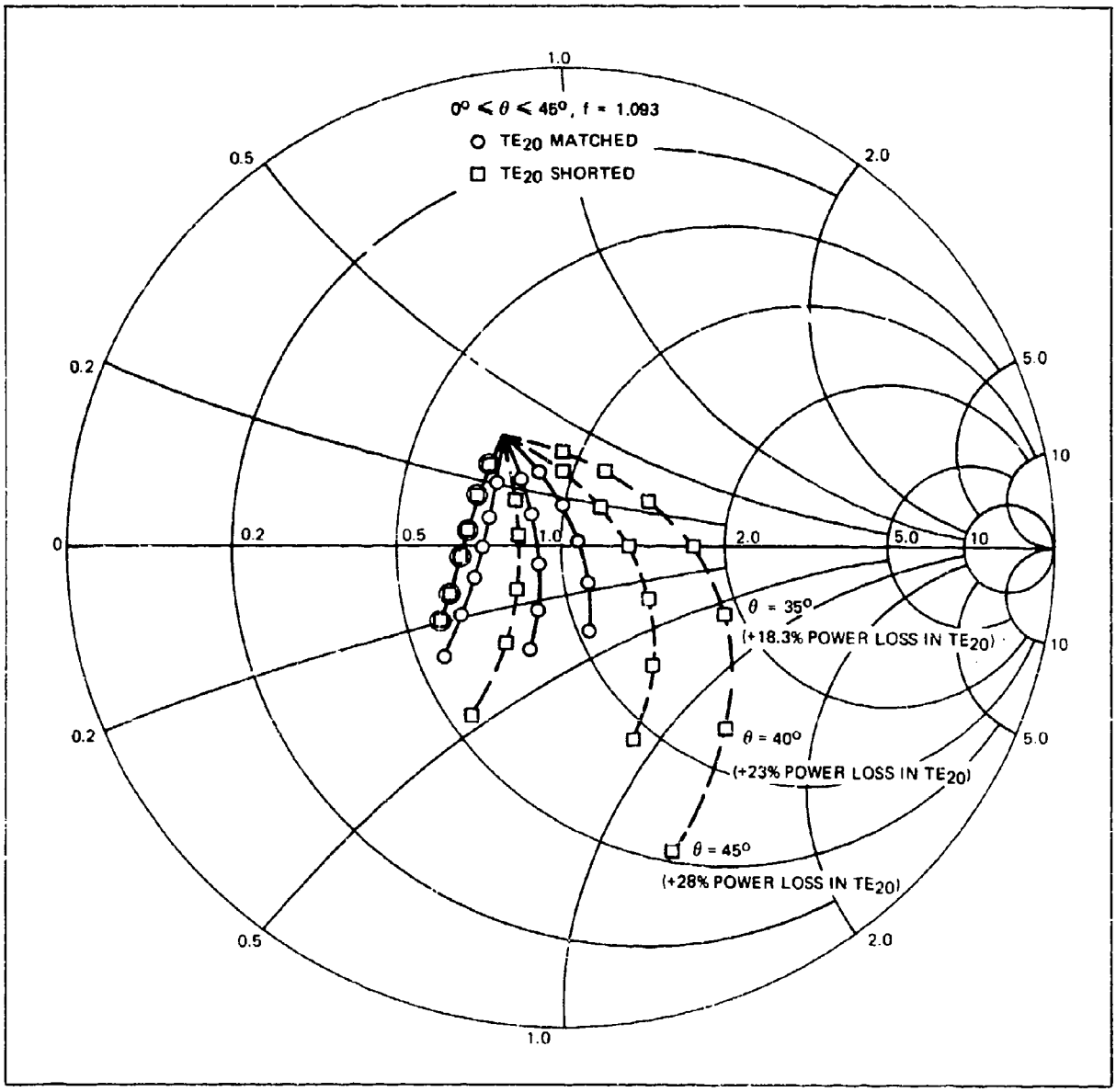

Figure 2-11. Comparison of Impedance Match Condition Between Two Arrays, One with TE_{20} Matched Termination, the Other with TE_{20} Shorted at 2.7λ From the Aperture in the Feed Waveguide

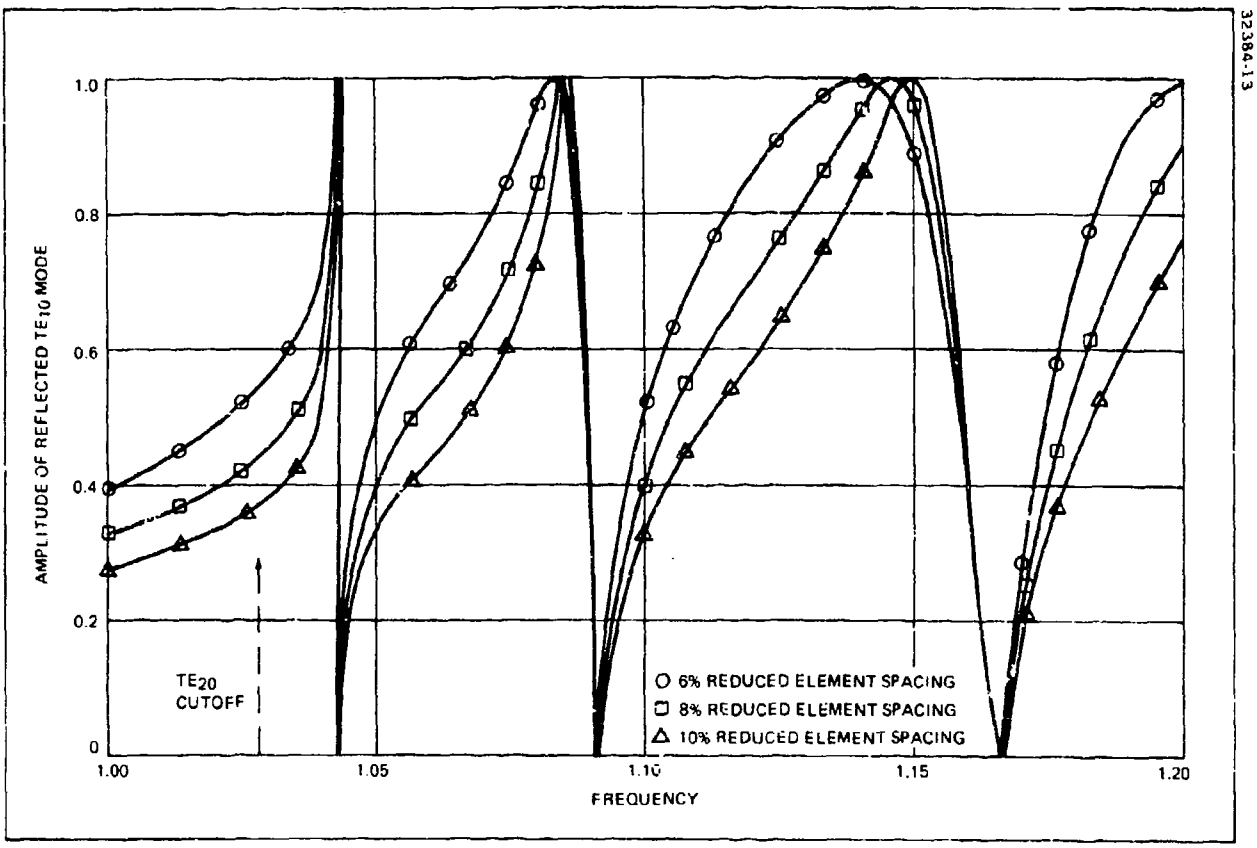

Figure 2-12. Amplitude of Reflected TE_{10} Mode at the Edges of Scan Limit in H-Plane for the Array with TE_{20} Shorted Termination Located at 2.7λ From the Aperture in the Feed Waveguide versus Frequency

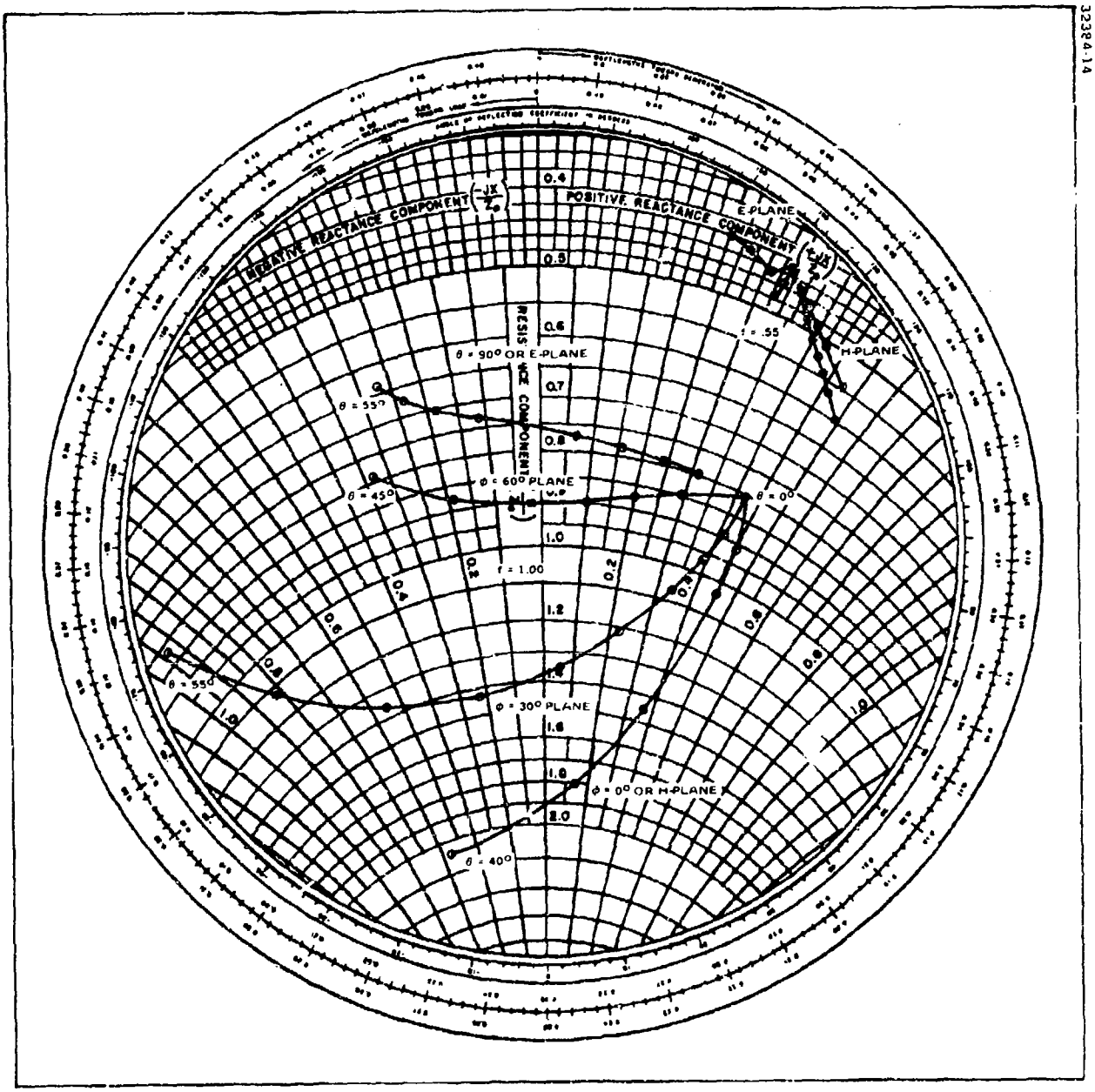

Figure 2-13. Active Element Impedance at f = .55 and 1.00 for the Array Specified in Equation (2-6)

means of a computerized network analyzer set up at Hughes. The simulated angle of incidence ranges from 23.5 to 73.3 degrees within the test frequency band. Both calculated and measured data are presented in Figure 2-14. The close agreement between the calculated and measured results proves that the computer prediction is very accurate and reliable.

In addition to the waveguide simulator, a 254-element array as shown in Figure 2-15 with the array parameters specified in Equation (2-5) has been constructed. Active element patterns in the E, H, and ϕ=45^{o} planes were taken from 3.12 GHz to 5.66 GHz at every 0.2 GHz step. No radiation blindness nor significant dips in φ=60^{o} range is observed. The high end of frequency band for a 60-degree half angle conical scan volume is 5.22 GHz. Since the impedance mismatch is always worst at the high end of the frequency band due to the trapped TE_{20} mode, only patterns at 5.22 GHz in E, H and ϕ = 45^{o} plane are shown. In Figure 2-16, it is observed that the maximum drop in gain at the edges of each scan volume from the ideal cosine drop off agree with the analytical results presented in Figure 2-6.

2.8 COAXIAL TO WAVEGUIDE TRANSITION

The waveguide radiator is excited by a magnetic loop located at the end of the waveguide wall. The configuration of this coaxial to waveguide transition is shown in Figure 2-17 and the measured VSWR from 3.4 to 7.0 GHz is shown in Figure 2-18. Within a 2:1 bandwidth, the VSWR is less than 1.54:1.

72-10-276

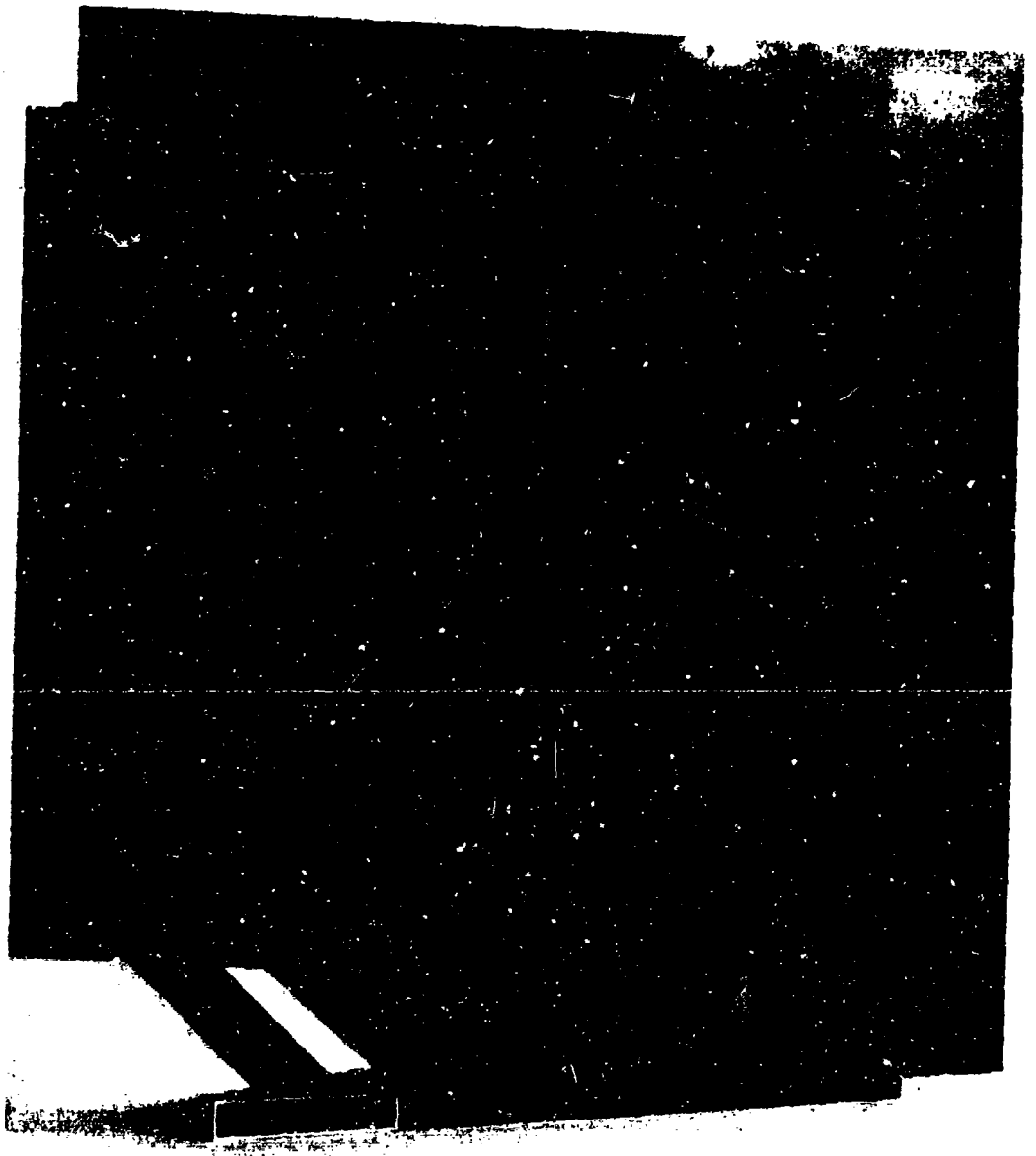

Figure 2-15. Experimental 254 Element Array

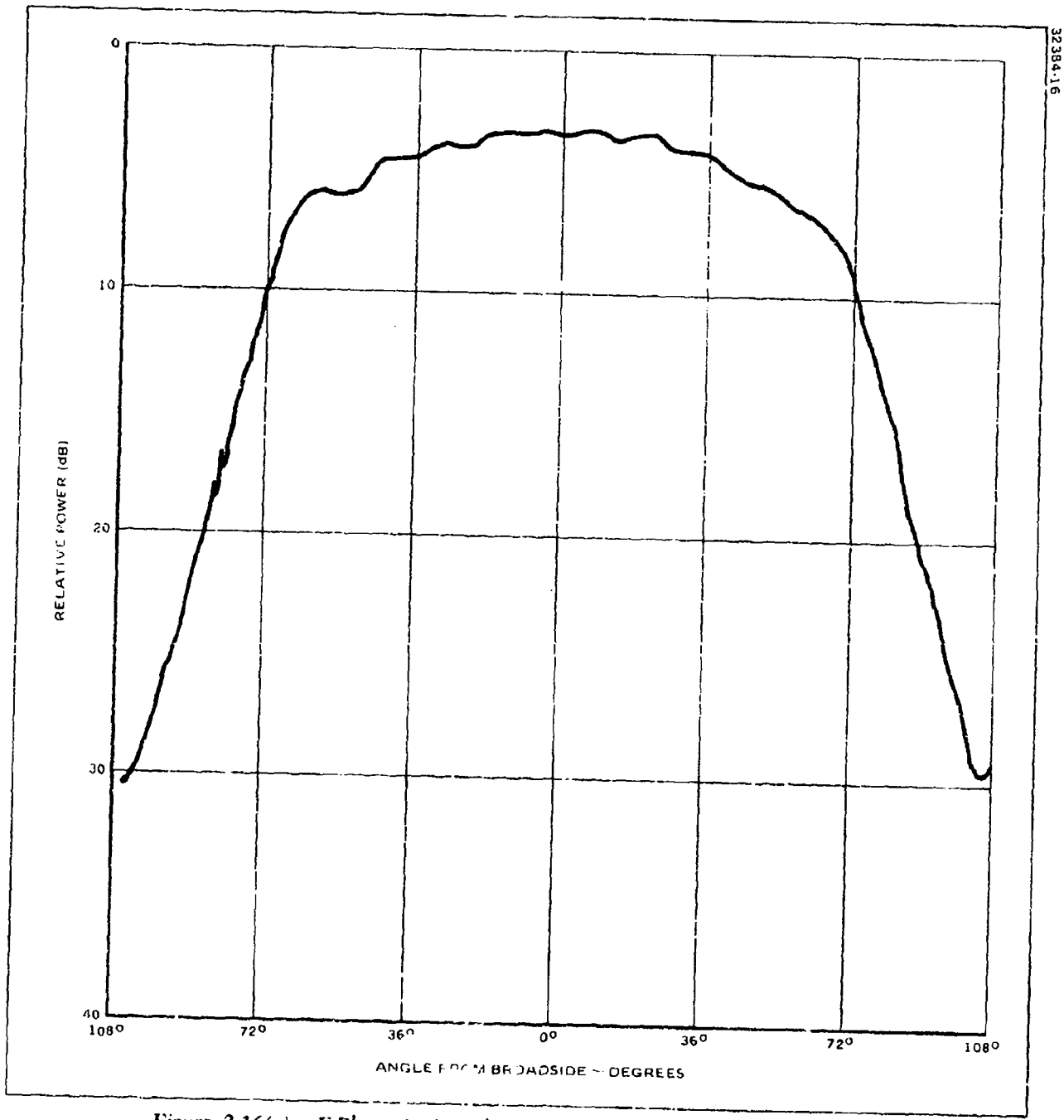

Figure 2-16(a). E-Plane Active Element Pattern, f = 1.00 or 5.22 GHz

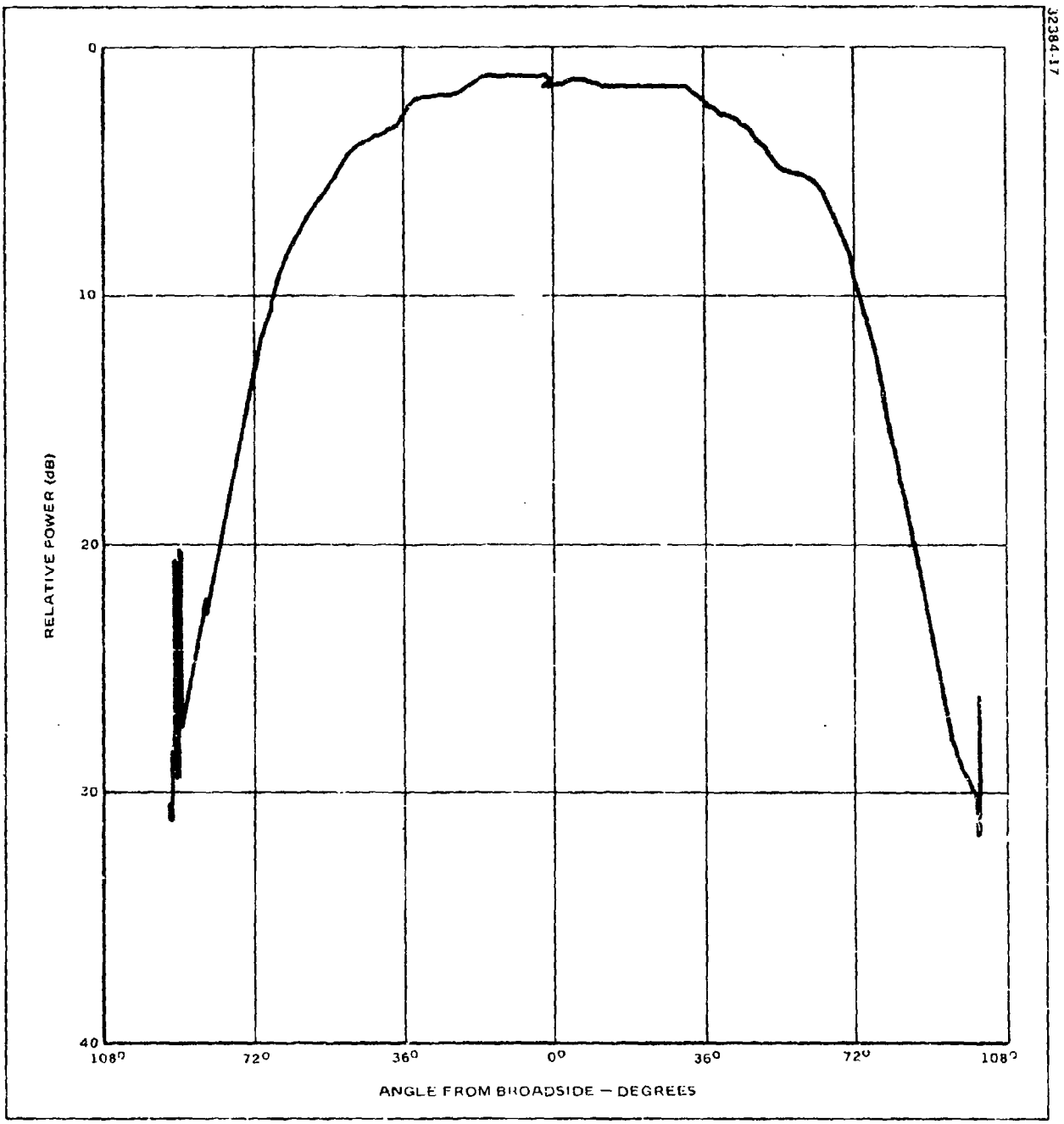

Figure 2-16(b). H-Plane Active Element Pattern, f = 1.00 or 5.22 GHz

Figure 2-16(c). ϕ = 45° Plane Active Element Pattern, f = 1.00 or 5.22 GHz

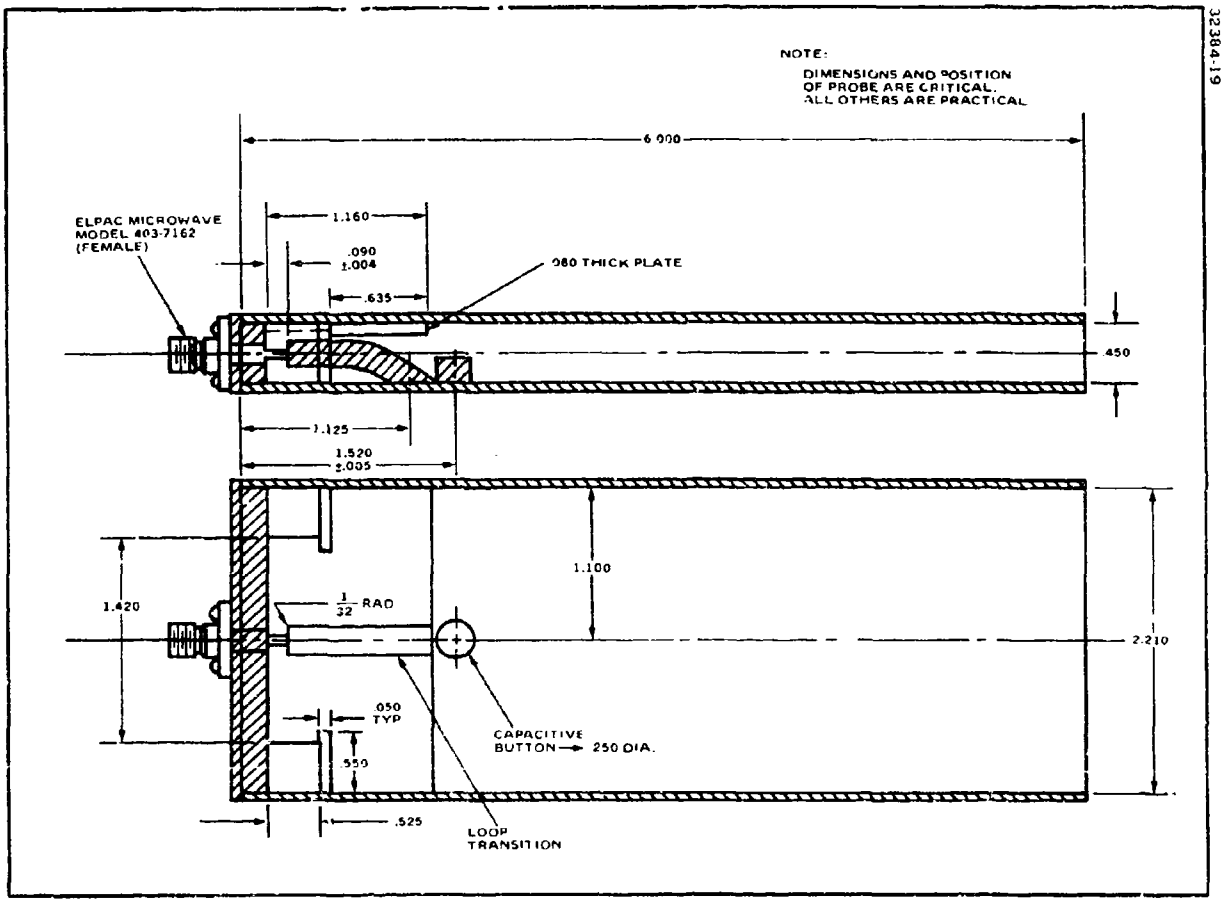

Figure 2-17. Geometry of a Coaxial to Waveguide Transition

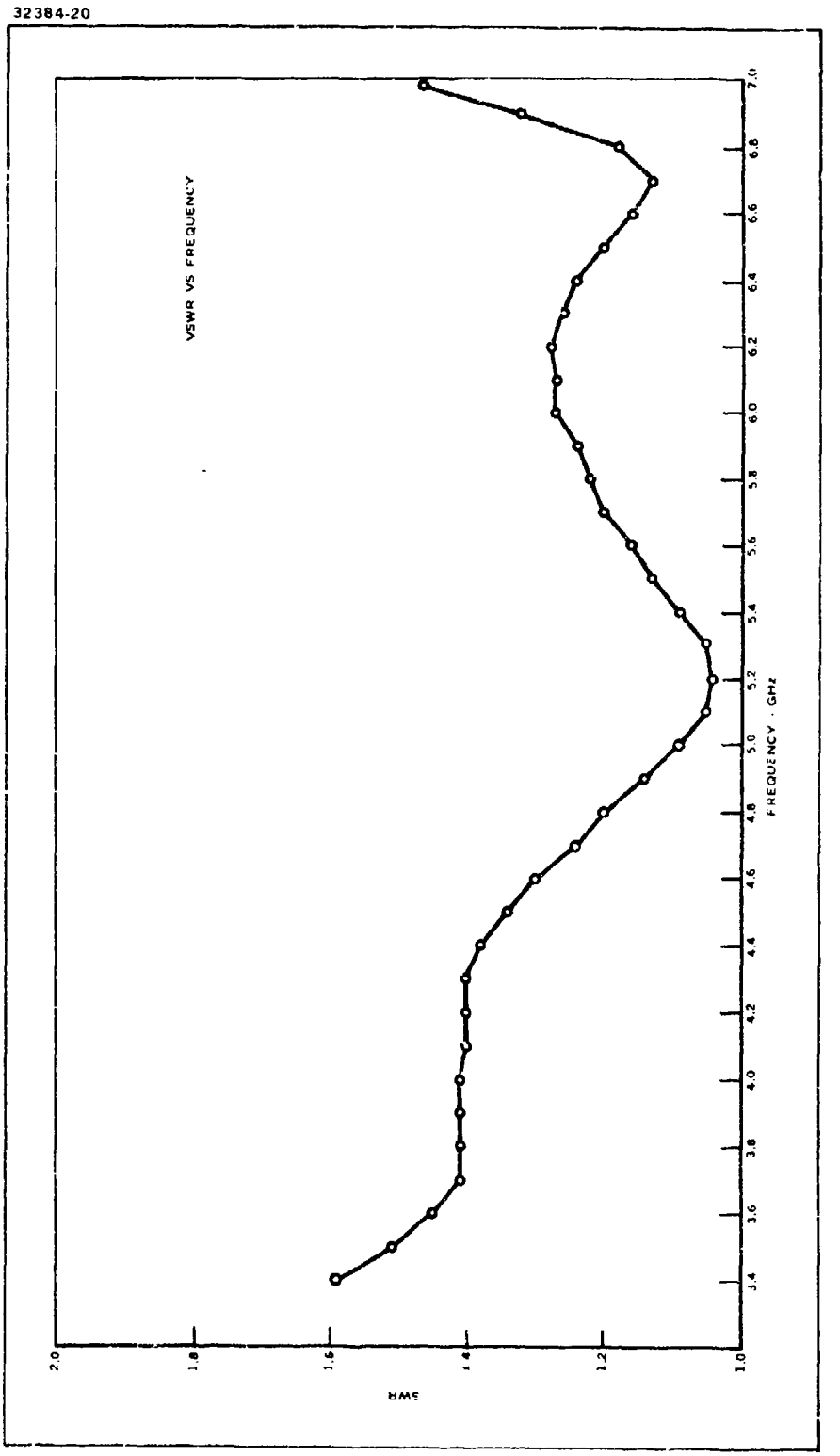

Figure 2-18. Performance of the Coaxial to Waveguide Transition

SECTION III
DOUBLE RIDGE RECTANGULAR WAVEGUIDE ARRAYS

In the previous section, it has been demonstrated that the active element impedance of a waveguide phased array can be well matched over nearly an octave band of frequencies. Basically, the TE_{20} cutoff frequency sets the high end of the frequency band and the low end of the frequency band is limited by the waveguide cutoff of the TE_{10} mode. One of the logical approaches to extend the tunable bandwidth of the waveguide phased array is to use ridge-loaded rectangular waveguide.

3.1 DESIGN CONSIDERATIONS

A frequency range of four to one or more can be easily obtained between the cutoff frequencies of the TE_{10} and TE_{20} modes by using ridge loading in a straight rectangular waveguide. These cutoff frequencies depend upon the size of the ridge. The guide which has a lower TE_{10} cutoff frequency also has a lower intrinsic impedance than that of the unloaded waveguide. From Figure 2-6, it is shown that the active element impedance of an open-ended waveguide radiator is at the level of 120π ohms or higher. Therefore, a tapered section of ridge from a uniformly ridge-loaded waveguide to an unloaded waveguide is used to provide a gradual match to the external free space.

Configuration of the element is shown in Figure 3-1. The radiating element is a double ridged rectangular guide with a ridge tapered to zero thickness at the open end, and a pair of thin irises which partially cover the aperture. The size of ridges is chosen so that it raises the TE_{20} mode cutoff and lowers the TE_{10} mode cutoff so as to propagate more than an octave band of frequencies without higher order modes.

3.2 OCTAVE BAND PHASED ARRAY

The design objective of the tested array is a 2:1 bandwidth for a ±60 degree conical scan volume. The rectangular guide has a 1.1" x .226" cross section arranged in an equilateral triangular lattice so that it has a unit cell area of $.293\lambda_h^2$ where $\lambda_h = 1.1315$" free space wavelength at the high frequency end, $f_h = 10.438$ GHz. Twenty-five percent of the width of the aperture is covered with iris. A .031" thick fiberglass radome with $\epsilon_r = 7.5$ is placed at .1" off the aperture. The cross section of the ridges is .300" x .125". The measured TE_{10} cutoff frequency of the ridge-loaded guide is about 4.4 GHz and TE_{20} cutoff is about 11.8 GHz. Both ridges are linearly tapered to zero height at the aperture within a distance of .375". This taper does not create a mismatch of more than 1.25:1 VSWR from an unloaded guide to a ridge loaded guide in the high frequency region. Therefore, no significant affects on aperture matching is expected in the high frequency region. However, it lowers the TE_{10} cutoff by 20 percent so that the array can be operated near or below the cutoff frequency of the straight rectangular guide without ridges.

The measured amplitude of reflection in the three H-plane waveguide simulators are shown in Figures 3-2 to 3-5. The designed frequency range for $\pm 60^\circ$ and $\pm 45^\circ$ conical coverage is from 5.22 GHz to 10.44 GHz and 11.38 GHz, respectively. The estimated maximum VSWR of this array is about 3.6:1 throughout the above specified bandwidth. Without the radome, the average measured transmission loss in these three simulators is about 0.6 dB higher than the case shown in Figure 3-2. Without the iris and the radome, radiation blindness or severe aperture mismatch in the high frequency region is observed.

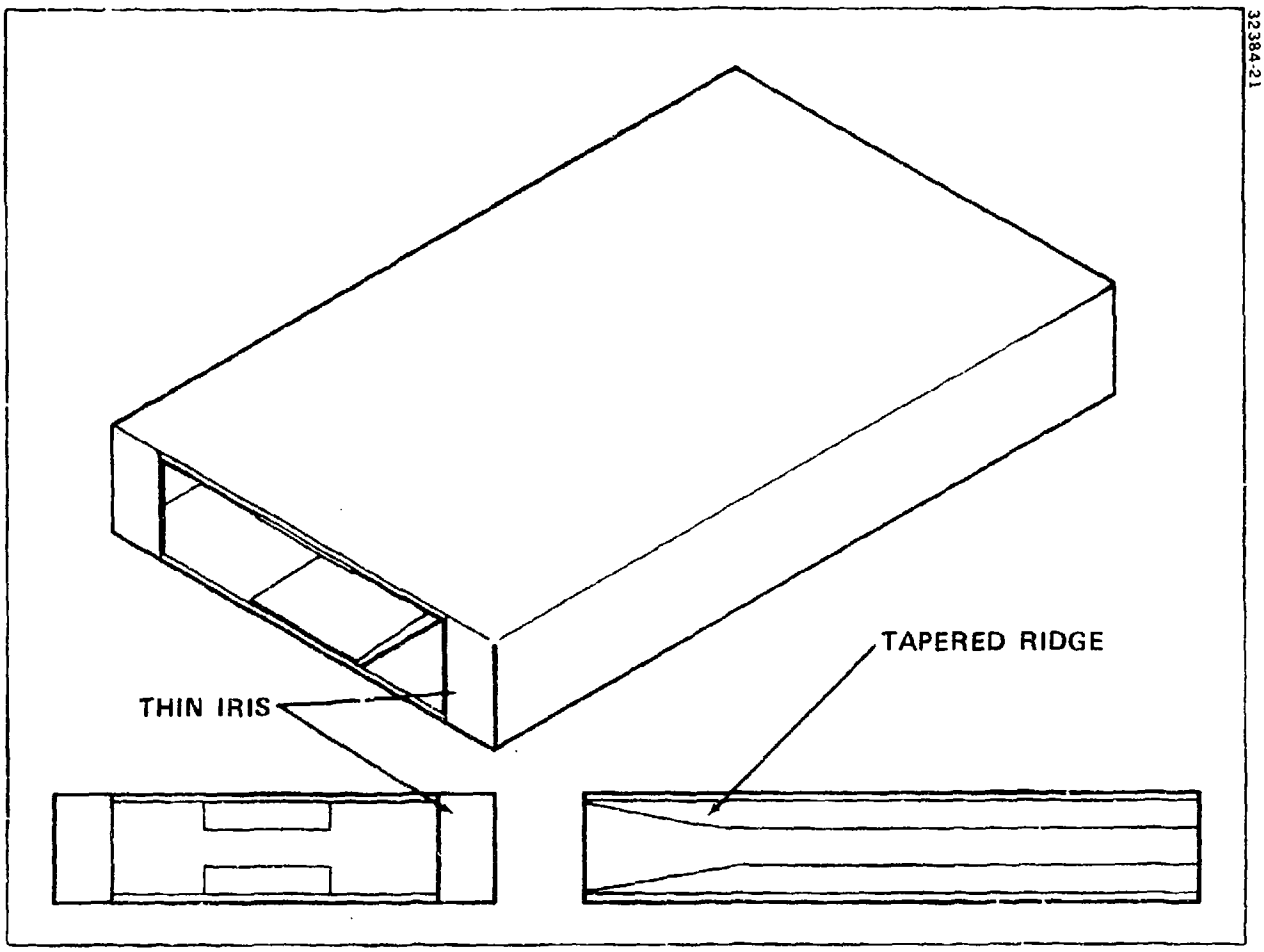

Figure 3-1. Configuration of Double Ridge Waveguide Element

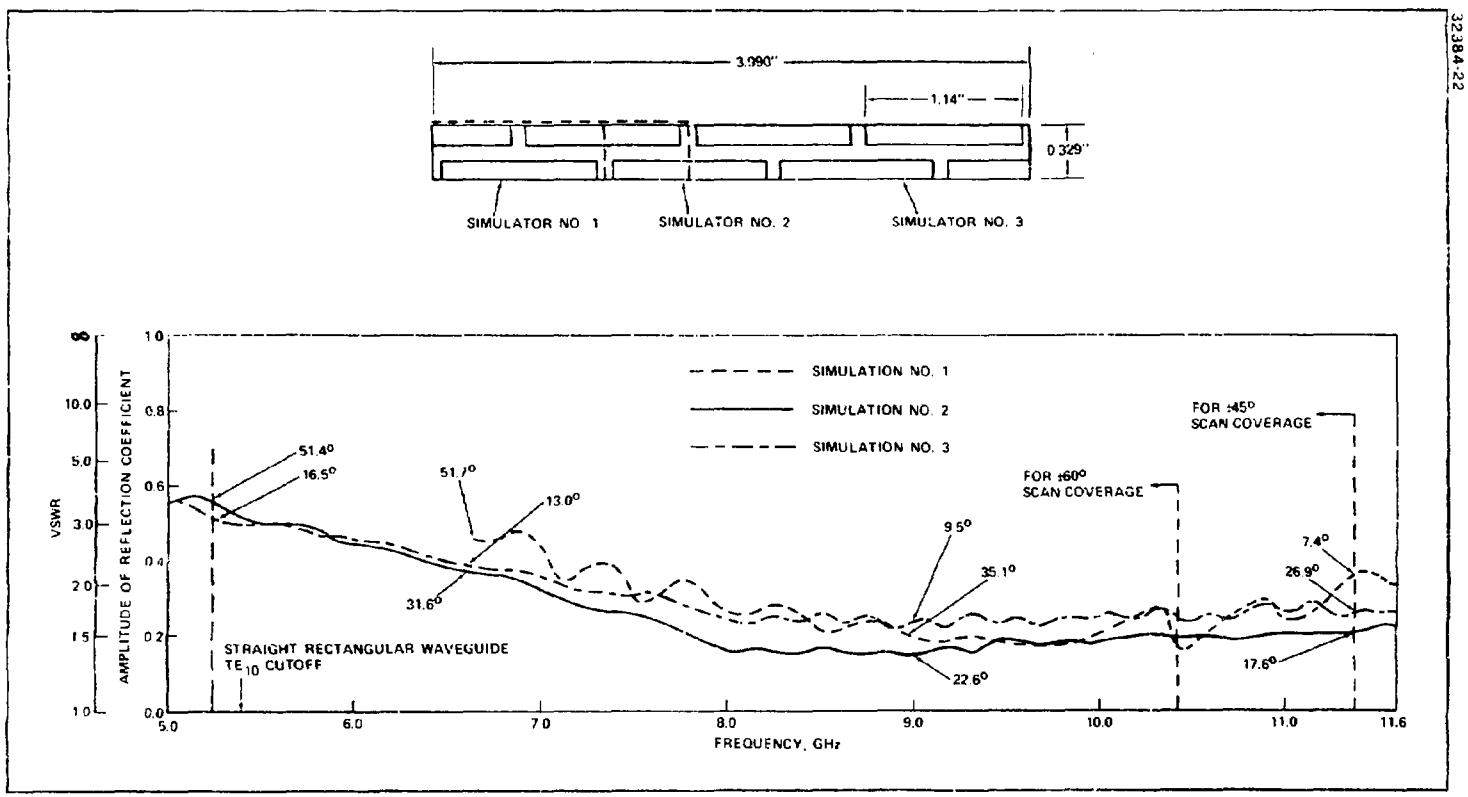

Figure 3-2. Measured Reflection Coefficient in Three H-Plane Simulators

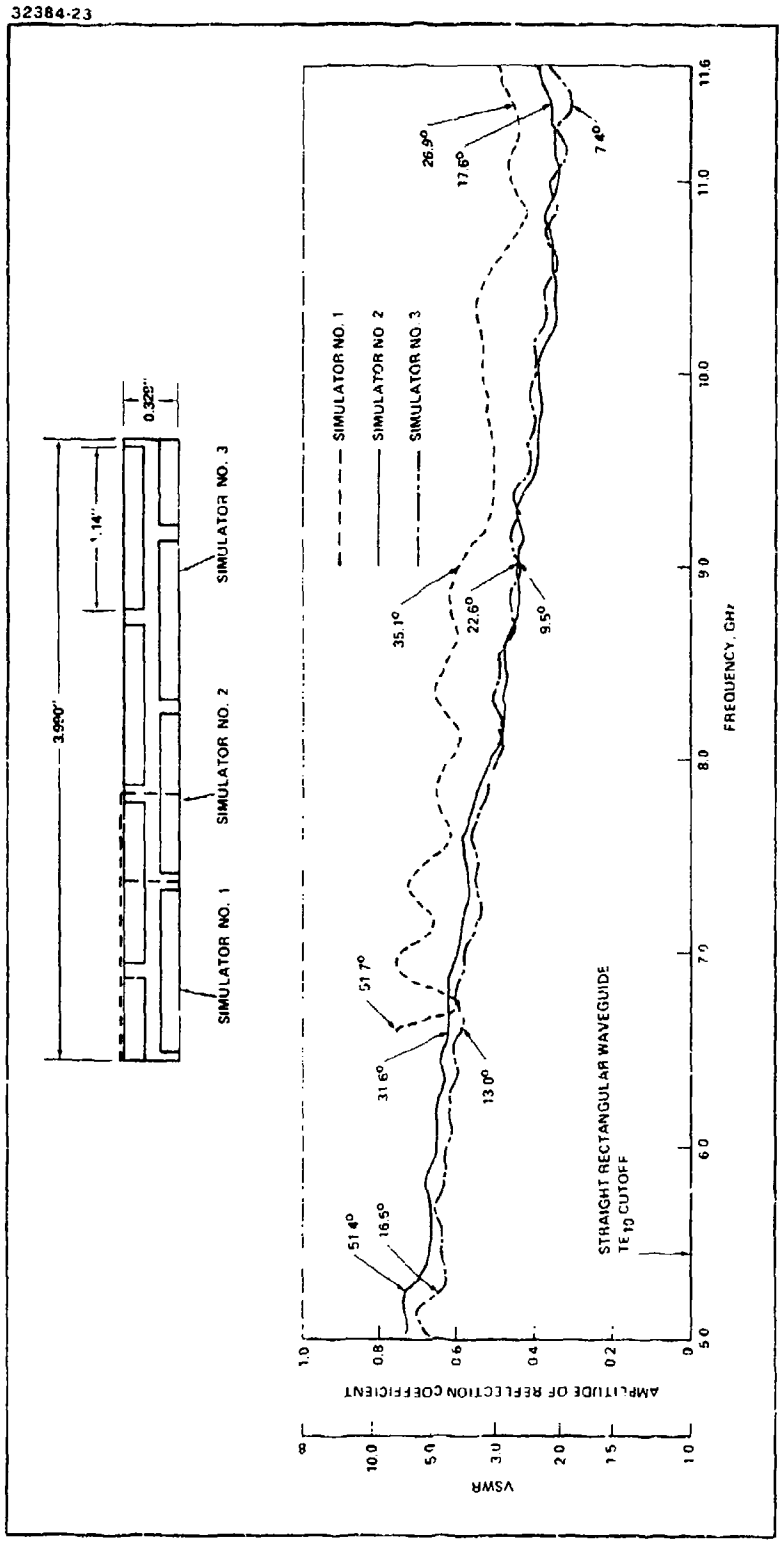

Figure 3-3. Measured Reflection Coefficient in Three H-Plane Simulators; No WAIM Dielectric Sheet in the Aperture

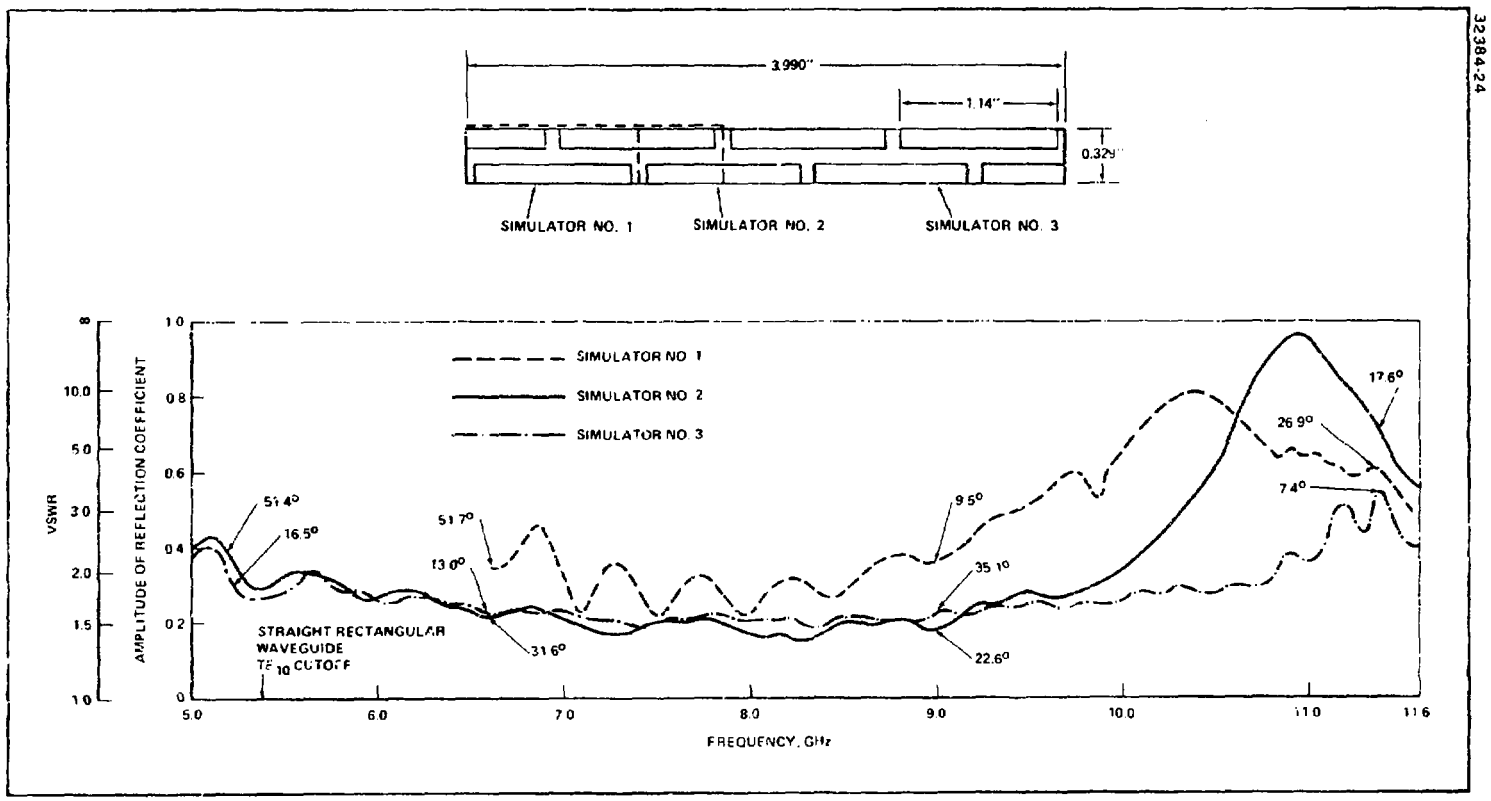

Figure 3-4. Measured Reflection Coefficient in Three H-Plane Simulators; No Iris in the Aperture

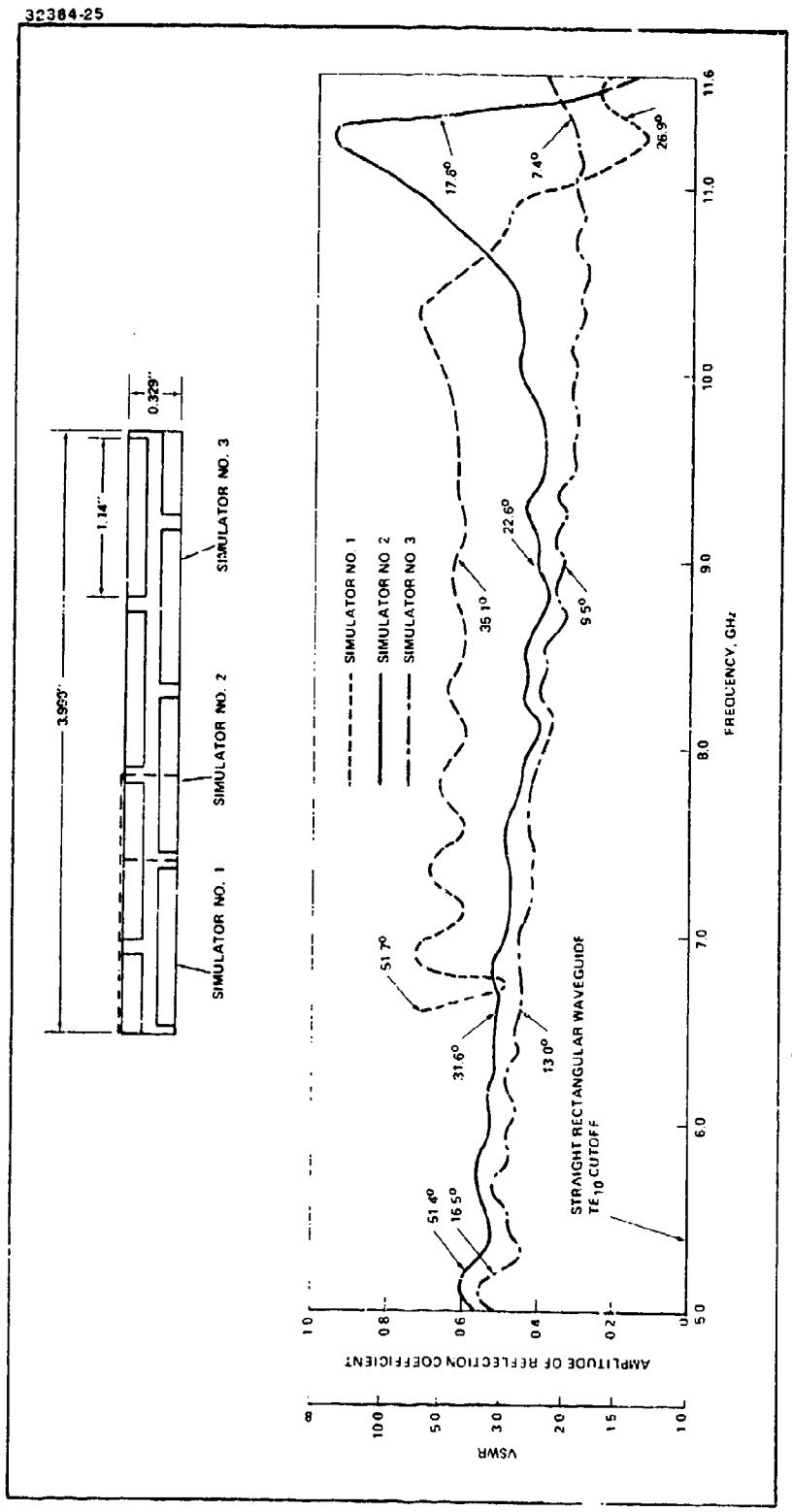

Figure 3-5. Measured Reflection Coefficient in Three H-Plane Simulators; No Iris, No WAIM Dielectric Sheet in the Aperture

SECTION IV
DIELECTRIC LOADED CIRCULAR WAVEGUIDE ARRAYS

Recently there has been considerable interest in wideband phased arrays with electronically adjustable polarization capability which includes dual circular or linear polarization. In order to obtain arbitrary polarization, two orthogonally linear or circular polarizations are required. Because of this requirement, broadband helices or spirals are ruled out from consideration. There are two possible solutions: one is a dipole-waveguide combination antenna in which a wideband dipole element is added to each of the existing rectangular waveguide element to obtain the required two orthogonally linear polarizations. The other is an array of circular or square waveguides. Since the latter is mechanically rigid and simple, we direct most of our efforts in the design and development of circular waveguide elements.

4.1 BANDWIDTH LIMITATIONS

The requirement for wide angle scanning limits the maximum element spacing and thus the size of element which can be used in the arrays. The requirements for dual polarization and wide bandwidth impose further restriction on the element. If circular or square waveguides are used, the above requirements necessitate the elements to be loaded with either dielectric or quadruple ridges in order to keep the element at least 10 percent or more above cutoff at the low end of the band. In the meantime, the element should be free from propagating any high order mode at the high end of the band. Applying the above restrictions, the maximum tunable bandwidth of uniform circular waveguide phased arrays is limited to 17 percent for $\pm 60^{\circ}$ scan coverage. In these studies, a 20 percent design is accomplished by the change of feed cross section. Studies on square waveguide phased arrays for dual polarization applications have been reported by Tsandoulas and Knittel[11]. A 20 percent bandwidth design using square waveguide element is achieved for one-fourth hemispherical scan coverage. However, if the scan coverage is raised to a 60-degree half-angle cone, the maximum bandwidth is reduced to approximately 10 percent.

4.2 ELEMENT CONFIGURATION

The configuration of the element is shown in Figure 4-1. The front end of the element has a circular aperture fed by a square waveguide. A gradual transition from square to circular cross-section is made to minimize the mismatch due to this transition. The dielectric constant, ϵ_2, of the plug is selected to prevent TM_{01} mode from propagating in the plug. However, the dielectric loading in the transition and square guide region may have a dielectric constant ϵ_3 higher than ϵ_2 in order to obtain a good impedance match over a wideband of frequencies. The use of open-ended circular aperture provides better impedance match and polarization isolation over a wide angle of scan than the square waveguide radiator. The use of square waveguide as feed has the advantage of a wider bandwidth than the circular waveguide feed since it can prevent the TM_{01} circular waveguide mode from being excited from the internal source, while keeping the feed at least 10 percent or more above cutoff at the low frequency end.

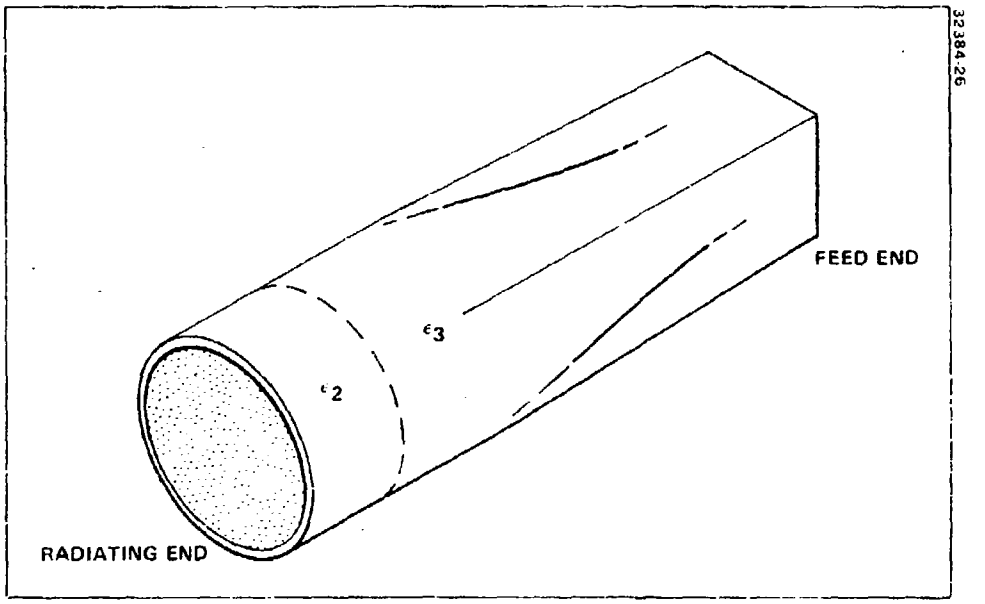

Figure 4-1. Dielectric-Loaded Square to Circular Waveguide Element

4.3 METHOD OF ANALYSIS

Analysis of the array performance is divided into two steps. The first step is the analysis of a planar circular waveguide array without the feed transition. Geometry of this mathematical model is shown in Figure 4-2. The method of moments is used to solve this boundary value problem. Assume all propagating modes are terminated internally into a matched load. The optimum design which results into the least transmission loss is selected for further investigation in the second step analysis. The second step analysis takes into account the TM_{01} mode reactive termination in the transition region. All higher order modes may be excited in the aperture due to mutual coupling. At the high frequency end, however, fraction of the TM_{01} mode excited in the aperture may leak through the dielectric plug and enter into the transition region. Since the square waveguide is designed to propagate only TE_{10} and TE_{01} modes, the TM_{01} mode will be terminated reactively in the transition region. The effects of this reactive termination can be simulated by an equivalent TM_{01} mode short termination at a distance from the inner face of the dielectric plug. All the other higher order modes are evanescent in the plug region and thus do not see the transition. The impedance mismatch of the dominant modes due to the change of cross-section in the transition is assumed to be negligible.

A brief description of the mathematical formulation and some terminologies is given in Section 2.2. The following section is a continuation of the analysis to deal with the polarization characteristics. All equations are general and fundamental. They can be applied to either circular or square waveguide arrays.

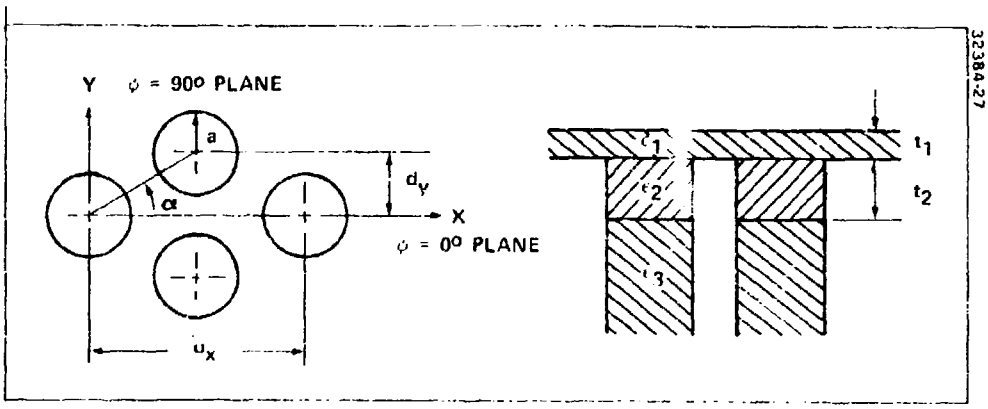

Figure 4-2. Geometry of Planar Circular Waveguide Arrays

4.4 ANALYSIS OF THE POLARIZATION CHARACTERISTICS

It is well known that the polarization characteristics of an array antenna is substantially different from that of an isolated element. The polarization ellipse at the peak of main beam varies with scan angle and strongly depends upon the array environment such as element spacing, element lattice, and size of the array. For an infinite planar array with uniform amplitude excitation, the radiated far field components at the peak of the main beam are related to the transmission coefficients of Φ_{00r} modes as defined in Section 2.2. It can be written as:

$$\bar{E} = \bar{E}_\theta + \bar{E}_\phi = \frac{1}{\cos\theta}\iint \bar{E}_t \ \bar{\Phi}^*_{002}\, da + \iint \bar{E}_t \, \Phi^*_{001}\, da \tag{4-1}$$

The polarization status of the far field can be described by the axial ratio and the tilt angle τ, which is the angle between the θ vector of the spherical coordinate and the major axis of the polarization ellipse. They can be written as:

$$\text{Axial Ratio} = \frac{\bar{E}_\theta \sin\tau + \bar{E}_\phi \cos\tau}{\bar{E}_\theta \cos\tau - \bar{E}_\phi \sin\tau} \tag{4-2}$$

and

$$\tau = \frac{1}{2}\tan^{-1}\left[\frac{2R_e\,(\bar{E}_\theta \cdot \bar{E}^*_\phi)}{\bar{E}_\theta \cdot \bar{E}^*_\theta - \bar{E}_\phi \cdot \bar{E}^*_\phi}\right] \tag{4-3}$$

In addition to the polarization ellipse, the problems of the polarization mismatch between the two antennas are significant in radar as well as communications applications. The polarization mismatch or isolation of phased arrays referred here is defined as the polarization coupling level at the peak of two beams, one with vertical or right-hand screw sense of incidence at the aperture, the other with horizontal or left-hand screw sense of incidence at the aperture. Thus, the polarization coupling or isolation can be obtained from the formula,

Polarization Coupling (dB)

$$= 10 \log \frac{\bar{E}_1 \cdot \bar{E}_2^*}{\sqrt{\bar{E}_1 \cdot \bar{E}_1^*}\sqrt{\bar{E}_2 \cdot \bar{E}_2^*}} \tag{4-4}$$

where $\bar{E}_1$ is the vector electric field at the peak of radiation when the array elements are excited with one sense of polarization and $\bar{E}_2$ is the field when the array elements are excited with another sense of polarization.

The computer program used in the following computations accounts for 10 waveguide modes and about 180 grating lobes surrounding the main beam. Reflection coefficient, cross polarization component of the incidence wave, amplitude of all waveguide modes, far field components, axial ratio at the peak of the main beam and polarization isolation between two orthogonal modes are printed out from the program.

4.5 DIELECTRIC-LOADED CIRCULAR WAVEGUIDE ARRAYS WITH INTERNAL MATCHED TERMINATION

A summary of several nearly optimum designs from the first step computation for ±45 degrees and ±60 degrees conical coverage are listed in Table I. The array parameters for ±45 degree conical scan are:

$$\begin{aligned} d_x &= 1.1013\lambda_h & d_y &= .3179\lambda_h & \alpha &= 30^o \\ a &= .28\lambda_h & t_1 &= .0229\lambda_h & t_2 &= .210\lambda_h \\ \epsilon_1 &= 4.2 & \epsilon_2 &= 1.8 & \epsilon_3 &= 2.53 \end{aligned} \tag{4-5}$$

The array parameters for ±60 degree conical scan are:

$$\begin{aligned} d_x &= 1.0075\lambda_h & d_y &= .2909\lambda_h & \alpha &= 30^o \\ a &= .26\lambda_h & t_1 &= .021\lambda_h & t_2 &= .200\lambda_h \\ \epsilon_1 &= 4.2 & \epsilon_2 &= 2.1 & \epsilon_3 &= 3.0 \end{aligned} \tag{4-6}$$

Where λ_h is the free space wavelength at the high frequency end, f_h. The transmission loss listed in the table includes reflection of the two orthogonal modes and the TM_{01} mode leaked through the dielectric plug. Figures 4-3(a) and (b) shows the impedance loci of the array specified in equation 4-6 for a $\pm 60^o$ scan coverage when operated in a dual linear mode at the high end of the band. Figure 4-4 shows the polarization isolation between the vertical and horizontal polarization when the array

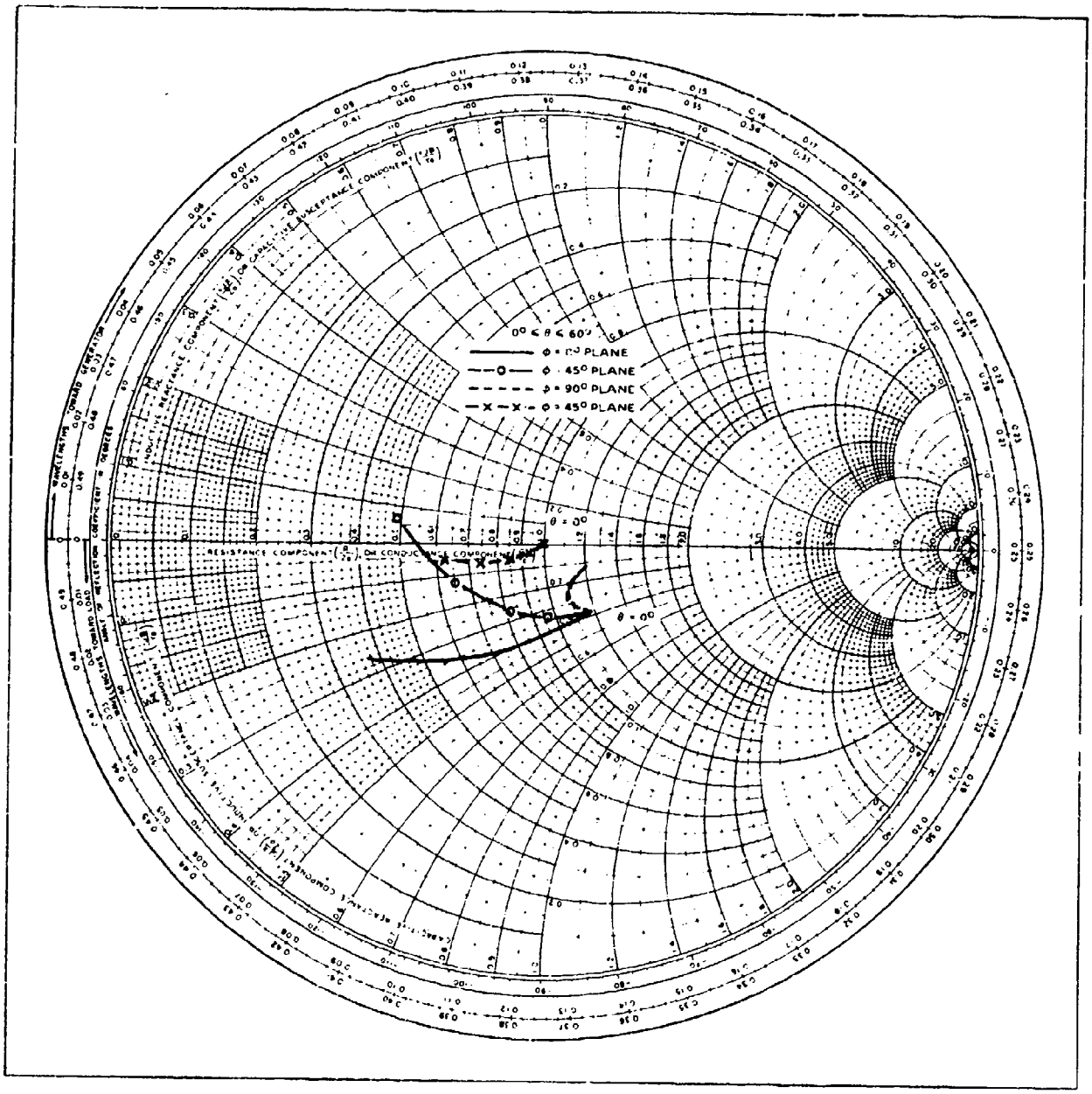

Figure 4-3(a). Impedance Loci at f_h for a Vertically Polarized Array

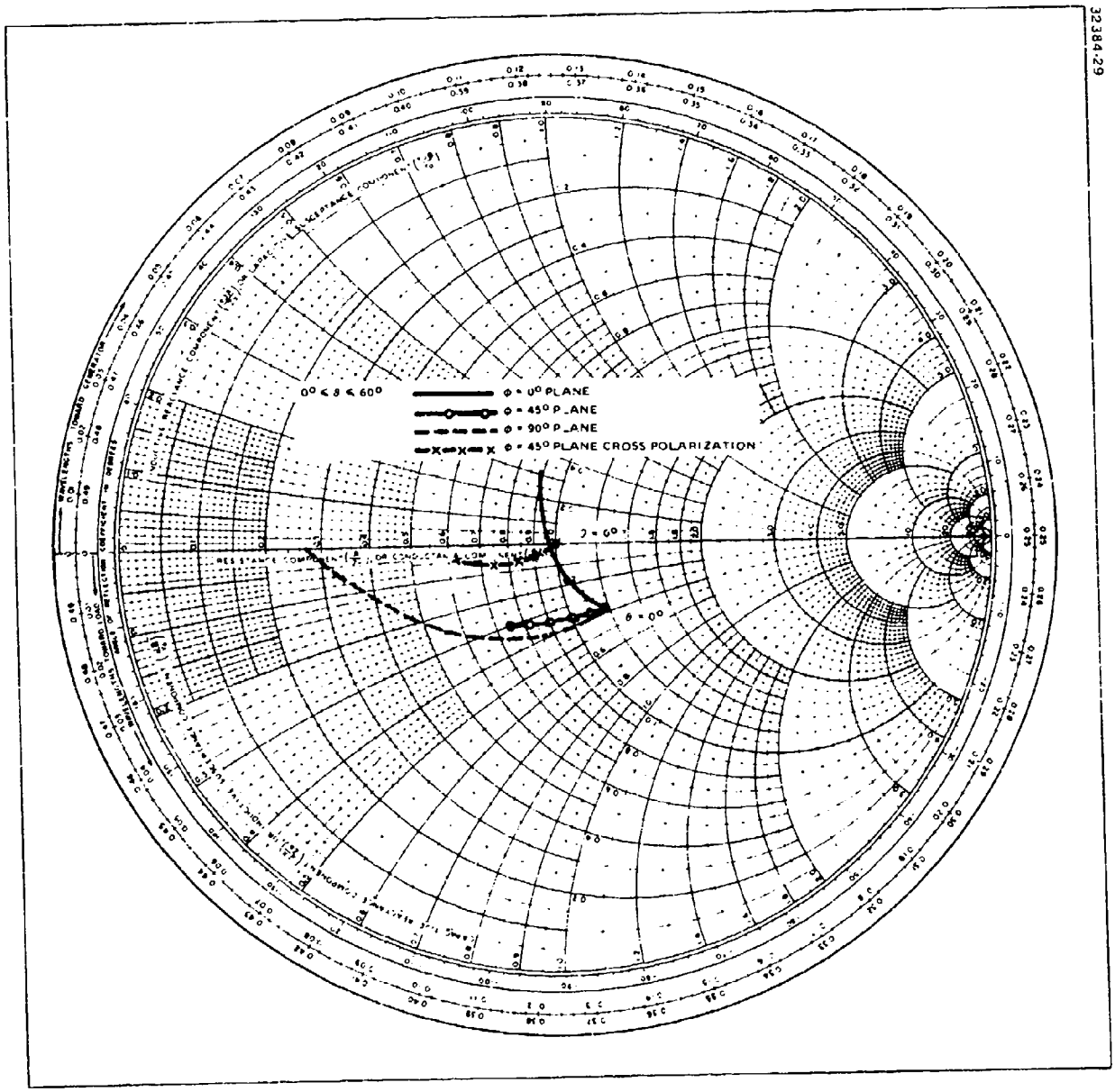

Figure 4-3(b). Impedance Loci at f_h for a Horizontally Polarized Array

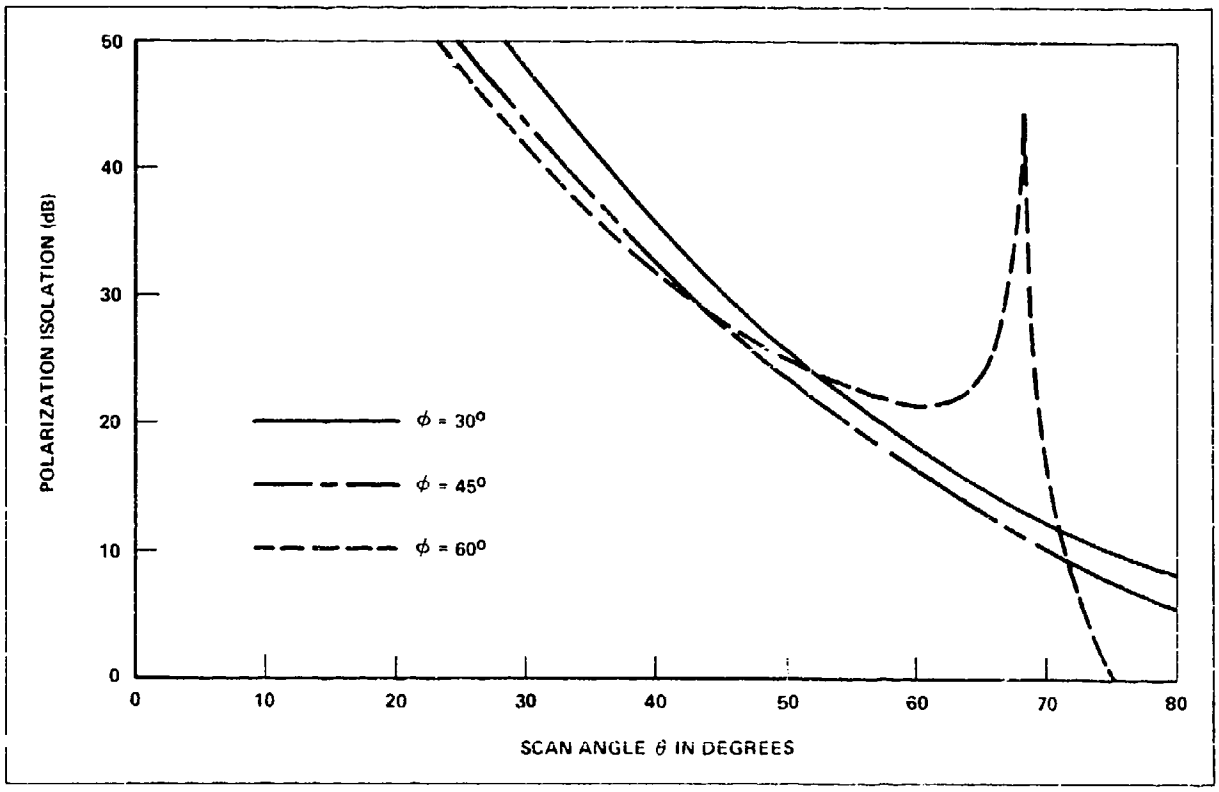

Figure 6-4. Polarization Isolation versus Scan Angle θ, Dual Linear Polarization

TABLE I. PERFORMANCE OF WIDEBAND DUAL POLARIZED PHASED ARRAYS WITH INTERNAL MATCHED TERMINATION

Scan Volume	Polarization State	Percent Bandwidth	Minimum Polarization Isolation in dB	Maximum Transmission Loss in dB	Maximum TM01 Power and Total Transmission Loss at that Scan Angle
$\pm 45^{\circ}$	Dual Linear	20	22.47 at f_h	1.16 at f_ℓ 1.06 at f_h	5.8% at f_h 0.57 dB
$\pm 45^{\circ}$	Dual Circular	20	20.27 at f_h	0.97 at f_ℓ 0.78 at f_h	4.2% at f_h 0.52 dB
$\pm 60^{\circ}$	Dual Linear	16	18.53 at f_h	1.80 at f_ℓ 1.82 at f_h	6.31% at f_h 0.80 dB
$\pm 60^{\circ}$	Dual Circular	20	15.08 at f_h	1.73 at f_ℓ 1.29 at f_h	5.33% at f_h 0.59 dB

f_ℓ = low frequency = low frequency end, f_h = high frequency end

Transmission loss includes two orthogonal modes and TM_{01} mode.

is scanned in $\phi = 30^{\circ}$, 45°, and 60° planes of scan. At the high frequency end, the worst aperture mismatch occurs in $\phi = 90^{\circ}$ plane at the edge of scan volume for the horizontal polarization. For the vertical polarization, the worst mismatch occurs in $\phi = 0^{\circ}$ plane. A compromise in aperture matching between these two points at high and low end of the frequencies are made for the desired tunable bandwidth. In practical applications, occasionally, only vertical and one sense of circular polarization are required. In this case the mismatch loss of the array can be improved further from that of this listed data presented in Table I. Since there is no cross polarization component excited in the symmetric plane of scan for the case of linear polarization, the worst polarization isolation always occurs in the $\phi = 45^{\circ}$ plane. The computation also indicates that the TM_{01} mode is not excited at all in the H-plane scan and is negligibly small in the E-plane scan.

Aperture matching of circular polarization is always better than that of the linear case because it is a compromise between two orthogonal linear polarizations. However, the polarization isolation is worse than the linear case since the horizontal polarization has the worst impedance match in $\phi = 90^{\circ}$ plane, while the vertical polarization has the best match in this plane. As a result of this unbalance in transmitted power from two orthogonal linear components, the minimum polarization isolation occurs in $\phi = 90^{\circ}$ plane. Figure 4-5 shows the transmission loss of the same array when operated in the dual circular mode at f_h. Figure 4-6 shows axial ratio and polarization isolation of the array. It is noted that the axial ratio of righthand circular polarization (RHCP) is better than the left hand circular polarization (LHCP) in the $\phi = 45^{\circ}$ scan plane. Performance of the array along the edge of a $\theta = 60^{\circ}$ cone is shown in Figure 4-7. It is interesting to see that there is a tradeoff between polarization characteristics and

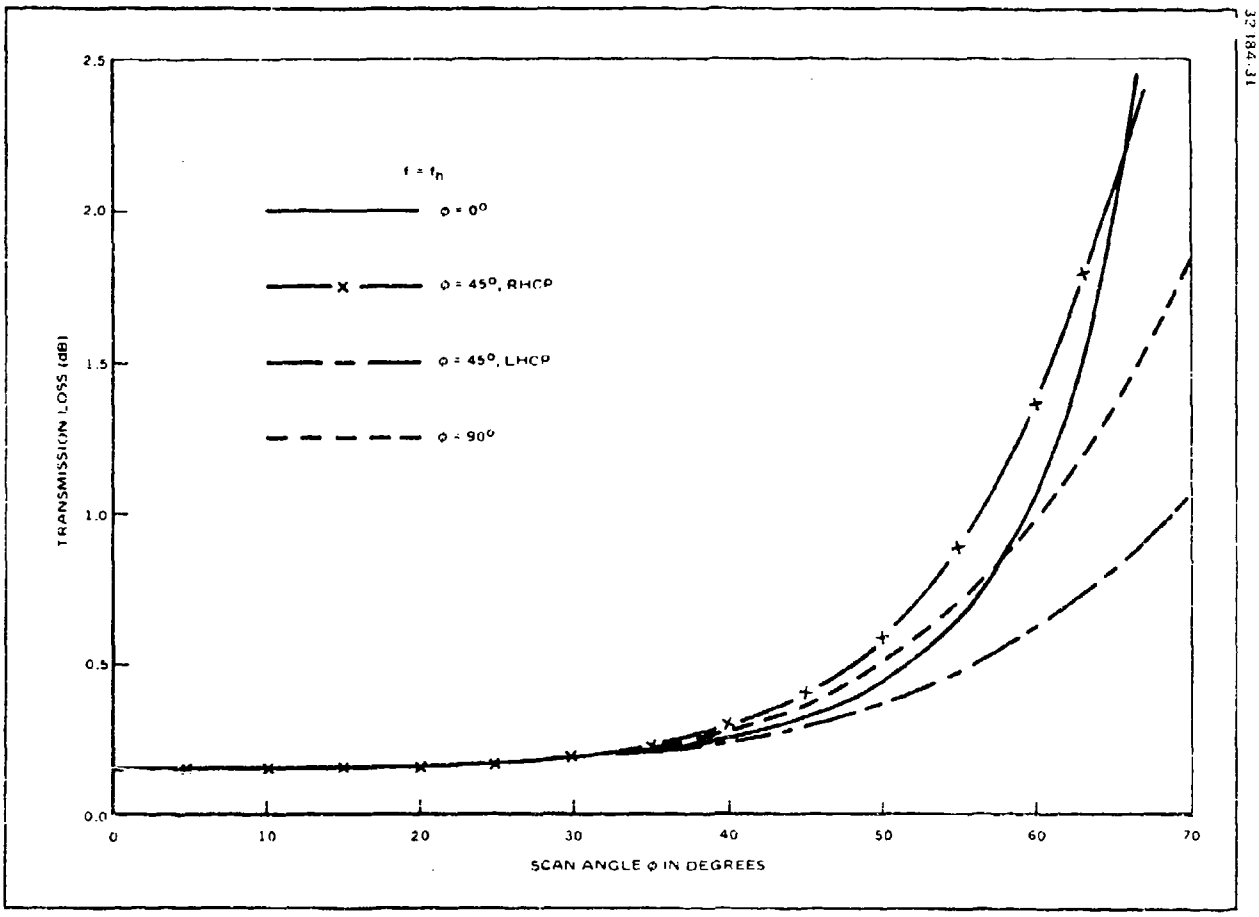

Figure 4-5. Transmission Loss of the Array as Specified in Equation (4-6) Dual Circular Polarization

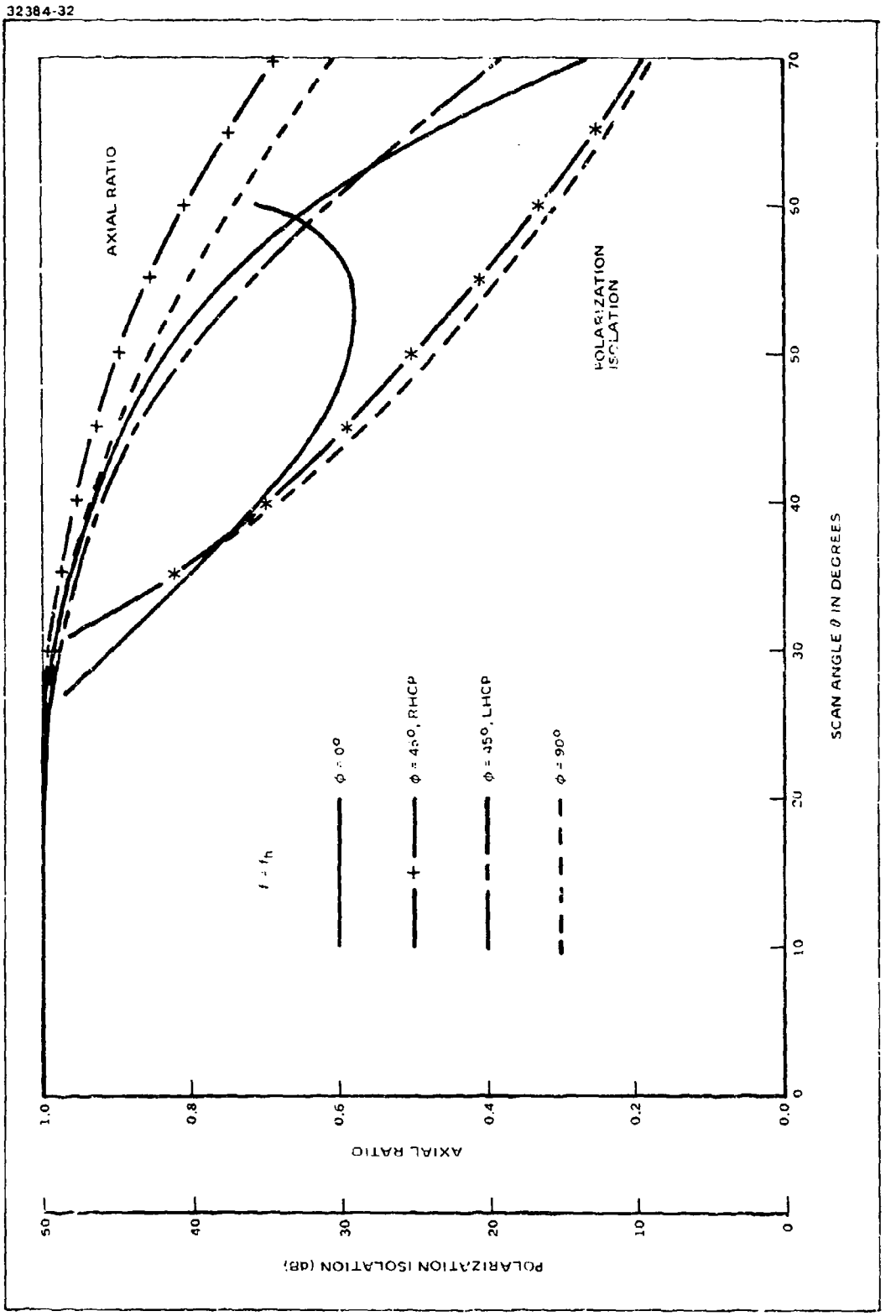

Figure 4-6. **Polarization Characteristics of the Array is Specified in Equation (4-6), *Dual Circular Polarization***

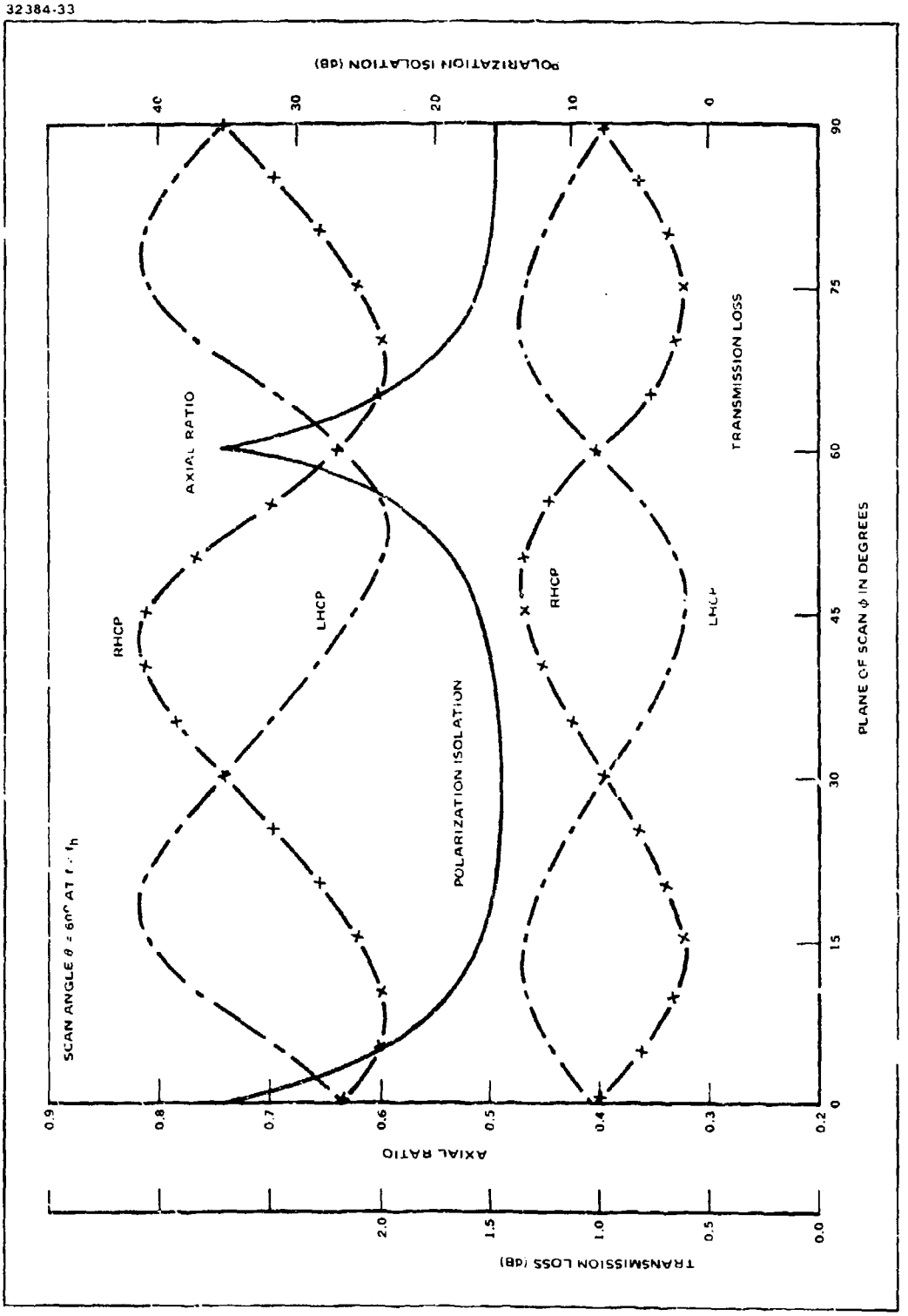

Figure 4-7. Performance of the Array as Specified in Equation (4-6) at the Edge of a $\theta = 60^{\circ}$ Cone

transmission loss in different scan plane. Performance of the array at a lower frequency of f = .85 f_h is shown in Figure 4-8 and Figure 4-9. As the operational frequency moves down farther to f = .8175 f_h, the average aperture mismatch over the scan volume becomes 1.35 dB. However, the axial ratio and polarization isolation improves in the low frequency region.

The polarization characteristics of phased arrays not only depends upon frequency and scan angle, it also varies substantially with the element spacing. Figure 4-10 shows the axial ratio of an array with array parameters as specified in Equation (4-6) except the d_y dimension varies from $0.2909\lambda_{l_1}$ to $0.500\lambda_{l_1}$. The first grating lobe emerges at end fire as the main beam is scanned to $\theta = 80^{\circ}$. It is observed that even though the array is scanned in one plane only, the equilateral triangular lattice still gives the best polarization characteristic.

The accuracy of these computations has been verified by measurement of reflection coefficient over a wideband of frequencies in H-plane waveguide simulator. Figures 4-11(a) and (b) shows two sets of computed and measured data; one case is with a dielectric plug at the open end as shown in Figure 4-2 and the other is uniformly dielectric loaded waveguide element.

A close agreement between computed and measured results is obtained in both cases. In fact, the measured amplitude of reflection is always slightly lower than the calculated result which is to be expected.

4.6 DIELECTRIC-LOADED CIRCULAR WAVEGUIDE ARRAYS WITH REACTIVE TM_{01} MODE TERMINATION

Reactive termination of the TM_{01} mode in the transition region does not seem to be a problem, since the worst aperture match always occurs in the H-plane at f_h and the TM_{01} mode is not excited at all in this plane of scan. In Table I, it is observed that the transmission loss is relatively low when reflected TM_{01} energy is high. In the second step calculation the TM_{01} mode admittance at the plane of the aperture looking into the feed end was varied from $-j\infty$ to $+j\infty$. For most cases, the performance is more or less the same as that listed in Table I. Except when the TM_{01} admittance looking into the element approaches zero, which corresponds to an open circuit for the TM_{01} mode at the aperture, it may cause a 4 to 5 dB transmission loss at the edge of scan volume. Therefore, it is decided to assume an equivalent TM_{01} short circuit at half of the TM_{01} guide wavelength at f_h from the inner face of the dielectric plug in the transition. This can be done physically by adjusting the length of the transition to get a TM_{01} short circuit at the inner face of the dielectric plug. As the frequency goes down, the TM_{01} energy diminishes, thus the TM_{01} mode has less or no effect in the low frequency region. Results of the second step calculation are listed in Table II.

Transmission loss, axial ratio and polarization isolation of the ±60 degree scan array are shown in Figures 4-12 and 4-13. Comparison between Figures 4-5, 4-6, and 4-12, 4-13 shows that the TM_{01} reactive termination slightly improves the impedance match but it deteriorates the polarization isolation and axial ratio.

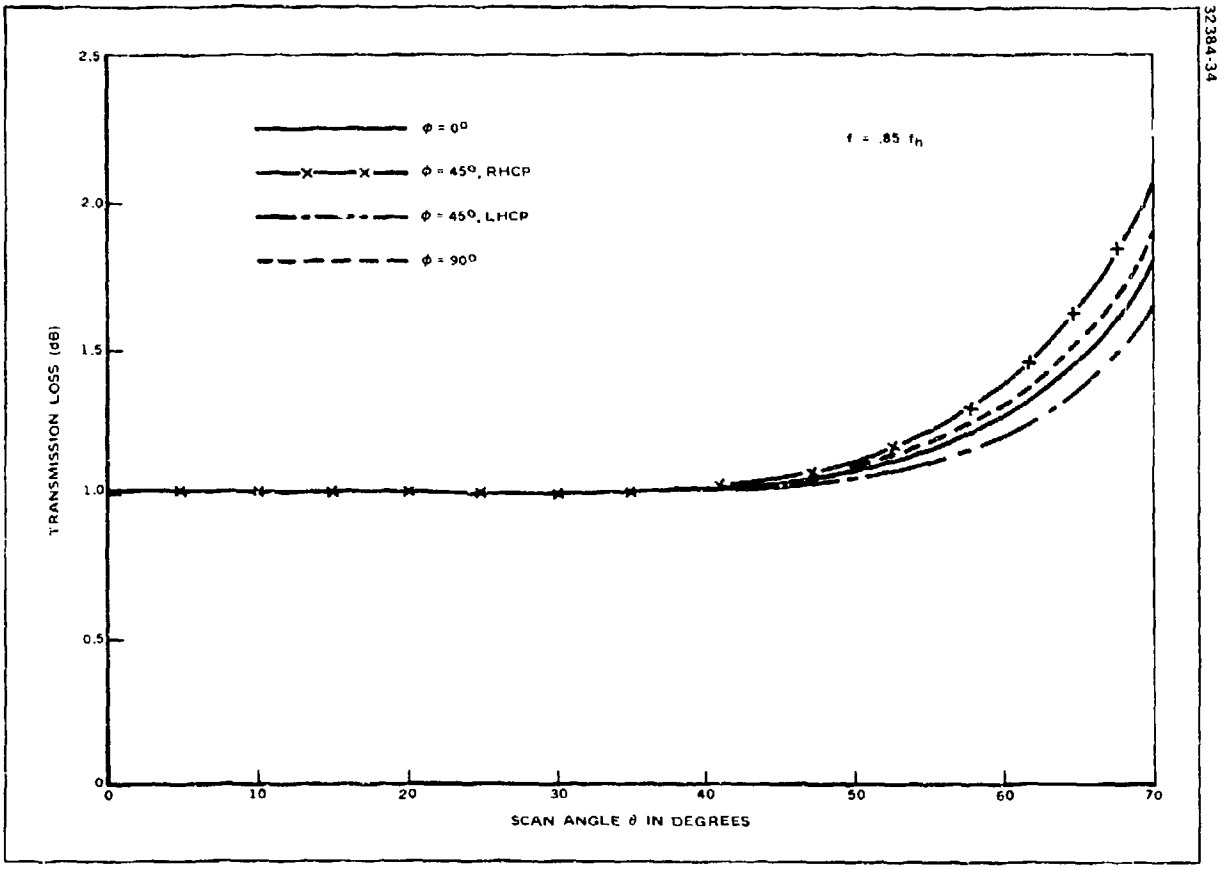

Figure 4-8. Transmission Loss of the Array as Specified in Equation (4-6), Dual Circular Polarization

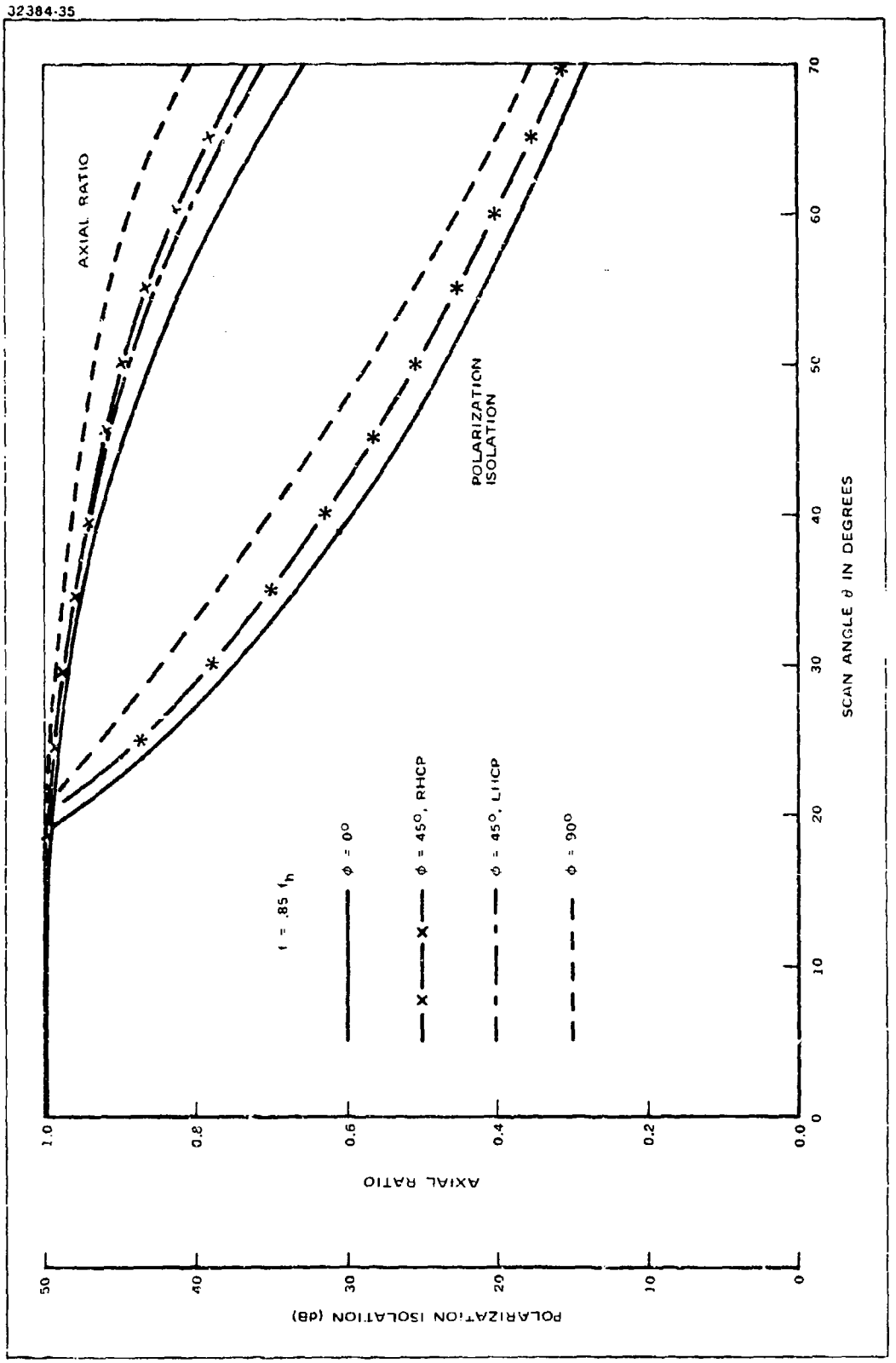

Figure 4-9. Polarization Characteristics of the Array as Specified in Equation (4-6) Dual Polarization

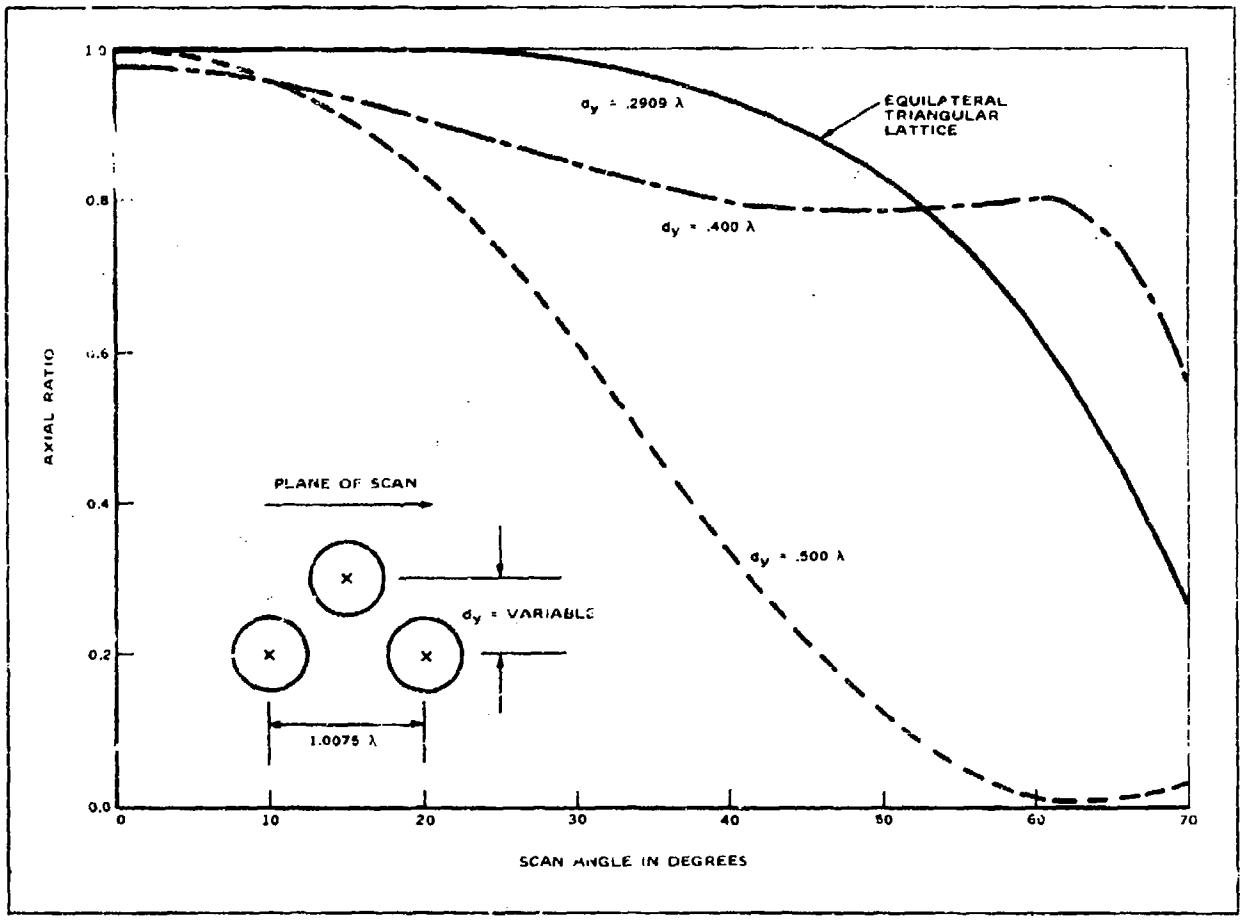

Figure 4-10. Axial Ratio versus Scan Angle for the Array Specified in Equation (4-6) Except d_y is Variable

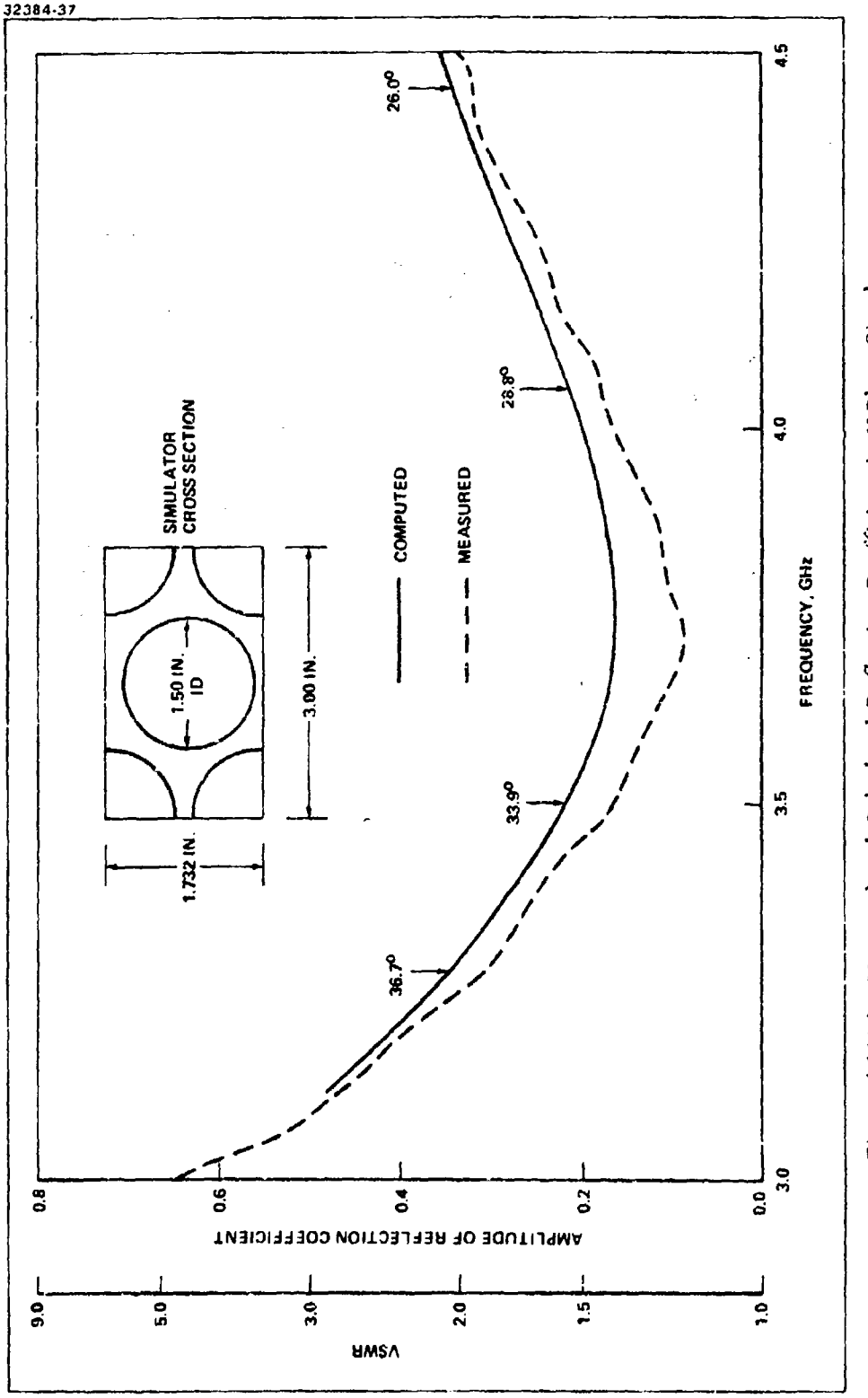

Figure 4-11(a). Measured and Calculated Reflection Coefficient in H-Plane Simulators

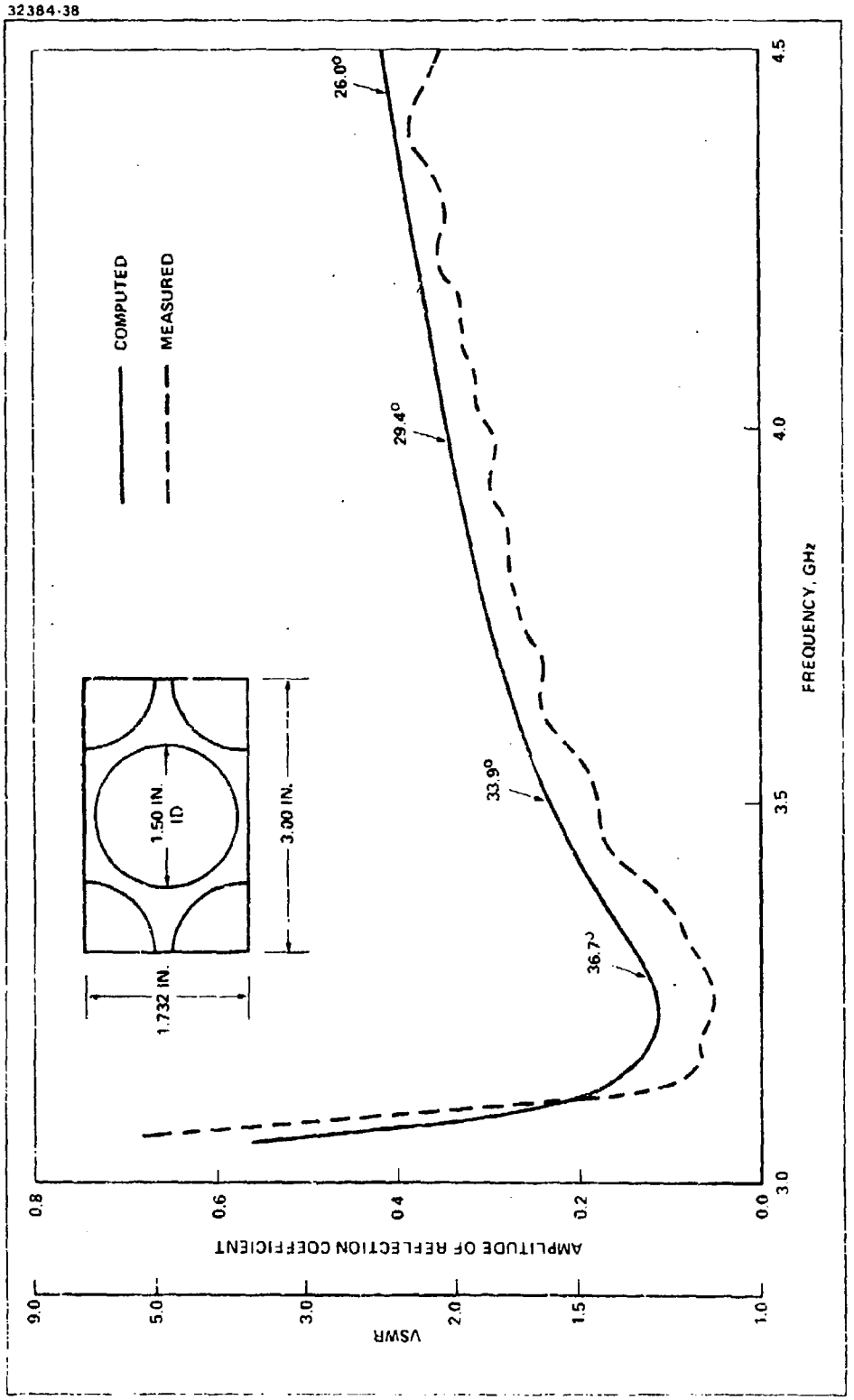

Figure 4-11(b). Measured and Calculated Reflection Coefficient in H-Plane Simulator

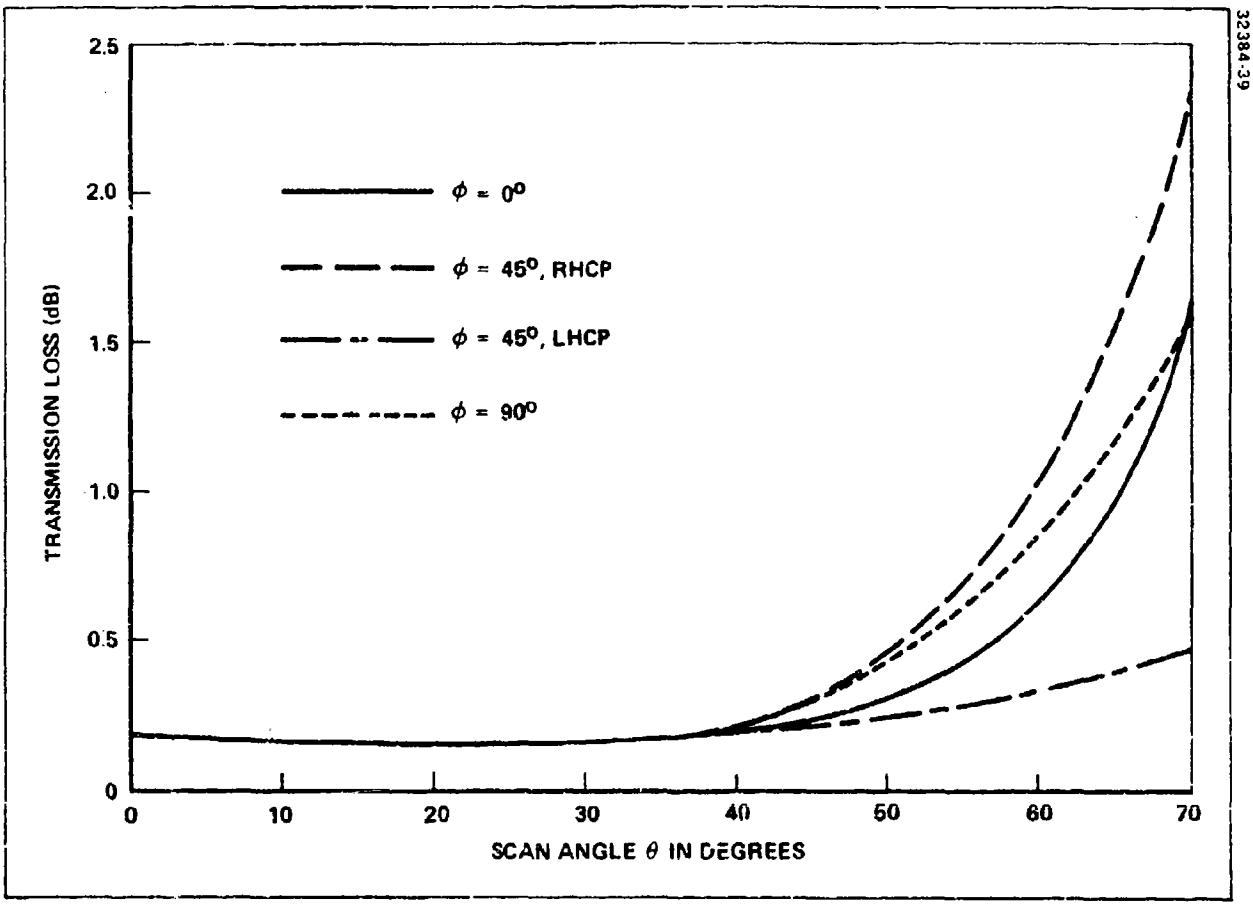

Figure 4-12. Transmission Loss of the Array with Reactive TM_{01} Termination, Dual Circular Polarization

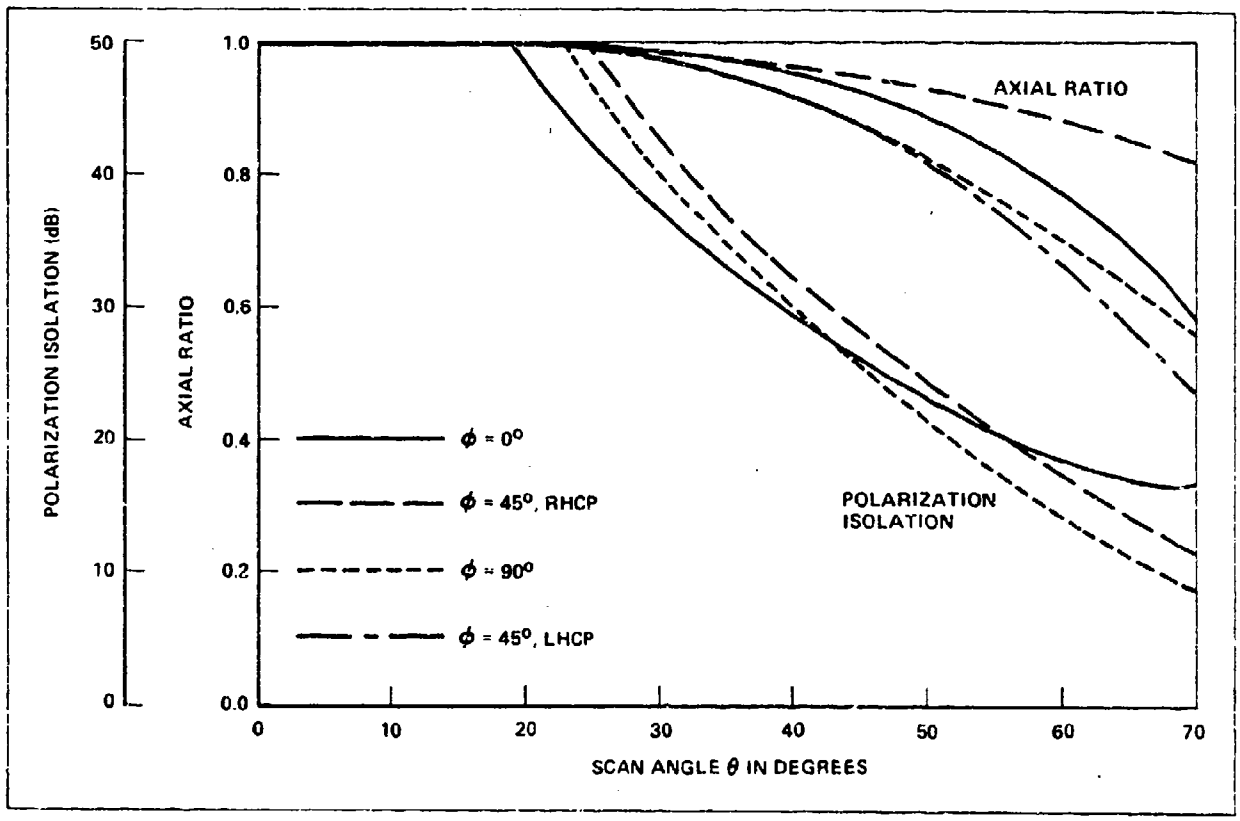

Figure 4-13. Polarization Characteristics of the Array with Reactive TM_{01} Termination, Dual Circular Polarization

TABLE II. PERFORMANCE OF WIDEBAND DUAL POLARIZED PHASED ARRAYS AT f_h WITH EQUIVALENT TM01 SHORT TERMINATION OF HALF TM01 GUIDE WAVELENGTH FROM THE PLUG

Scan Volume	Polarization State	Min. dB Polarization Isolation at $\theta = 60^o$ Cone	Min. dB Polarization Isolation at $\theta = 30^o$ Cone	Max. dB Transmission Loss
$\pm 45^o$	Dual Linear	23.69	42.2	1.06
$\pm 45^o$	Dual Circular	18.52	37.3	0.79
$\pm 60^o$	Dual Linear	16.33	41.8	1.82
$\pm 60^o$	Dual Circular	14.03	37.3	1.27

4.7 SUMMARY

The polarization characteristic of a phased array depends substantially on array environment. A hexagonal array of circular waveguide radiators gives the best polarization characteristic over the scan volume. However, the bandwidth is limited to 20 percent or less because of the 1.3:1 frequency separation between the cutoff frequencies of the TM_{01} and the TE_{11} mode. At the edge of scan volume, the minimum polarization isolation of the circular waveguide arrays is more than 6 dB higher than that of the square waveguide phased arrays[11].

SECTION V
QUADRUPLE RIDGE-LOADED CIRCULAR WAVEGUIDE ARRAYS

In the previous section we have shown that the dielectric-loaded circular waveguide phased array can be operated satisfactorily over 20 percent frequency band. In practical application, however, fabrication of this array is very cumbersome from the standpoint of weight, cooling, packaging, efficiency and cost effectiveness. In this section, we will develop a method to replace the dielectric-loaded elements by the quadruple ridge-loaded waveguide.

5.1 PROPERTIES OF QUADRUPLE RIDGE-LOADED CIRCULAR WAVEGUIDE RADIATORS

The configuration of the quadruple ridge-loaded circular waveguide element is shown in Figure 5.1. This type of elements have been developed and used successfully in the ADAR Program[12]. This kind of elements is attractive for use in the arrays because of the following advantages:

1. The reduced cutoff frequency of ridge-loaded waveguide permits a compact cross section to fit into the restricted element spacing for wide angle scanning arrays.

2. The ridge-loaded waveguide provides a wide bandwidth since ridge loading raises the cutoff frequency of the TM_{01} mode while lowering the cutoff of the TE_{11} mode from that of the ordinary circular waveguide modes.

3. The attenuation in the ridge-loaded waveguide is higher than that of the ordinary air loaded circular waveguide, but is still much less than that of the dielectric loaded waveguide.

4. A ridge-loaded waveguide to coaxial junction has been successfully developed. Either loop or probe transition can provide more than 30 dB isolation between two orthogonal polarizations.

The TE_{11} mode cutoff wavelengths λco of the ridge-loaded waveguide is determined by measurement of guide wavelength λg. In terms of λg and the free space wavelength λ_o, λ_{co} is given by:

$$\lambda co = \sqrt{\frac{\lambda_o^2 \lambda_g^2}{\lambda_g^2 - \lambda_o^2}}$$

The ratio of the TE_{11} mode cutoff frequency with the ridge to that without the ridge is plotted in Figure 5-2 for different ridge widths. It is seen that the cutoff frequency is not very sensitive to the ridge width. Figure 5-3 shows the relative cutoff frequency of TM_{01}, TE_{21} and TE_{01} modes in the ridge-loaded waveguide. It is noted that the cutoff frequency of the TM_{01} mode is higher than that of the TE_{21} mode when the size of ridge R/a exceeds .21.

The experimental work for determining the higher order mode cutoff frequencies was carried out by Clark[13]. Although the accuracy of this data is limited, it proved to be useful and sufficient for the present application.

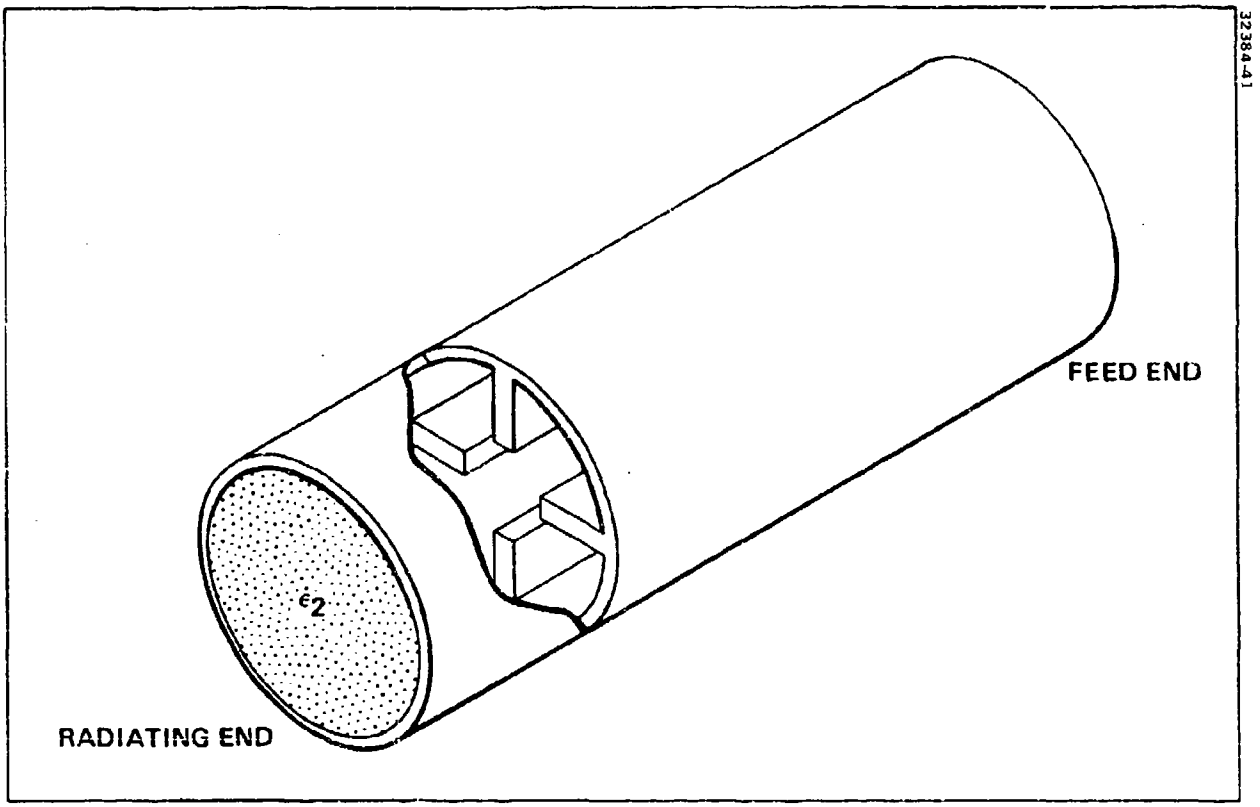

Figure 5-1. Quadruply-Ridged Circular Waveguide Element

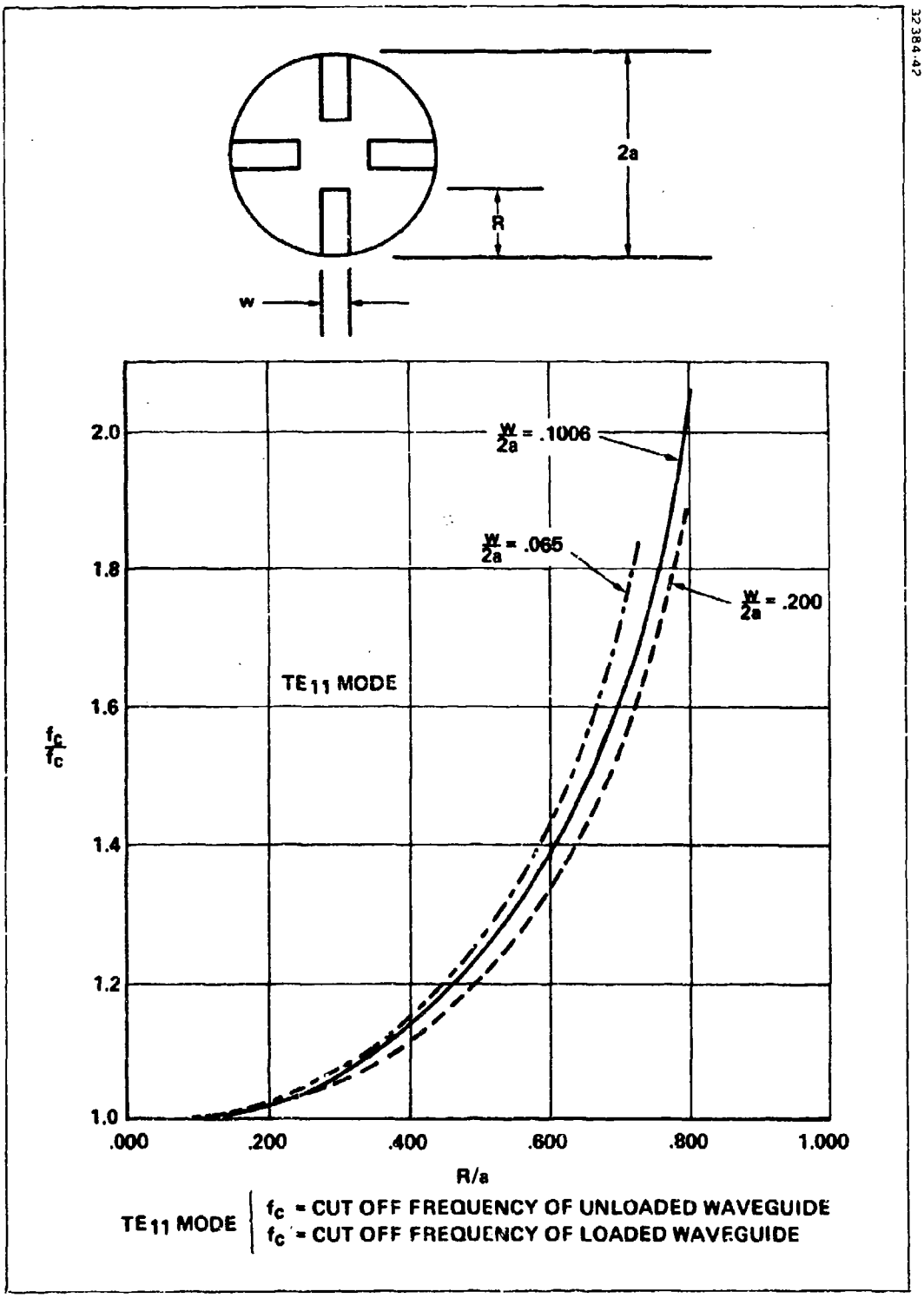

Figure 5-2. Cutoff Frequency of Quadruple Ridge-Loaded Circular Waveguide

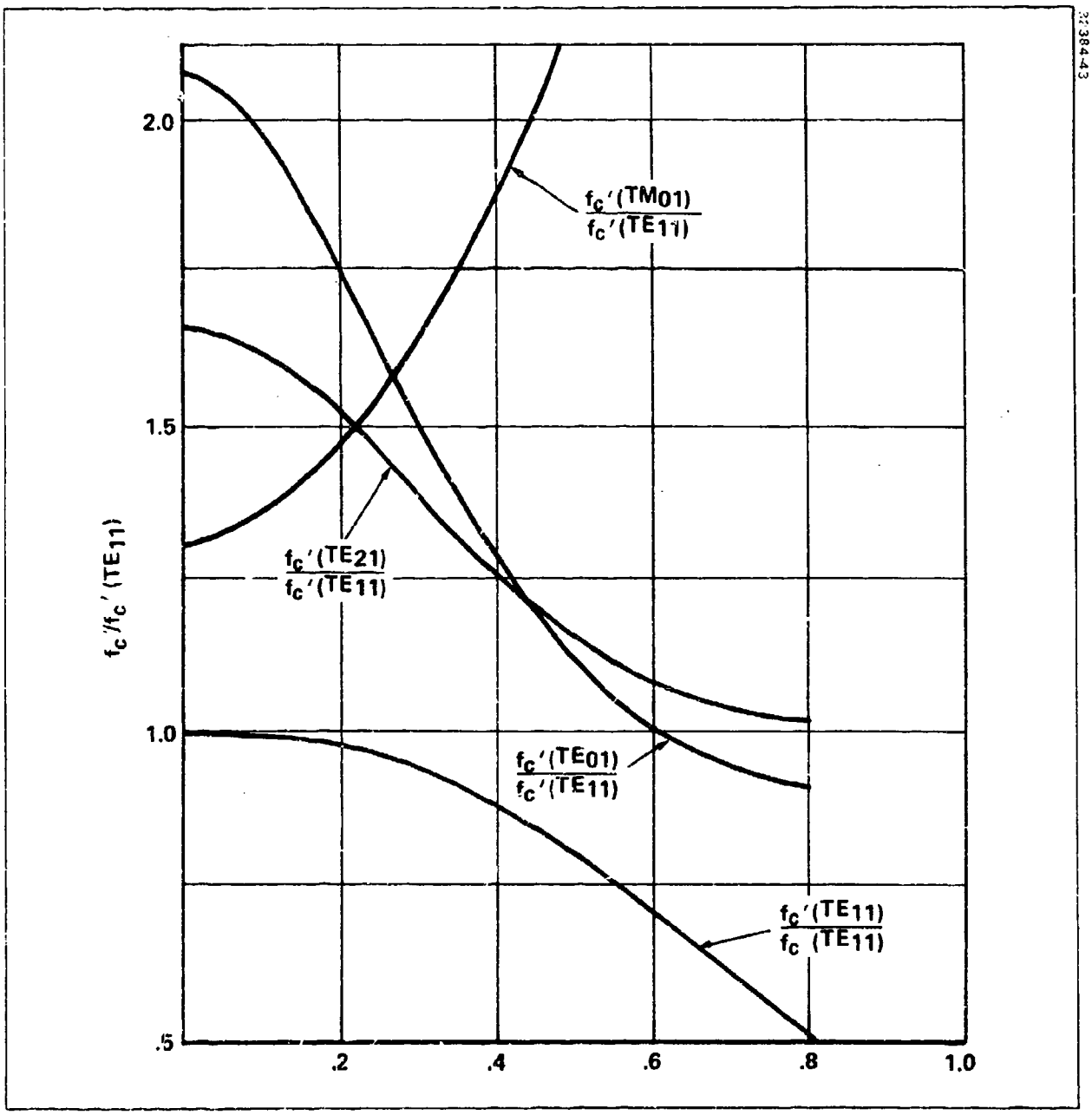

Figure 5-3. Cutoff Frequency of Quadruple Ridge-Loaded Circular Waveguide

5.2 ANALYSIS OF QUADRUPLE RIDGE-LOADED CIRCULAR WAVEGUIDE ARRAYS

A unit cell of an infinite quadruple ridge-loaded waveguide array and it is equivalent circuit is shown in Figure 5-4. In our present application, the TM_{01} mode is far below cutoff in the ridge-loaded region, and the TE_{21} mode is far below cutoff in the dielectric plug region. Therefore, neither one of them will propagate or leak through the entire element. The equivalent circuit parameters N and t_3 at the ridge to dielectric junction can be determined by a single impedance measurement, Z_{in} referred to the junction and looking into the ridge-loaded section with a matched termination[15].

The TE_{11} mode incident at the ridge to dielectric waveguide junction does not excite the TM_{01} mode in the dielectric plug because of the symmetric cross sectional discontinuity. Thus, the incident field at the aperture can be approximated by the TE_{11} mode. Due to external mutual coupling, the TM_{01} mode generated in the aperture will see a short or capacitive susceptance at the ridge to dielectric junction. This TM_{01} mode susceptance "B_c" can be measured experimentally. For the case we consider in the following, the susceptance B_c will approximate to a short circuit since the TM_{01} mode is far below cutoff in the ridge-loaded waveguide region. The admittance Y_{out}, looking out from the junction, can be computed by the method described in Section (2.2) and the looking in admittance, Y_{in}, at the junction can be measured directly. With all these circuit parameters known, amplitude of reflection can be calculated fairly closely from the equivalent circuit. The equivalent circuit shown in Figure 5-4 is not restricted to the ridge-loaded waveguide element. It is also directly applicable to a radiating element with internal matching iris or post.

5.3 APERTURE MATCHING TECHNIQUE

The equivalent circuit method provides a valuable guideline for the synthesis and optimization of an internal matching network. The steps in this optimization are:

1. Determine the element lattice and element spacing which minimize total number of elements in the array.

2. Select a dielectric material or dielectric constant ϵ_2 which is less than the value to keep the TM_{01} mode in the circular waveguide to below cutoff at the high end of the frequency band.

3. Compute the locus of impedance variation within the scanning limits. Select a scan angle which is to be matched. Usually a point near the center of the impedance locus on the impedance Smith Chart is selected for minimizing the overall average aperture mismatch loss.

4. Synthesize an internal matching network so that the impedance looking toward the source equals the conjugate of the selected matching point on the Smith Chart.

5. Repeat the above steps for optimum aperture matching.

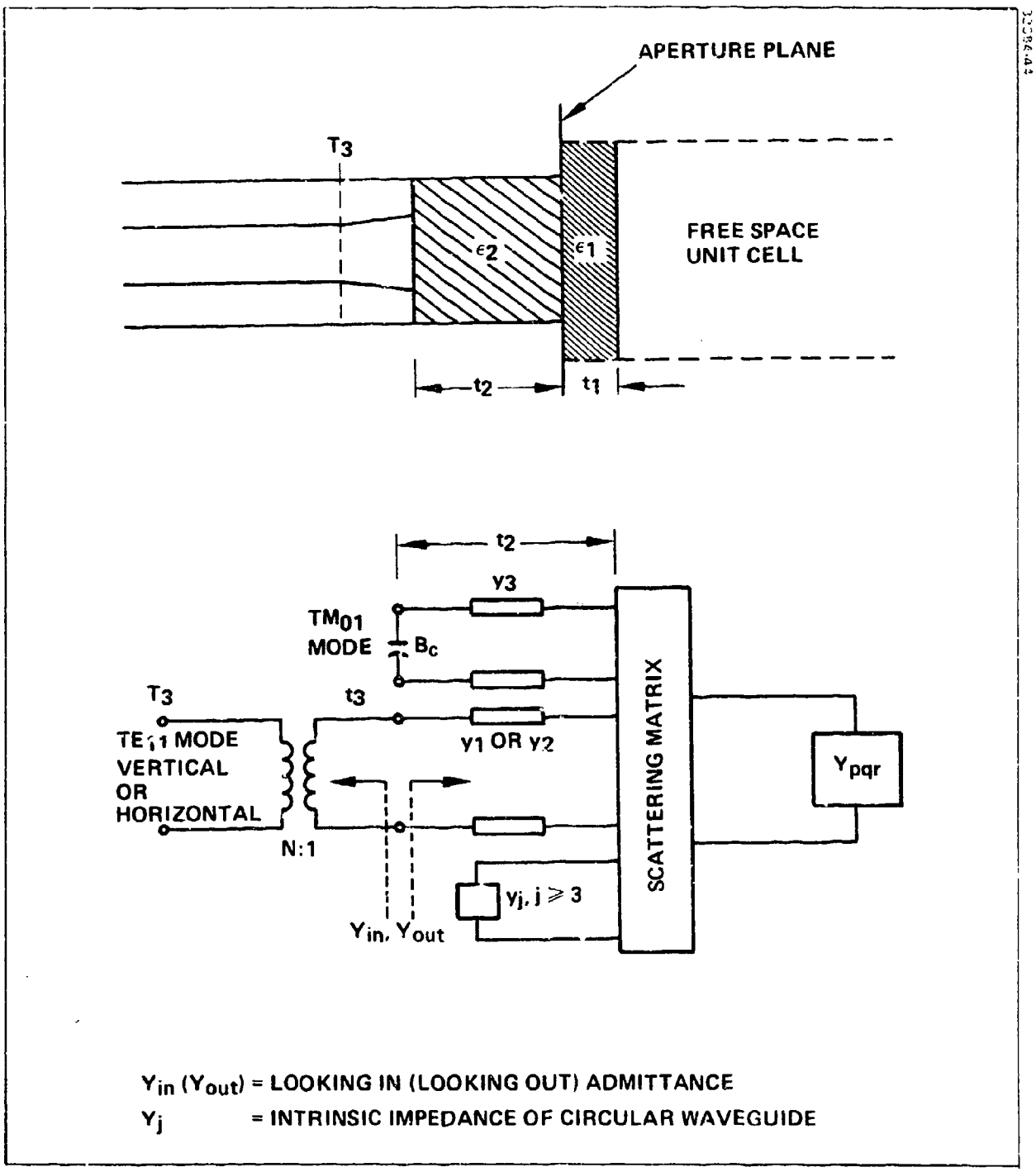

Figure 5-4. Unit Cell Geometry in the Array and Its Equivalent Circuit Representation

5.4 PERFORMANCE OF QUADRUPLE RIDGE-LOADED CIRCULAR WAVEGUIDE ARRAYS

Applying the foregoing procedure for a design which requires to scan over a $\pm 60^{o}$ half-angle cone, we have arrived at the following array parameters:

$d_x = 1.0075\lambda_h$ $\quad d_y = .2909\lambda_h$ $\quad \alpha = 30^{o}$

$a = .252\lambda_h$ $\quad t_1 = .0315\lambda_h$ $\quad t_2 = .188\lambda_h$

$\epsilon_1 = 4.2$ $\quad \epsilon_2 = 2.3$

$\lambda_h = 2.97$ inches $\quad f_h = 3.937$ GHz

The quadruple ridged waveguide has a R/a ratio of .7 and linear tapered to .57 within a .5 inch distance. The measured impedance, referred to the junction, looking into the quadruple ridge-loaded circular guide is shown in Figure 5-5. From this measurement, the equivalent circuit parameters, t_3 and N are determined. The parameter, N, essentially equals to the measured VSWR. The calculated aperture impedance (voltage reflection coefficient) at $f = f_h$ and $.85\ f_h$ which corresponds to 3.937 and 3.346 GHz, respectively, are also shown in Figure 5-5. By selecting a .56 inch thick dielectric plug, the looking out impedance locus is rotated by a distance t_2 and matched to the conjugate of the looking in impedance Z_{in}. The calculated results of power transmission loss versus scan angle at $f = f_h$, $.925\ f_h$, and $.85\ f_h$ are shown in Figure 5-6. An excellent aperture match from high to the center of the band is obtained.

Validity of this equivalent circuit was checked experimentally in an H-plane waveguide simulator with dimensions shown in Figure 5-7. The measured amplitude of reflection coefficient was found to be very close to the calculated value by the foregoing equivalent circuit method except at the low end of the band where the dielectric loaded region is near the cutoff condition. The discrepancy is due to the difficulties in determining the looking in impedance accurately since the impedance as well as the waveguide attenuation varies rapidly at frequencies close to the waveguide cutoff. In fact, the measured data always shows a dip near the cutoff frequencies. If it is not due to loss, the array may have a wider bandwidth than what was calculated.

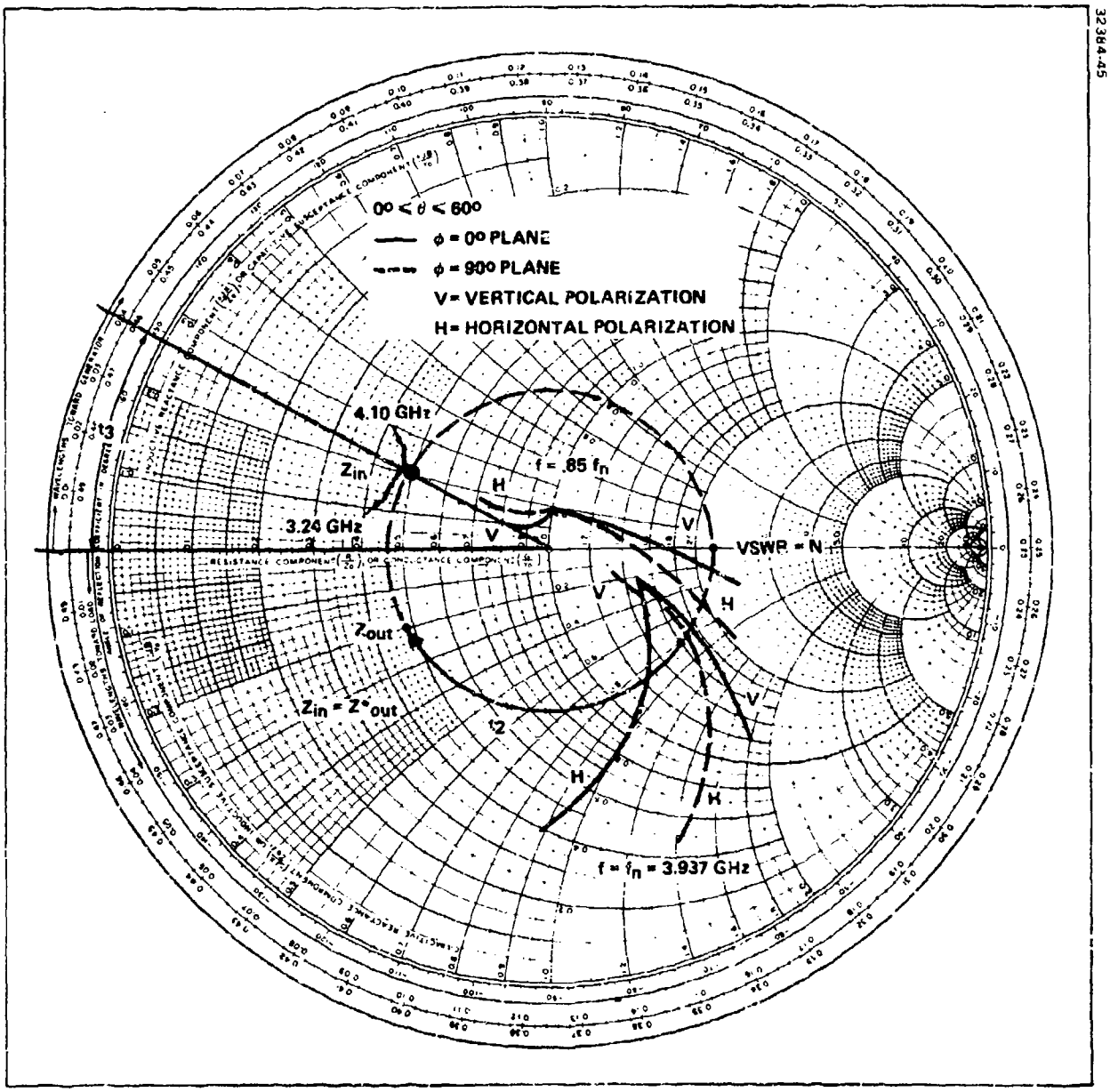

Figure 5-5. Looking-in and Looking-out Impedance

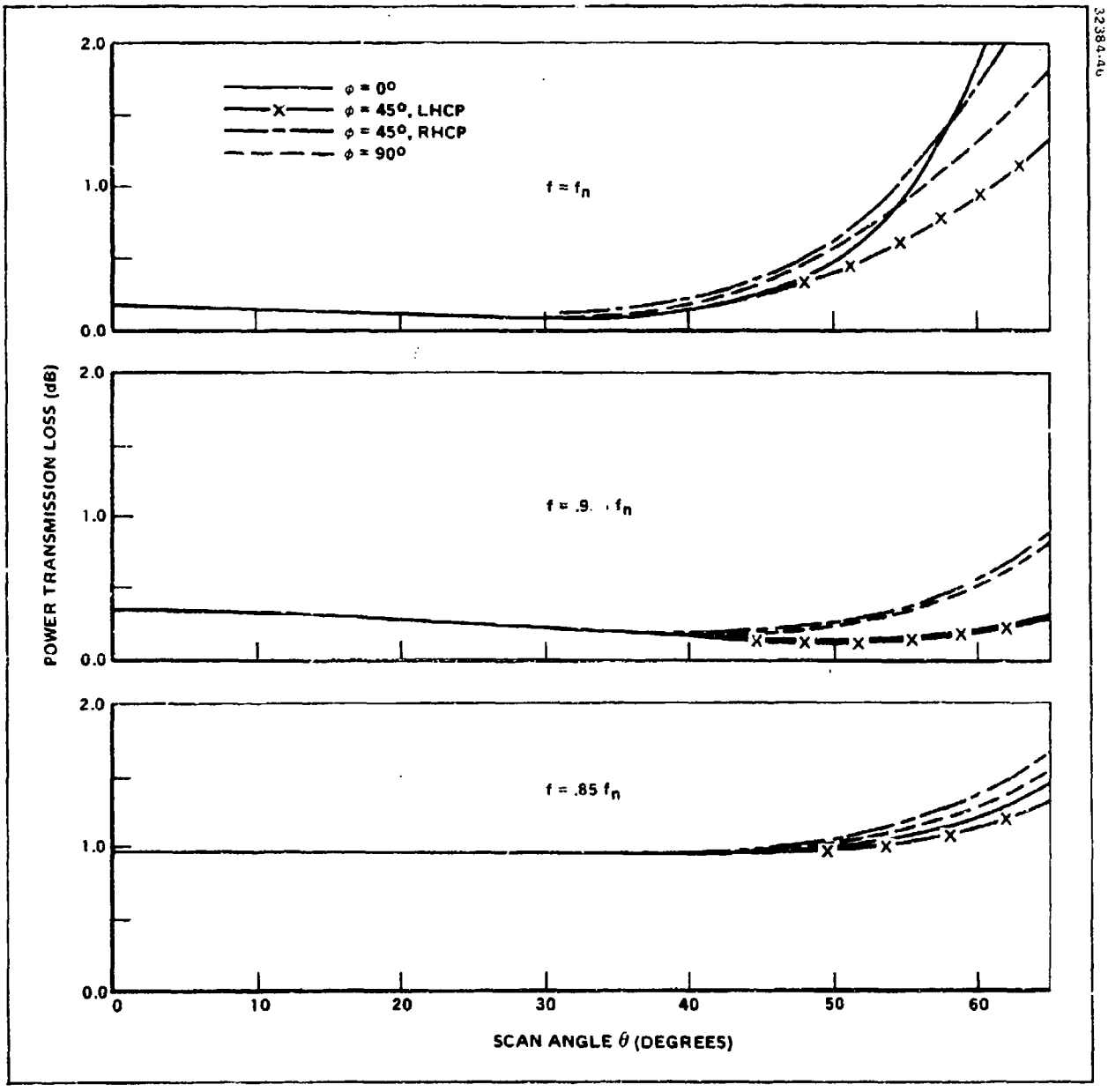

Figure 5-6. Power Transmission Loss versus Scan Angle at f = f_n, P25 f_n and .85 f_n

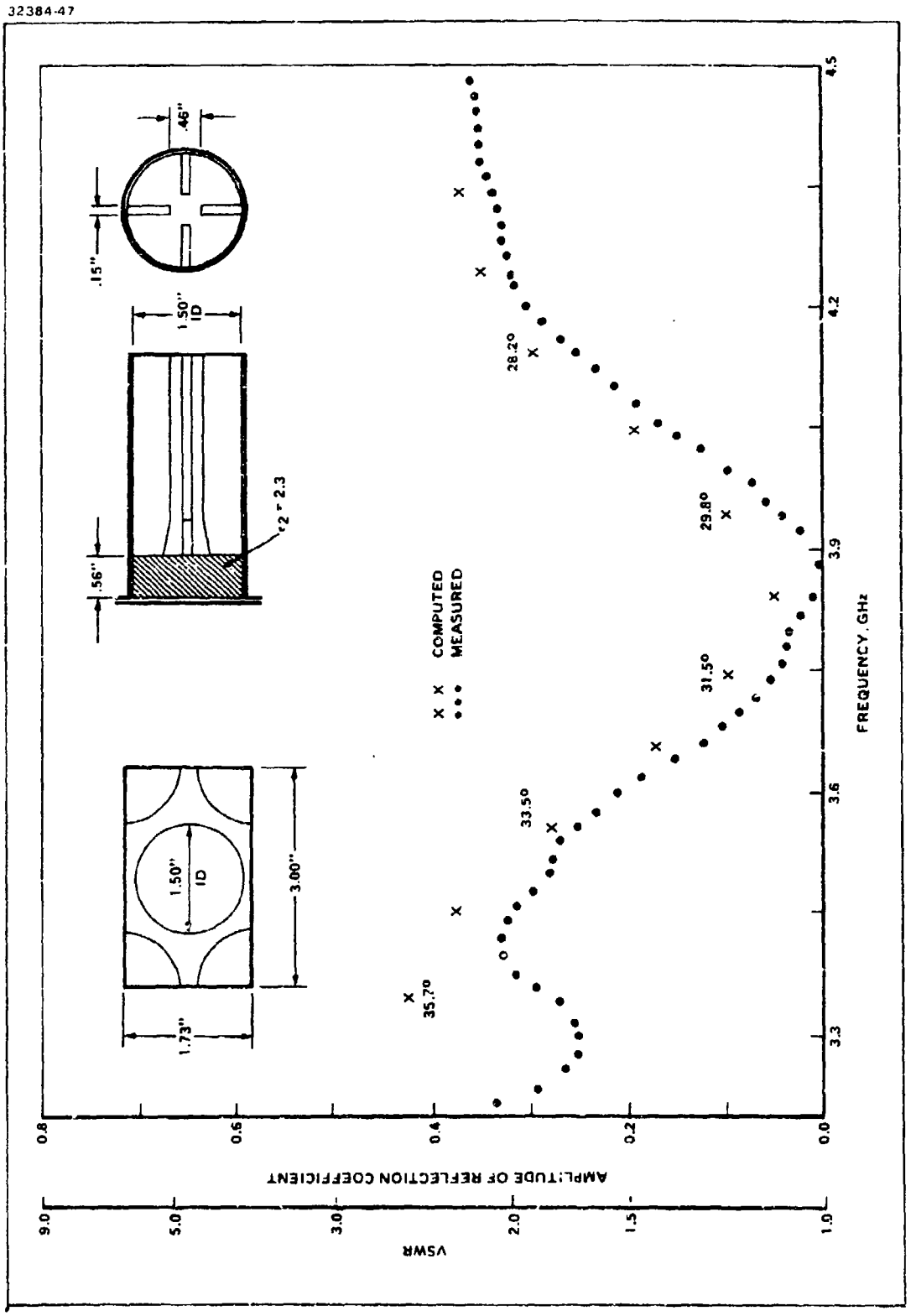

Figure 5-7. Measured and Calculated Results

SECTION VI
CONCLUSIONS

Throughout this program, our design has been emphasized on good performance as well as simplicity for low cost fabrication while we try to broadbanding the element design. In each task, two types of radiating elements have been developed; one designed for the nearly maximum bandwidth obtainable and the other with less bandwidth but with less bandwidth but with good performance.

In Task 1, the 50 percent band rectangular waveguide arrays is not only simple and cost effective, but also possesses excellent impedance match within the scan volume. The double ridge-loaded waveguide arrays is the first one to achieve an octave bandwidth. If the scan volume is reduced from that of 60-degree conical volume, the double ridge-loaded waveguide arrays may be matched over a multi-octave bandwidth.

The dual polarization and simultaneously wide angle scanning requirements limit the bandwidth of an arbitrarily polarized phased array. A 20 percent bandwidth for both the dielectric-loaded circular waveguide arrays and the quadruple ridge-loaded circular waveguide arrays are probably in the limit which can be realized unless the required scan volume is relaxed. The axial ratio and polarization isolation vary rapidly at the edge of scan volume. The polarization characteristics depend substantially with element lattice and element spacing. In some planes of scan, the axial ratio for one sense of circular polarization is better than the other opposite sense. A further tradeoff study of aperture mismatch and depolarization loss will be very helpful in determining the optimum antenna design.

REFERENCES

1. G. H. Knittel, "Wide Angle Impedance Matching of Phased Array Antennas A Survey of Theory and Practice," 1970 Phased Array Antenna Symposium, pages 62-65.

2. G. N. Tsandoulas, "Wideband Limitations of Waveguide Arrays," Microwaves, September 1972, pages 49-56.

3. G. J. Laughlin, E. V. Byron, and T. C. Cheston, "Very Wideband Phased Array Antenna," IEEE Trans. on Antennas and Propagation, Volume AP-20, November 1972, pages 699-704.

4. E. G. Magill and H. A. Wheeler, "Wide-Angle Impedance Matching of a Phased Array Antenna by a Dielectric Sheet," IEEE Trans. on Antennas and Propagation, Volume AP-14, January 1966, pp. 49-53.

5. S. W. Lee and W. R. Jones, "On the Suppression of Radiation Nulls and Broadband Impedance Matching of Rectangular Waveguide Phased Arrays," IEEE Trans. on Antennas and Propagation, Volume AP-19, No. 1, January 1971, pages 41-51.

6. N. Amitay and V. Galindo, "The Analysis of Circular Waveguide Phased Arrays," Bell System Tech. Journal, Volume 47, pages 1903-1931, November 1968.

7. R. F. Harrington, "Matrix Methods for Field Problems," Proc. IEEE Volume 55, pp. 136-149, February 1967.

8. S. W. Lee, W. R. Jones, and J. J. Campbell, "Convergence of Numerical Solutions of Iris Type Discontinuity Problems," IEEE Trans on Microwave Theory and Techniques, MTT-19, June 1971, pages 528-536.

9. G. V. Borgiotti, "Model Analysis of Periodic Planar Arrays of Apertures," Proceedings of IEE, Volume 56, November 1968, pages 1881-1892.

10. J. J. Gustincic, "The Determination of Array Impedance with Multi-element Waveguide Simulators," IEEE Trans. Antennas Propagation, Vol. AP-20, pp. 589-595, September 1972.

11. G. N. Tsandoulas and G. H. Knittel, "The Design and Performance of Dually Polarized Square Waveguide Arrays," 1972 G-AP International Symposium Digest, pp. 157-160.

12. ADAR Semiannual Technical Summary Report, Volume III, "Prototype Systems Development," Submitted to Rome Air Development Center by Hughes Aircraft Company, Contract No. AF 30(602)4240, Document No. FR 67-14-130, SDN A-90968/10G, 15 April 1967.

13. R. T. Clark, "Ridge Loaded Circular Guide," Hughes Aircraft Company IDC Ref No. 71/1422.00-54.

14. P. W. Hanan and M. A. Balfour, "Simulation of a Phased-Array Antenna in Waveguide," IEEE Trans. Antenna Propagation, Vol. AP-13, pp. 342-353, May 1965.